RADAR INTERFEROMETRY FOR MONITORING LAND SUBSIDENCE AND COASTAL CHANGE IN THE NILE DELTA, EGYPT

A Dissertation

by

MOHAMED HASSAN ALY

Submitted to the Office of Graduate Studies of
Texas A&M University
in partial fulfillment of the requirements for the degree of

DOCTOR OF PHILOSOPHY

August 2006

Major Subject: Geology

RADAR INTERFEROMETRY FOR MONITORING LAND SUBSIDENCE AND COASTAL CHANGE IN THE NILE DELTA, EGYPT

A Dissertation

by

MOHAMED HASSAN ALY

Submitted to the Office of Graduate Studies of
Texas A&M University
in partial fulfillment of the requirements for the degree of

DOCTOR OF PHILOSOPHY

Approved by:

Co-Chairs of Committee,	John R. Giardino
	Andrew G. Klein
Committee Members,	Howard A. Zebker
	Vatche P. Tchakerian
	Christopher C. Mathewson
Head of Department,	Richard L. Carlson

August 2006

Major Subject: Geology

ABSTRACT

Radar Interferometry for Monitoring Land Subsidence and Coastal Change in the Nile Delta, Egypt. (August 2006)

Mohamed Hassan Aly, B.S., Zagazig University;

M.S., Zagazig University

Co-Chairs of Advisory Committee: Dr. John R. Giardino
Dr. Andrew G. Klein

Land subsidence and coastal erosion are worldwide problems, particularly in densely populated deltas. The Nile Delta is no exception. Currently, it is undergoing land subsidence and is simultaneously experiencing retreat of its coastline. The impacts of these long-term interrelated geomorphic problems are heightened by the economic, social and historical importance of the delta to Egypt. Unfortunately, the current measures of the rates of subsidence and coastal erosion in the delta are rough estimates at best. Sustainable development of the delta requires accurate and detailed spatial and temporal measures of subsidence and coastal retreat rates.

Radar interferometry is a unique remote sensing approach that can be used to map topography with 1 m vertical accuracy and measure surface deformation with 1 mm level accuracy. Radar interferometry has been employed in this dissertation to measure urban subsidence and coastal change in the Nile Delta. Synthetic Aperture Radar (SAR) data of 5.66 cm wavelength acquired by the European Radar Satellites (ERS-1 and ERS-2) spanning eight years (1993-2000) have been used in this investigation. The ERS data

have been selected because the spatial and temporal coverage, as well as the short wavelength, are appropriate to measure the slow rate of subsidence in the delta. The ERS tandem coherence images are also appropriate for coastal change detection.

The magnitude and pattern of subsidence are detected and measured using Permanent Scatterer interferometry. The measured rates of subsidence in greater Cairo, Mansura, and Mahala are 7, 9, and 5 mm yr^{-1}, respectively. Areas of erosion and accretion in the eastern side of the delta are detected using the ERS tandem coherence and the ERS amplitude images. The average measured rates of erosion and accretion are -9.57 and +5.44 m yr^{-1}, respectively. These measured rates pose an urgent need of regular monitoring of subsidence and coastline retreat in the delta.

This study highlighted the feasibility of applying Permanent Scatterer interferometry in inappropriate environment for conventional SAR interferometry. The study addressed possibilities and limitations for successful use of SAR interferometry within the densely vegetated delta and introduced alternative strategies for further improvement of SAR interferometric measurements in the delta.

ACKNOWLEDGEMENTS

This work has been made possible through the generous support of several organizations. It was supported financially by the Egyptian Ministry of Higher Education and by the National Aeronautics and Space Administration (NASA). The ERS InSAR data were provided by the European Space Agency (ESA), the SRTM data were provided by the Jet Propulsion Laboratory (JPL), and the precise ERS orbital data were provided by the Delft Institute for Earth-Oriented Space Research (DEOS), Delft University of Technology.

Special thanks go to Rick Giardino and Andrew Klein, Texas A&M University, for their tireless advice, constructive comments and great support throughout the five years in which I have had the privilege of being their student. Thanks also to Vatche Tchakerian and Christopher Mathewson, Texas A&M University, for serving on my committee and reviewing my dissertation.

I am also grateful to Howard Zebker, Stanford University, for reviewing my dissertation and my proposals to NASA and ESA. I am proud to have had the opportunity to have Howard in my advisory committee. His encouragement and insightful suggestions contributed a lot to my work.

Finally, I reserve the utmost appreciation and gratitude to my family. I eternally thank my parents for their guidance, encouragement, and support, and I am grateful to my wife and daughter for their unique contribution to my work. Words can not express my sincere gratitude for the support they have given me.

TABLE OF CONTENTS

CHAPTER Page

Page

LIST OF TABLES

LIST OF FIGURES

FIGURE Page

FIGURE Page

FIGURE Page

CHAPTER I

INTRODUCTION

1. Background

Land subsidence is a major worldwide problem, particularly in vulnerable coastal areas such as the Nile Delta. Currently, the delta is undergoing land subsidence and is simultaneously experiencing coastline retreat. The impacts of these long-term interrelated geomorphic problems are heightened by the economic, social and historical importance of the delta to Egypt. A major debate has evolved in the last decade concerning whether or not the land surface of the Nile Delta is subsiding. The debate is certainly problematic in light of the fact that current measures of subsidence in the delta are rough estimates at best. To date, no precise geodetic measurements have been conducted within the Nile Delta to capture present-day subsidence. Prior to this study, knowledge of subsidence rates in the delta was limited to long-term geologic averages that assumed spatial and temporal uniformity.

Stanley (1988 and 1990) estimated the subsidence rates near the coast of the delta to be between 1.00 and 2.50 mm yr^{-1} in the west and 5.00 mm yr^{-1} in the east based on radiocarbon dating of Holocene deltaic sediments. Warne and Stanley (1993) reassessed these estimates and suggested that they were minimum rates because sediment reworking can cause radiocarbon dated cores to be older than the burial age. Subsidence rates estimated based on this geologic process assume uniform extension across the eastern and western parts of the delta, thus, yielding spatial and temporal averages that

---

This dissertation follows the style of the *Journal of Geophysical Research*.

can not assign unique rates to any particular region.

In the fifth century BC, Herodotus observed the annual growth of the Nile Delta from annual flooding (Bloom, 1998). Today, it can be argued that human alteration of the Nile River system through damming and irrigation, which has stopped sediment supply, has turned the delta into a relic coastal plain and has lead to high rates of land subsidence and coastal erosion (Stanley and Warne, 1993; Stanley, 1996). Tectonic setting, aquifer system compaction, and natural compaction of deeply buried strata all contribute to the rate of land subsidence in the Nile Delta (Stanley, 1988).

Acting together, subsidence, eustatic sea-level rise, and reduced sediment supply since closure of the High Aswan Dam in 1964 could cause a relative rise in the sea level over the northeastern delta plain of approximately 1 m by the year 2100 (Stanley, 1990). This incursion would submerge much of the delta in the eastern part to as far south as 30 km from the present coast. For example, in only three coastal cities, Alexandria, Rosetta and Port Said, over two million people would be forced to abandon their homes, 214,000 jobs would be lost and over US $35 billion in land value, property, and tourism income would also be lost as a direct result of a sea level rise of 50 cm (El Raey, 1997). The loss of world famous historic, cultural and archeological sites, thousands of acres of fertile agricultural land, and the vulnerability of other low land cities in the delta outside these three cities are not counted (El Raey, 1997). Thus, the Nile Delta sinking threatens the existence of the coastal zone cities and sustainable urban development across the entire delta. Therefore, there is an urgent need to update maps of the delta coastline position on a regular basis.

2. Research Motivation

Land subsidence in the Nile Delta has induced marked environmental changes particularly with respect to coastline retreat and sea-level rise in the Mediterranean Sea. The Nile Delta has witnessed a significant urban development over the past century. Groundwater pumping is the primary water supply for drinking water and industrial projects. Oil exploitation and natural gas extraction in the northern part of the delta have been also dramatically increased in the last decade. Groundwater, oil and gas pumping in addition to sediment natural compaction, as well as seismic activities directly have resulted in an increased compaction of the aquifer system in the delta.

There is an increasing demand for regular monitoring and accurate measuring of subsidence and coastline retreat in the Nile Delta to gain a broad understanding of these two phenomena and to provide decision-makers with useful information for integrated development and sustainable use of the natural resources in the delta. Several tools such as terrestrial leveling survey and Global Positioning System (GPS) can be used to measure rates of coastal change and land subsidence in the delta; however, these tools provide point measurements that are spatially and/or temporally limited. Radar interferometry, in contrast, is employed in this study to provide subtle measurements of surface changes in the delta at a significantly improved spatial resolution with millimeter-level accuracy and over large areas (100 km^2).

3. Problem Statement

Integrated sustainable development of the Nile Delta requires accurate and detailed spatial and temporal measures of subsidence and coastline retreat rates that this

research attempts to provide using radar interferometry. The main focus of this study addresses the research question “is the land surface of the Nile Delta experiencing subsidence?” If so, what are the magnitudes and patterns of spatial and temporal deformation? Coastal changes, including erosion and accretion will also be addressed using Synthetic Aperture Radar (SAR) interferometric coherence images.

4. Study Objectives

This study employs SAR Interferometry (InSAR) techniques to detect and measure rates of land subsidence and coastal change in the Nile Delta. The specific objectives of this research are four-fold: (1) measure and accurately map subsidence across broad regions in the delta; (2) measure and map coastline retreat rates in the eastern side delta; (3) determine the spatial and temporal patterns of deformation in the selected study sites; and (4) address the potential and limitations for successful use of various InSAR approaches to study crustal deformation within problematic, non-ideal areas of slow rate of deformation, such as the Nile Delta, for InSAR application.

It is also the objective of this study to make a recommendation to the European Space Agency (ESA) either to continue or to stop regular SAR acquisitions over the Nile Delta and areas of similar conditions by ERS-2 and ENVISAT satellites. This, in turn, will help in development and preparation for future operational use of SAR satellites.

5. Study Approach

The Permanent Scatterer (PS) approach is applied to detect and measure urban subsidence in three selected cities in the Nile Delta. Additionally, the tandem coherence

images are employed to detect and measure coastal change in the eastern side of the delta in the 1993-2000 period.

Data from several spaceborne radar missions were considered and evaluated and only the European ERS-1/2 C-band radar instruments were found to provide the required spatial and temporal data coverage. From the large number of archived ERS-1/2 InSAR pairs, 73 ERS InSAR scenes were selected on a time-scale of eight years (1993-2000). Thirty nine ERS scenes were selected for the eastern part of the delta (Track: 436, Frame: 2979), and thirty four ERS scenes were selected for the Cairo area (Track: 436, Frame: 2997).

Several InSAR pairs with short baselines (<200 m) have been selected to test the feasibility of applying the conventional SAR Interferomtery (InSAR) in the Nile Delta. Low baseline values limit the potential for geometric decorrelation in InSAR. Several ERS Tandem pairs were also selected to generate reference DEMs and to create tandem coherence images for accurate detection of the coastline positions. Furthermore, low Doppler Centroid differences were ensured for all selected raw data.

6. Study Area

The Nile River Delta is located in northern Egypt and has an area of about 22,000 km². Its 225 km long, smooth coastline is located approximately 160 km north of Cairo, which resides at the apex of the delta (Figure 1.1). Elevations decrease gently in the delta from south to north, with an 18 m elevation near Cairo decreasing to sea level along the coast. Elevations decrease across the delta at approximately 0.1 m km^{-1}, but the average gradient is considerably lower in the northern delta plain near the Mediterranean Sea.

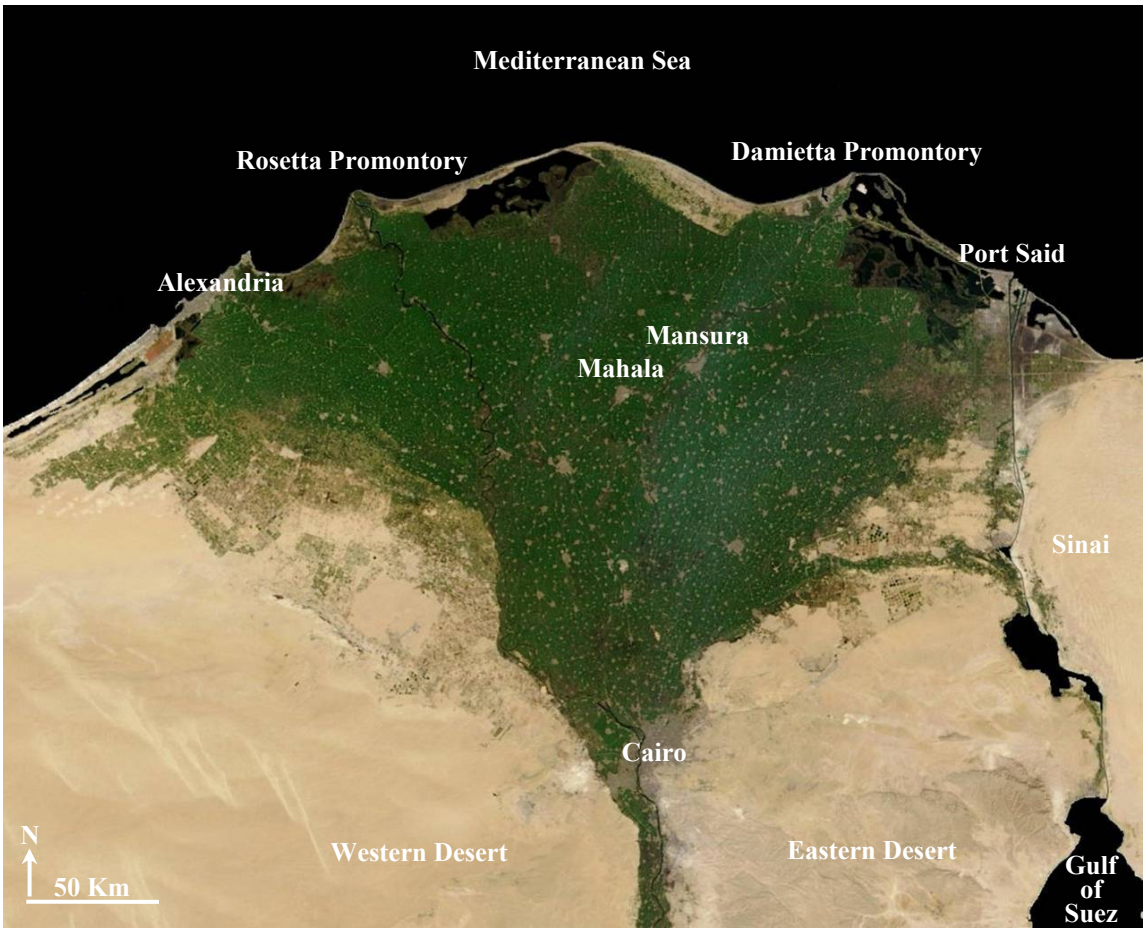

Figure 1.1. The Nile Delta as seen by MODerate resolution Imaging Spectrometer (MODIS), acquired on February 05, 2003. Major cities appear in grayish color and vegetated areas appear in green color

With 50 million people occupying its 22,000-km^2 area, the Nile Delta is one of the most densely populated areas on Earth (average population density of 2,300 people km^{-2}). About 97% of the Egyptian population lives on the Nile River banks and its delta, which compose approximately 4% of the total land area of Egypt. This densely populated coastal delta houses a multitude of significant archeological sites and has many strategic natural resources including natural gas, oil, groundwater, and black sands. In addition, the fertile soils in the delta account for two-thirds of the agricultural land in Egypt and the region supports numerous fisheries (Stanley, 1996). It is also a vibrant tourist destination and an essential recreation outlet for the residents of congested interior cities of Egypt. Thus, the Nile Delta is strategically and economically the most important region in Egypt.

The delta has an arid climate with temperatures exceeding 30º C in July, and mean annual precipitation approximately 200 mm at the coast and less than 100 mm on the delta. Mean potential evapotranspiration rates are approximately 600 - 1100 mm yr^{-1}. Potential evapotranspiration is the maximum amount of evaporation and transpiration from a vegetated surface when an abundant and continuous supply of soil moisture content is available (Beaumont et al., 1976; Stanley and Warne, 1993).

The aquifer system in the Nile Delta consists of alluvial sediments containing two water-bearing layers. The lower layer is highly permeable Pleistocene graded sand and gravel. The upper layer is a Holocene clay-silt layer of relatively low horizontal hydraulic conductivity and very low vertical permeability. The base of the system is the Pliocene clay (Idris and Nour, 1990).

The delta aquifer is bounded by the Mediterranean Sea in the north and the Suez Canal in the east. The thickness of the aquifer is diminished and seems to be isolated from the aquifer of Upper Egypt Nile Valley by thick layers of Pliocene and/or Miocene clay approaching the clay cap near Cairo in the south. The aquifer is in direct contact with that of the Western Desert in the west (Idris and Nour, 1990). The thickness of the Pleistocene aquifer is 100-900 m, with thickness decreasing towards the delta fringes and southward to Cairo. The saturated zone of fresh water attains a maximum thickness of 300 m with less than 1000 ppm. Main recharge of the delta aquifer system is through infiltration from irrigation systems and irrigation water through the clay cap. The total annual amount of water pumped from the delta aquifer is estimated to be 1.6×10^9 m^3 (Idris and Nour, 1990).

The Nile Delta began to develop in the Messinian time. During the Messinian lowering of sea level, the Nile River deposited its sediment load on a broad, subareal-exposed continental margin. The early Pliocene transgression resulted in invading and filling the down-faulted Nile valley to the Middle Egypt (Sestini, 1989).

Tectonic activities in the eastern part of Egypt impacted the Nile system during the Pliocene and Pleistocene (Sestini, 1989). Field mapping, seismic exploration, and well logs suggest a thick accumulation exceeded 3,000 m of superposed and partially overlapping terrigenous sediments underlying the Holocene delta plain (Zaghloul et al., 1977a,b; Rizzini et al., 1978; Zaghloul et al., 1979; Shawky Abdine, 1981; Schlumberger, 1984; Stanley and Warne, 1998). Late Quaternary subsurface stratigraphy of the delta consists of alluvial sand and stiff mud of about 12 Ka age. It is unconformably overlain by shallow marine to coastal transgressive sands with ages of

about 12 - 8 Ka. These sands are unconformably overlain by a variable sequence of Holocene deltaic sands, silts and muds of about 7.5 Ka age (Stanley and Warne, 1998).

Northern Egypt, including the Nile Delta, has been affected by three major tectonic phases from the early Mesozoic to the Recent (Abdel-Aal et al., 1994; Mosconi et al., 1996). The first tectonic phase involved a left lateral oblique extension as a result of the westward movement of Eurasia relative to Africa during the Triassic and the Jurassic. This movement created NE-SW and ENE-WSW fault systems either as normal faults or strike-slip faults with left lateral motions (Meshref, 1990; Abdel-Aal et al., 1994). The second major phase of tectonic activities was a NW-SE oblique contraction related to the closing of the Tethys Sea during the late Cretaceous - early Tertiary. The second phase resulted in a fold system trending ENE associated with the thrust faults of the Syrian Arc System and a fault system trending NW-NNW (Meshref, 1990). The final tectonic phase began in the late Eocene and continued to the Recent and created three major fault systems: (1) the NNW normal fault system, parallel to the Gulf of Suez, developed in the late Eocene and continued to the Miocene, (2) the NNE fault system, parallel to the Gulf of Aqaba, formed by a left lateral oblique slip in the Miocene and continued to the Recent, and (3) the NS fault system formed by rejuvenating and reactivating the older pre-Tertiary structures during the early Miocene (Orwig, 1982; Meshref, 1990).

The previous geologic studies revealed that tectonic activities occurred in north Egypt impacted the eastern side of the Nile Delta and the region of greater Cairo more than the western side of the delta. This implies a major contribution of the tectonic factor to the long-term subsidence rates in the eastern side of the delta and in greater Cairo.

7. Synopsis

This investigation employed Synthetic Aperture Radar Interferometry (InSAR) to study urban subsidence and coastal change in the densely vegetated Nile Delta. A review of SAR interferometry for measuring topography and crustal deformation is presented in Chapter II with a short discussion of radar interferometry principles. Chapter III and Chapter IV present the results of the land subsidence investigations using InSAR. Chapter III discusses land subsidence in greater Cairo in the southern part of the delta. Land subsidence in two other cities, Mansura and Mahala in the middle of the Nile Delta, is presented in Chapter IV. Chapter V discusses the use of SAR tandem coherence images to detect and measure coastal change at Damietta Promontory in the eastern side of the Nile Delta. The last chapter, Chapter VI, discusses the potential and limitations for successful use of InSAR approaches to study crustal deformation, particularly in densely vegetated areas such as the Nile Delta. This chapter also summarizes the conclusions of this study and suggests avenues for future work.

CHAPTER II

SAR INTERFEROMETRY FOR MEASURING TOPOGRAPHY AND CRUSTAL DEFORMATION

1. Introduction

Synthetic Aperture Radar Interferometry (InSAR) is a revolutionary remote sensing approach capable of mapping terrain heights with 1 m vertical accuracy and detecting subtle surface deformation with 1 mm level accuracy. InSAR data can be acquired both day and night, in all-weather conditions, with SAR spatial resolutions, on a global scale, and over day to year periods. InSAR has been used worldwide for a wide variety of applications, including, but are not limited to, mapping terrain heights and monitoring active volcanoes, active tectonics, land subsidence, landslides, and earthquake activities, as well as studying glacier dynamics.

Active radar systems illuminate the surface of Earth and detect radar backscatters; thus, radar images can be acquired independent of the solar illumination. Generally, imaging radar systems include Real Aperture Radar (RAR) and Synthetic Aperture Radar (SAR). The RAR system requires a long antenna and a high power output to achieve an acceptable resolution and a dynamic range, as the resolution is proportional to the antenna length and inversely proportional to the range. SAR systems overcome the limitation of the antenna length by synthesizing an antenna that receives a series of reflected radar signals and electronically combines them with reference

wavelengths. The resolution of SAR images remains the same over all ranges (Elachi, 1988; Curlander and McDonough, 1991).

2. Historical Review

Numerous studies have been published demonstrating the unique contribution of InSAR to the science community. The first use of InSAR dates from the 1960s when observations of the surface of Venus using Earth-based antennas were conducted by Rogers and Ingalls (1969) and Rumsey et al. (1974). Zisk (1972a,b) applied the same technique to measure the topography of Moon. Graham (1974) was the first to introduce InSAR for Earth topographic mapping using a military airborne SAR system.

The first civilian InSAR application was accomplished by NASA scientists at the Jet Propulsion Laboratory (JPL) in Pasadena, California. Zebker and Goldstein (1986) presented the first practical results of InSAR topographic measurements utilizing a side-looking airborne system. They mounted two SAR antennas on an aircraft with a baseline of 11.1 m length. One antenna transmitted the radar signals, and the backscattered signals were received by the two antennas.

The produced complex images from this experiment had approximately 10 m resolution and were not corrected for the aircraft roll as a result of the lack of information about the aircraft attitude. The achieved accuracy was quite limited, with elevation deviations of 2-10 m Root Mean Square (RMS) error over the ocean and with larger RMS values over the land. Nevertheless, the experiment showed the promise of the interferometric approach. Gabriel and Goldstein (1988) adapted the existing

interferometric technique to crossed orbits using SIR-B repeat-pass data acquired over the Rocky Mountains, British Columbia, Canada, in October 1984. This applied technique was computationally complicated and required precise knowledge of orbit parameters, as the orbits were not parallel.

A remarkable improvement occurred when Gabriel et al. (1989) introduced the differential interferometric approach. They produced a double difference interferogram using two interferograms generated from repeat-pass SEASAT observations. It was demonstrated that SAR interferometry could detect elevation differences on the order of sub-centimeter. The multi-baseline approach was first presented by Li and Goldstein (1990). They studied the effect of using various baselines to detect topography. Their study showed that the sensitivity of height measurements is proportional to the baseline length, but the phase error also increases as the baseline increases.

Since the launch of the ERS-1 satellite by the European Space Agency (ESA) in July 1991, a huge archive of C-band InSAR data has become available, and numerous papers covering InSAR limitations and its potential applications have been published. Applications of spaceborne InSAR were greatly extended after the launch of the ERS-2 satellite by ESA in April 1995. The tandem mode of the ERS-1 and ERS-2 satellites acquired InSAR data with only one-day separation. This, in turn, allowed comprehensive investigations of slight change in terrain heights, atmospheric effects, and temporal decorrelations in InSAR data.

Currently, SAR data appropriate for InSAR applications are available from several spaceborne and airborne missions, including ERS-1, ERS-2 and ENVISAT satellites operated by the European Space Agency, JERS-1 and ALOS operated by the National Space Development Agency of Japan, RADARSAT-1 and RADARSAT-2 operated by the Canadian Space Agency, and SIR-C/X-SAR operated by the National Aeronautics and Space Administration (NASA), the German Space Agency (DARA), and the Italian Space Agency (ASI). A wide variety of InSAR data acquired by airborne interferometers are also available throughout the world. The availability of various kinds of InSAR data, open-source InSAR processors as well as commercial InSAR processing packages, in addition to InSAR expertise led to numerous publications in various fields.

3. System Design and Implementation

Whereas conventional SAR systems utilize a single antenna to acquire data, InSAR systems acquire data using two antennas separated by a known baseline. SAR interferometric data can be acquired by systems of three different designs: along-track, across-tack, and repeat-pass interferometric systems. Those system names refer to the relative positions of the antennas with respect to each other. In along-track systems, the baseline is parallel to the flight path. In across-track systems, the baseline is perpendicular to the flight path. However, in repeat-pass systems, only one antenna is mounted on the system and the second antenna is simulated by repeating the pass at a later time. It is actually a way of conducting across-track interferometry utilizing a single antenna.

3.1. Along-track interferometry

In along-track interferometry, two SAR antennas are placed parallel to the flight path. Both SAR antennas transmit and receive the microwave signals in a single pass. Currently, the along-track interferometry is limited to airborne SAR platforms. Feasible applications are the detection of moving objects such as glaciers and ice sheets, the mapping of ocean currents, and the measurement of the directional wave spectra (e.g., Goldstein and Zebker, 1987; Goldstein et al., 1989; Marom et al., 1991; Orwig and Held, 1992).

3.2. Across-track interferometry

In across-track interferometry, two SAR antennas are placed perpendicular to the flight direction. In across-track interferometry, one antenna transmits the radar signals and the radar backscatter is received by the two SAR antennas simultaneously in a single pass. The system captures information on the terrain heights. The problem with the system geometry is that errors caused by the aircraft roll can not be distinguished from the influence of terrain slope. The across-track interferometry is suitable for topographic mapping.

The Shuttle Radar Topography Mission (SRTM) is a good example for cross-track interferometry utilizing dual antennas to acquire InSAR data in a single pass. SRTM acquired InSAR data over approximately 80% of the entire landmass of Earth in eleven days during February 2000. SRTM data are acquired in C- and X-bands and processed into a global DEM by NASA-JPL and the German aerospace center (DLR),

respectively. SRTM DEMs are publicly available at resolution levels of one and three-arc sec (Rabus et al., 2003).

3.3 Repeat-pass interferometry

In repeat-pass interferometry, a single antenna is used to acquire InSAR data by imaging the same area at different times and with a slightly different viewing geometry. The baseline in this case is determined by the separation between the platform passes. The repeat-pass approach requires precise orbital parameters. Thus, it is most suited to spaceborne platforms. ERS, ENVISAT, RADARSAT, JERS, and ALOS satellites are repeat-pass spaceborne systems.

Numerous studies applied the repeat-pass approach using InSAR data from various SAR systems such as SIR-B (Gabriel and Goldstein, 1988), SEASAT (Li and Goldstein, 1990), and ERS-1 (Prati and Rocca, 1992). Gray and Farris-Manning (1993) applied the repeat-pass approach using an aircraft of the Canadian Center for Remote Sensing (CCRS) operated with one SAR antenna.

4. InSAR Theory

Synthetic Aperture Radar Interferometry (InSAR) is an active radar system that transmits and receives microwave signals using two SAR antennas. It works by accurately measuring the distance between the sensor and a point on the surface of Earth. The interferometric data acquired by the two SAR antennas are representations of both amplitudes and phases of the radar backscatter. A phase preserving SAR processor can

be used to transform these data into two separate complex SAR images for the same area. The two complex SAR images will be quite similar; however, the phase of the corresponding pixels will be slightly different. In across-track interferometry, this phase difference can be interpreted as the pixel height (Figure 2.1).

In an InSAR image, the phase difference and the pixel height are related by:

$$\phi = \phi_1 - \phi_2 = \frac{2\pi}{\lambda}\Delta\rho = \frac{2\pi}{\lambda}(\rho_1 - \rho_2) \qquad (2.1)$$

$$z = h - \rho_1 \cos\theta \qquad (2.2)$$

where ϕ is the phase difference between the phases (ϕ_1 and ϕ_2) of the radar backscatters at the two SAR antennas, λ is the radar wavelength, ρ_1 and ρ_2 are the ranges respectively from the two successive SAR antennas S_1 and S_2, z is the height to be calculated, h is the height of the reference orbital antenna S_1 above the datum, and θ is the look angle of the reference interferometer S_1.

Equation (2.1) represents the case of a single-pass InSAR system where one of the two SAR antennas mounted on the platform transmits the radar signals and both antennas receive the radar backscatter simultaneously. In repeat-pass interferometry, the relationship demonstrated in equation (2.1) can be expressed as:

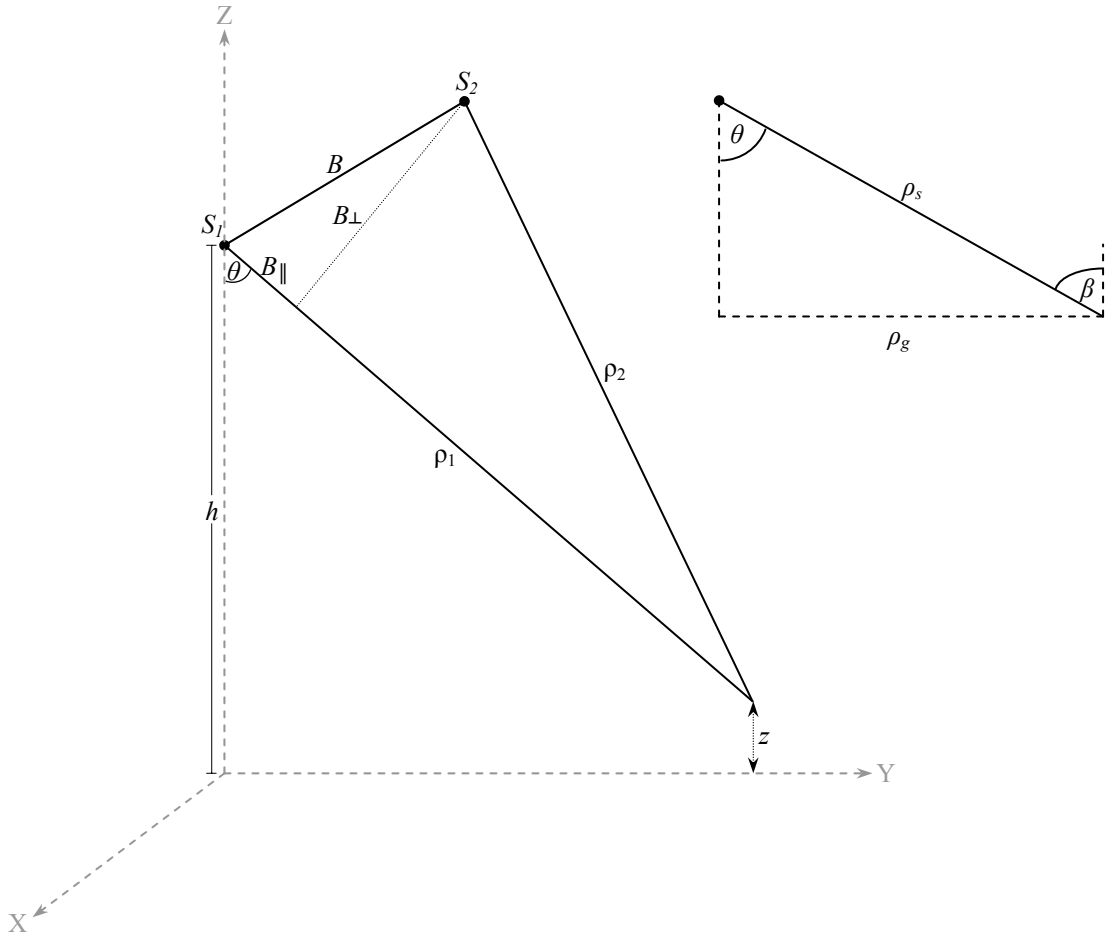

Figure 2.1. General geometry of across-track interferometry. The two SAR interferometers, S_1 and S_2, are flying parallel to the X-axis (azimuth direction) with a perpendicular baseline $B_\perp$ and a parallel baseline $B_\parallel$. ρ_1 and ρ_2 are the ranges respectively from the two successive SAR antennas S_1 and S_2, z is the height to be calculated, h is the height of the reference orbital antenna S_1 above the datum, θ is the look angle of the reference interferometer S_1, ρ_g and ρ_s are the ground range and the slant range, respectively, and β is the incident angle

$$\phi = \phi_1 - \phi_2 = \frac{4\pi}{\lambda}\Delta\rho = \frac{4\pi}{\lambda}(\rho_1 - \rho_2) \qquad (2.3)$$

where ϕ is the phase difference between the phases (ϕ_1 and ϕ_2) of the radar backscatters at the two SAR antennas, λ is the radar wavelength, and ρ_1 and ρ_2 are the ranges respectively from the two successive SAR antennas S_1 and S_2.

In surface deformation studies, the topographic phase contribution has to be estimated and removed from the interferometric signals. The topographic phase can be expressed as:

$$\phi_{topo} = -\frac{4\pi B_\perp z}{\lambda\rho\sin\theta} \qquad (2.4)$$

where ϕ_{topo} is the topographic phase, $B_\perp$ is the perpendicular baseline between the two SAR antennas, z is the topographic height, λ is the radar wavelength, ρ is the range (the distance between the radar and a point on the ground), and θ is the look angle of the reference interferometer.

In along-track interferometry where two SAR antennas are positioned horizontally along the flight path, the phase difference can be interpreted as the target motion proportional to the radial distance moved in the time required for the rear antenna to occupy the position of the forward antenna (Goldstein and Zebker, 1987). The

relationship of the phase difference and the radial velocity of the target can be represented as:

$$\phi = \frac{4\pi uB}{\lambda v} \tag{2.5}$$

where u is the radial velocity of the target, B is the baseline between the two SAR antennas, and v is the velocity of the radar platform.

The basic task in processing InSAR data is to extract information about three-dimensional objects from the complex InSAR data. The real (Re) and the imaginary (Im) components of the complex signals contain information about the interferometric phase (ϕ) and the amplitude (A) of the radar backscatters.

$$\phi = \arctan\frac{\mathrm{Im}}{\mathrm{Re}} \tag{2.6}$$

$$A = \sqrt{\mathrm{Im}^2 + \mathrm{Re}^2} \tag{2.7}$$

With pairs of complex values (C_1 and C_2), equation (2.6) can be re-written as:

$$\phi = \arctan\left[\frac{\mathrm{Im}\left[\sum_{i=1}^{N} C_1^{(i)} C_2^{*(i)}\right]}{\mathrm{Re}\left[\sum_{i=1}^{N} C_1^{(i)} C_2^{*(i)}\right]}\right] \tag{2.8}$$

This maximum likelihood estimator provides the phase difference for homogenous distributed targets (Allen, 1995), where N is the number of looks to be averaged (Rodriguez and Martin, 1992) and * denotes the complex conjugate.

5. Common Processing Approaches

5.1. Two-pass interferometry

In two-pass interferometry, two SAR images acquired at different times for the same area are needed to create an interferogram containing both topography and surface deformation. The approach requires an external Digital Elevation Model (DEM) for the same area be geocoded to the SAR geometry for topographic phase removal.

The advantages of the two-pass approach are: (1) only one pair of SAR images is required, which saves money, time, effort, and complication in processing, (2) no need for phase unwrapping of a topographic interferogram, avoiding errors in phase unwrapping and computation load, and (3) the geolocation process is not affected by the quality of an unwrapped topographic interferogram.

The disadvantages of the two-pass approach are mostly associated with the use of an external DEM. The external DEM may contain significant errors, the datum of the DEM may be not known, or most importantly the DEM itself may be unavailable or available but inappropriate with regard to accuracy and spatial resolution.

5.2. Three-pass interferometry

Three-pass interferometry requires three SAR images taken for the same area at different times. Two of them should be acquired within a very limited time period to create a topographic interferogram that can be used later for topographic correction. The tandem mode of the ERS satellites, in which images are acquired with only one day apart, is appropriate for this purpose. The reference image used for the creation of the topographic interferogram is used with the third image to produce another interferogram containing both topographic and surface deformation contributions.

Three-pass interferometry has the advantages that the three radar images are all in SAR coordinates. It does not require an external DEM, thus avoiding errors associated with external DEMs and interpolation errors associated with topographic phase simulation and geocoding. The disadvantages of the three-pass interferometry include difficulty in finding an appropriate SAR triplet, and errors in phase unwrapping of the topographic interferogram can produce errors in the deformation estimation and the geolocation process.

5.3. Four-pass interferometry

Four-pass interferometry requires four SAR images taken for the same area at different times; two of them are used to construct an interferogram containing both topography and deformation. The other two images are used to create a topographic interferogram for topographic correction. The four-pass approach is quite similar to the three-pass approach. However, in the four-pass approach, the two interferograms are

processed independently using two different reference images. Therefore, one of the interferograms has to be resampled to the other for topographic phase removal.

Critical limitations for applying conventional SAR interferometry, including, two-, three- and four-pass interferometric approaches, are basically related to temporal decorrelation, geometric decorrelation, and atmospheric path delay. A detailed discussion of these limitations is provided in Chapter VI.

5.4. Permanent scatterer interferometry

The Permanent Scatterer interferometric approach has been recently introduced by Ferretti et al. (2000) as a new approach to monitor surface deformation. This pixel-by-pixel approach uses Permanent Scatterers of sufficient spatial density that exhibit coherence over long time periods, such as man-made features and bare rocks, to capture motion of the scatterers. The approach enables the exploitation of the individual phases of the Permanent Scatterers in areas of low coherence where conventional InSAR fails as a result of temporal and geometrical decorrelations, as well as atmospheric heterogeneities.

Over conventional InSAR, the advantages of the Permanent Scatterer interferometry are: (1) the critical baseline and the Doppler Centroid difference defined as critical limitations for conventional InSAR approaches are no longer limitations for the Permanent Scatterer interferometry, (2) target motion can be accurately tracked on a pixel-by-pixel basis over long time periods, (3) elevations of the Permanent Scatterers (PSs) can be estimated with good accuracy by combining very long perpendicular

baselines, (4) atmospheric artifacts can be accurately estimated and eliminated by using a long time series, and (5) isolated coherent scatterers, such as urban areas and bare rocks, can be detected and tracked among incoherent scatterers, such as densely vegetated areas.

The disadvantages of Permanent Scatterer interferometry are: (1) it requires a large number of SAR acquisitions of the same area (at least 20 scenes), (2) data are expensive and it is difficult to find the appropriate time series needed, (3) stable reflectors need to be of sufficient spatial density, and (4) it does not work properly over low reflectivity areas of smooth surfaces. More details on the approach can be found in Ferretti et al. (2000 and 2001).

6. Basic Processing Steps

There are significant differences in the degree to which processing facilities prepare the raw signal of the InSAR data for distribution. ERS SAR raw data, which are used in this research, are delivered in the CEOS format. CEOS stands for the Committee on Earth Observation Satellites. The CEOS format consists mainly of four files: a volume directly file, a leader file, a data file, and a null volume file. The volume directory file contains general information on the arrangement of the data on the distributed media. The leader file contains specific information about the distributed data, such as raw data file size, spacecraft state vectors, scene center latitude and longitude, and time of acquisition. The data file contains the raw signal product. It consists of a header record and the raw data usually stored as one data line per record.

Each record consists of a prefix, raw data and a suffix. Finally, the null volume file contains information about ending the medium of storage.

6.1. Image formation

All SAR interferometric approaches require that SAR acquisitions for the same area be processed consistently relative to each other before the coregistration process. To produce Single Look Complex (SLC) images appropriate for InSAR processing, InSAR raw data have to be subject to a series of processing steps, including range spectrum estimation, missing line correction, estimation of the Doppler ambiguity, Doppler Centroid estimation, range compression, azimuth prefilter, azimuth auto-focus, and azimuth compression. Several technical parameters are needed for the process of image formation. The important parameters of the ERS satellites are given in Table 2.1.

The orbital information provided with the CEOS raw data is a rough estimate and can dramatically affect the results. Precision state vectors are essential for accurate estimation of the interferometric baselines. Precise state vectors of the ERS satellites are available at the European Space Agency (ESA) and the Delft Institute for Earth-Oriented Space Research (DEOS). The quality of the DEOS orbital state vectors exceeds that of the ESA precision state vectors (PRC). For ERS satellites, DEOS orbital data are of about 5 cm vertical accuracy and of about 13 cm horizontal accuracy in along- and across-track directions. The several centimeters error in orbital estimations is repeatable in each cycle and it is the same for ERS-1 and ERS-2 along the same track and, thus, its effect is eliminated in InSAR processing.

6.2. Interferogram generation

A focused complex SAR image is a representation of amplitudes and phases of the radar backscatters in a two-dimensional record. Interferogram generation requires that complex SAR images be correctly focused and calibrated and be precisely coregistered to sub-pixel accuracy, 0.1 pixel. Phase value differences are calculated using the amplitude values of corresponding pixels in two precisely coregistered SAR images. The complex interferogram is produced by pointwise multiplication of the corresponding pixels in the two complex coregistered SAR images as follows:

$$I = C_1.C_2^* = A_1 e^{i\phi_1}.A_2 e^{-i\phi_2} = A_1 A_2.e^{i(\phi_1 - \phi_2)} = A.e^{i\phi} \qquad (2.8)$$

where C_1 is the complex value, amplitude and phase, of the reference image, C_2 is the complex values of the resampled image, the * denotes the complex conjugate, A is the amplitude of the interferogram, and ϕ is the phase of the interferogram.

6.3. Phase unwrapping

The measured interferometric phase is given modulo 2π, i.e. it is wrapped. The wrapped phase does not infer range differences, as it is limited to –π and +π; therefore, phase unwrapping is needed to convert the cyclic phase values into continuous values. To solve the interferometric phase ambiguity, it is necessary to add the correct integer number of phase cycles (n2π) to every phase measurement. A wide variety of algorithms

Table 2.1. Important technical parameters of ERS SAR satellites

Parameter	**Value**
Carrier frequency	5.3 GHz
Wavelength	5.656 cm
Pulse bandwidth	15.55 MHz
Pulse repetition interval	595.27 μs
Pulse repetition frequency	1679.9 Hz
Pulse length	37.1 μs
Sampling frequency	18.96 MHz
Chirp slope	419 GHz s^{-1}
Receiver noise temperature	3700 K
Range to first pixel	832 km
Orbital elevation	790 km
Orbital interval time	1, 3, 35 days
Look angle	20.5° – 25.9°
Incidence angle	23°
Swath width	100 km
Ground range resolution	25 m
Slant range resolution	10 m
Azimuth resolution	5 m
One look range pixel size	20 m
One look azimuth pixel size	4 m
Ground coverage of one scene	~100 km²
Nominal critical baseline	~ 1200 m

has been developed for phase unwrapping. A thorough discussion and review of the existing algorithms can be found in Chen (2001). The unwrapped interferometric phase (ϕ_{unw}) is a function of the topography (ϕ_{topo}), the surface deformation (ϕ_{def}) in the Line-Of-Sight (LOS), the atmospheric artifacts (ϕ_{atm}), and the phase noise (ϕ_{noise}). It can be expressed as the sum of these contributions:

$$\phi_{unw} = \phi_{topo} + \phi_{def} + \phi_{atm} + \phi_{noise} \tag{2.9}$$

Once the measured interferometric phase is unwrapped correctly, the absolute phase can be computed using a point of a known elevation within the SAR scene as an absolute elevation reference. Then, the unwrapped phase values in the topographic interferogram can be converted into height values, and the unwrapped phase values in the topographically corrected interferogram can be converted into displacement values.

This is usually followed by a geocoding step in which the interferometric products are projected to a common refernce system. Geocoding enables combination of the InSAR products with products from other sources.

For Permanent Scatterer interferometry, there is no single processing procedure to follow, as each dataset has its own characteristics and problems; however, a complete description of the procedures applied in this dissertation is given in chapter III.

7. Interferometric Decorrelations and Limitations

Coherency between SAR acquisitions is by far the most important requirement for successful use in SAR interferometry (Hanssen, 2001). Temporal and geometrical decorrelations (Zebker and Villasenor, 1992) and atmospheric heterogeneities (Goldstein, 1995; Massonnet and Feigl, 1995; Zebker et al., 1997) between SAR acquisitions are three major contributors to phase ambiguity in SAR interferometry. Temporal decorrelation hampers SAR interferometric measurements where positions of the scatterers change with time within the resolution cell.

Geometric decorrelation limits the utility of SAR interferometry to InSAR pairs of perpendicular baselines smaller than the critical one, ~1200 m for ERS (Zebker and Villasenor, 1992; Massonnet and Feigl, 1998). For surface deformation measurements, the phase gradient should be within one fringe per pixel (Massonnet and Feigl, 1998). Atmospheric heterogeneities superimpose an Atmospheric Phase Screen (APS) in SAR images, which seriously affect the accuracy of deformation measurements (Massonnet and Feigl, 1995 and 1998; Colesanti et al., 2003). Cycle ambiguity problems in conventional InSAR can be overcome by carrying out InSAR measurements on Permanent Scatterers (PSs), exploring a long temporal series of SAR acquisitions for the same area (Ferretti et al., 2000 and 2001; Colesanti et al., 2003).

Surface deformation studies are also limited by the swath width, 100 km for ERS, and the range pixel size, 20 m for ERS, of the SAR platform (Massonnet and Feigl, 1998). Additionally, rough topography in mountainous areas may lead to interferometric

decorrelation, but the effect of topography depends on the platform acquired the InSAR data.

In most cases, uncertainties in InSAR measurements are quantifiable and their effect can be eliminated. Uncertainties, in InSAR pairs that can be combined to construct interferograms, related to system errors are repeatable and comparable in all SAR acquisitions. Therefore, they have a slight effect on InSAR measurements, as all InSAR measurements are relative to a reference acquisition. Furthermore, InSAR acquisitions that are dramatically affected by errors and decorrelations or are not within the InSAR system limitations can not be combined originally in processing to produce interferograms.

8. Applications

8.1. Topographic mapping

Spaceborne SAR systems have been proven capable of acquiring images to produce global DEMs of high quality in few days. However, airborne SAR systems can produce DEMs of higher resolution, similar to optical streogrammetry, because they fly closer to the ground (Bürgmann et al., 2000). Unlike stereo-pair radar techniques, where the observable terrain height is the order of the resolution cell size, the measured terrain height with InSAR techniques is of the order of the radar system wavelength (Zebker et al., 1992).

Single-pass interferometry has many advantages for DEM generation over the repeat-pass systems utilizing a single antenna because the two SAR images are taken

simultaneously and the length and orientation of the baseline can be accurately determined. The simultaneous acquisition prevents interferometric decorrelations and neglects the effects of the atmospheric path delay. SRTM is a good example of this approach.

The InSAR data collected with the tandem mode of the ERS satellites are appropriate for DEM generation, as they are acquired with only one day apart. Zebker et al. (1994b) estimated the accuracy of DEMs derived from ERS-1 images. Their study indicated that there are two main errors in generating DEMs using this approach, which are the height estimation error, and the baseline error. The height estimation error is a function of the error in the phase estimation. Ferretti et al. (1996) introduced the multi-baseline approach for the automatic generation of high quality DEMs using InSAR data.

8.2. Crustal deformation studies

InSAR has a unique capability of detecting active processes that are not accessible with other geodetic tools. SAR interferometry is capable of detecting surface changes of the order of the radar wavelength. For the C-band, wavelength = 5.66 cm, radar systems, e.g., ERS and RADARSAT, one color cycle in a topographically corrected interferogram marks 2.83 cm of surface deformation in LOS.

8.2.1. Earthquakes

The Landers earthquake of 1992 was the first seismic event captured with InSAR (Massonnet et al., 1993 and 1994; Zebker et al., 1994a; Massonnet and Feigl, 1995a;

Hernandez et al., 1997; Price and Sandwell, 1998). Results from these studies to measure the co-seismic displacements agreed well with the conventional measurements. Some InSAR studies provided more insights into modeling of the earthquake motion (Pletzer et al., 1994; Massonnet and Feigl, 1995b).

8.2.2. Volcanoes

Monitoring active volcanoes is not feasible with traditional surveying methods. The first use of InSAR to study volcanoes was reported by Evans et al. (1992). They used TOPSAR airborne data to assess damage caused by lava flaws and the intercomparison of the volcano morphology. Massonnet et al. (1995) used ERS data to investigate volcanic deformation of Mount Etna. Several volcanoes across the world have been studied using InSAR such as Hawaiian volcanoes (Rosen et al., 1996), Alaskan volcanoes (Lu et al., 1997), localized inflation on Izu Peninsula, Japan (Fujiwara et al., 1998a), deformation of the active Yellowstone Caldera (Wicks et al., 1998), and volcanic deformation in the Long Valley (Thatcher and Massonnet, 1997). Zebker et al. (2000) reported sixteen active volcanoes detected with SAR interferometry. More recently, Hooper et al. (2004) introduced a new method for measuring deformation on volcanoes and other natural terrains using InSAR Persistent Scatterers.

8.2.3. Landslides

Landslides usually degrade the ground surface quickly reducing the interferometric coherence, as they commonly deform the ground surface in excess of the

high gradient limit. Studying landslides requires a very accurate DEM, as they usually occur in areas of rough topography (Massonnet and Feigl, 1998). All these factors limit the use of InSAR to study most of landslides across the world. Singhroy et al. (1998) studied landslide characterization in Canada using InSAR. Rott et al. (2003) investigated the InSAR techniques and applications for monitoring landslides. Another study for landslide monitoring using ground-based SAR interferometry was reported by Tarchi et al. (2003). Colesanti et al. (2003) applied the Permanent Scatterer interferometric technique to monitor landslides and tectonic motions. Hilley et al. (2004) addressed the dynamics of slow-moving landslides using the Permanent Scatterer analysis.

8.2.4. Land subsidence

Several recent studies have measured land subsidence using ERS interferometry. Carnec et al. (1996) detected land subsidence of coal mining near Gardanne, France. Massonnet et al. (1997) observed subsidence over a geothermal field in California. Fielding et al. (1998) mapped subsidence at the Lost Hills and Belridge oil fields as a result of oil and gas extraction. Galloway et al. (1998) studied land subsidence in the Lancaster area, California. Amelung et al. (1999) mapped subsidence in Las Vegas, Nevada. Hoffmann et al. (2001) studied seasonal subsidence and rebound in Las Vegas Valley, Nevada, using synthetic aperture radar interferometry. Buckley et al. (2003) measured successfully urban land subsidence in Houston, Texas, using conventional SAR interferometry. More recently, Dixon et al. (2006) studied land subsidence in New Orleans using the Permanent Scatterer technique.

CHAPTER III

LAND SUBSIDENCE IN GREATER CAIRO

1. Introduction

Land subsidence is a major global geomorphic problem, particularly in densely populated deltas. The Nile Delta (Figure 1.1) is no exception. However, to date, the magnitude and temporal and spatial patterns of land subsidence in the delta are not well known. Several factors contribute to the rate and patterns of subsidence in the Nile Delta. These factors are natural sediment compaction, tectonic setting of the region, groundwater pumping, and oil and gas extraction. Extraction of oil and gas is the major contributing factor in the northern coastal zone, particularly in the western side of the delta. However, groundwater pumping is the major contributing factor in the middle and the southern parts of the delta, especially in big cities such as Cairo, Mansura, and Mahala (Figure 1.1).

Over the past 100 years, the population of Egypt has increased from 10 million to approximately 65 million, with a growth rate of about one million people per year (World Bank, 1990). Currently, the approximate population of Egypt is 77 million; 50 million of them inhabit the Nile Delta.

Groundwater has been a major source of municipal and domestic water supply in the Nile Delta during the last few decades. The dramatic change in the population density in the delta has led to a significant increase in the rate of groundwater pumping, especially in the metropolitan areas. This, in turn, accelerated the rate of urban subsidence in the delta. Declining groundwater in the aquifer system in the delta

contributed also to the rate of the long-term subsidence as a result of the compaction of the aquifer system that consists mainly of unconsolidated sediments composed of a significant fraction of silts, clays and sands.

Stanley (1990) studied sediment borings collected from the Nile Delta and radiocarbon dated many of them. He investigated 65 sediment borings (Figure 3.1A) with depth ranging from 10 to 60 m obtained from Smithsonian Institution drilling expeditions. In addition, he consulted approximately 100 core lithologic logs to improve subsurface correlations. Figure 3.1B shows a summery of the late Quaternary stratigraphy in the Nile Delta. The study by Stanley (1990) revealed that the entire northern zone, where samples were collected, is presently subsiding.

Stanley (1990) speculated that mapping the base of the Holocene deltaic facies, dated at approximately 8000-6500 yr BP, indicates differential subsidence of the northern part of the delta. According to Stanley (1990), the average of long-term subsidence rates near the coast for the mid to upper Holocene ranges from approximately 1.0-2.5 mm yr^{-1} in the west to 5.0 mm yr^{-1} in the east (Figure 3.1A). Zaghloul et al. (1977b), Said (1981), Stanley (1988 and 1990), and Stanley and Warne (1993) attributed the rapid rate of subsidence in the eastern side of the delta to stratigraphic and tectonic factors.

Warne and Stanley (1993) studied archeological sites along the Nile Delta margin to re-assess and refine rates of subsidence in the delta. Their study indicated that subsidence rates estimated by Stanley (1990) for the northern part of the delta are minimum rates because sediment reworking generally produces radiocarbon dated core

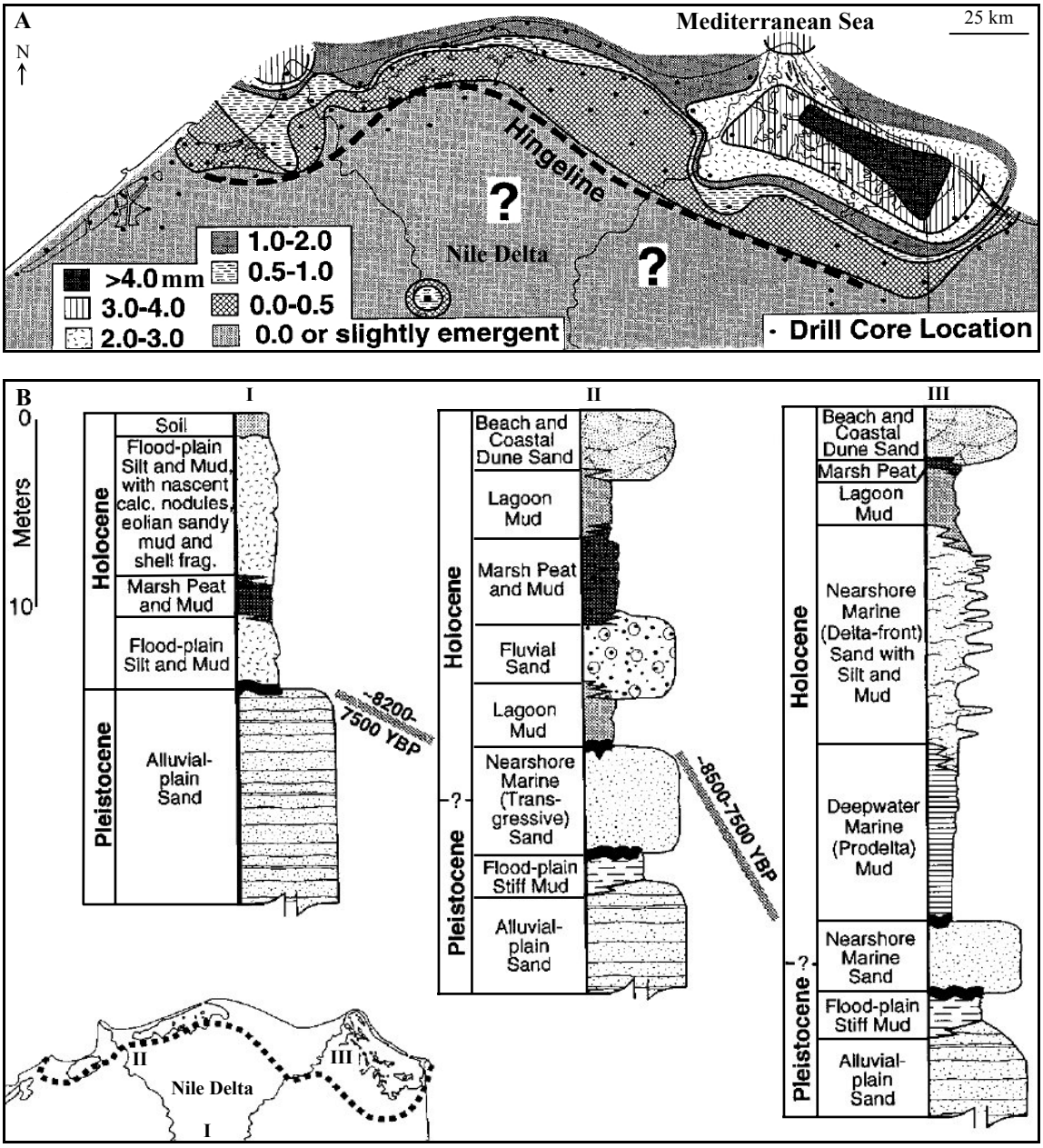

Figure 3.1. (A) Locations of sediment borings and land subsidence rates in the Nile Delta, (B) simplified stratigraphic logs depicting late Quaternary sequences in the Nile Delta from Stanley and Warne (1998)

ages being older than the ages of final burial. Zaghloul et al. (1990) studied the geomorphologic and geologic evolution, as well as subsidence in the Nile Delta, and reported similar rates of long-term subsidence during the Quaternary. A recent attempt has been made by Stabel and Fischer (2001) to measure urban subsidence in Cairo using satellite radar interferometry, but the study was not successful because they could not construct or even find a suitable DEM for the purpose of topographic correction.

To date, the actual rates of subsidence and its spatial and temporal variations across the Nile Delta are not well known, as the measures from the aforementioned studies are just rough estimates. Unfortunately, no research has been conducted so far to measure land subsidence in the delta using the traditional leveling survey methods. Recently, several GPS networks have been established in Egypt. One of these consists of eleven permanent GPS stations around greater Cairo established in 1995. The GPS network should be suitable for detecting and measuring both vertical and horizontal crustal deformations; however, only horizontal velocity vectors have been reported; e.g., Badawy et al. (2003) and El-Fiky et al., (2004). Several attempts have been made to obtain GPS data for the Nile Delta region from the Egyptian Organizations but, unfortunately, none of them has been successful.

Potential consequences of land subsidence in the Nile Delta include, but are not limited to, reduction of the aquifer system storage, sinking of the coastal zone cities, and damage of the utility infrastructure, wells, railroads, highways, and bridges, as well as buildings. Therefore, there is an increasing demand for regular monitoring and accurate measuring of the rates and patterns of land subsidence in the Nile Delta region. This particularly important to gain a broad understanding of the phenomenon and to provide

decision makers with useful information for integrated development and sustainable use of natural resources in the delta.

Traditional leveling survey and GPS are widely used to measure land subsidence but these all are point-measurement tools and, thus, provide spatially limited views of the ongoing surface deformation. In contrast, radar interferometry has the potential to provide subtle surface deformation measurements at a significantly improved SAR resolution with millimeter-level accuracy and over large areas (approximately 100 km² for ERS satellites). Numerous researches have successfully applied radar interferometry to measure land subsidence; e.g., Fielding et al. (1998), Galloway et al. (1998), Fruneau et al. (1999), Strozzi and Wegmüler (1999), Strozzi et al. (1999a), and Strozzi et al. (1999b), Ferretti et al. (2000), Bawden et al. (2001), Hoffmann et al. (2001), and Buckley et al. (2003).

Spaceborne ERS SAR interferometry is applied in this dissertation to detect and measure land subsidence in three major cities in the Nile Delta; Cairo, Mansura and Mahala (Figure 3.2). In an effort to provide a sufficient depth to the subject, the study of land subsidence is distributed over two chapters. Land subsidence in greater Cairo is discussed in this chapter and land subsidence in Mansura and Mahala is discussed in the next chapter, as a single ERS dataset is used for both cities.

Cairo, the capital of Egypt, is an ancient city occupying the area at the apex of the Nile Delta where the Nile River splits into two branches (Figure 3.2). The region of Cairo has been continuously inhabited for more than 3,500 years. With its 15 million inhabitants, Cairo is one of the largest cities in the world. Greater Cairo is characterized by very dense settlement structure with little vegetation, and the mountains at its eastern

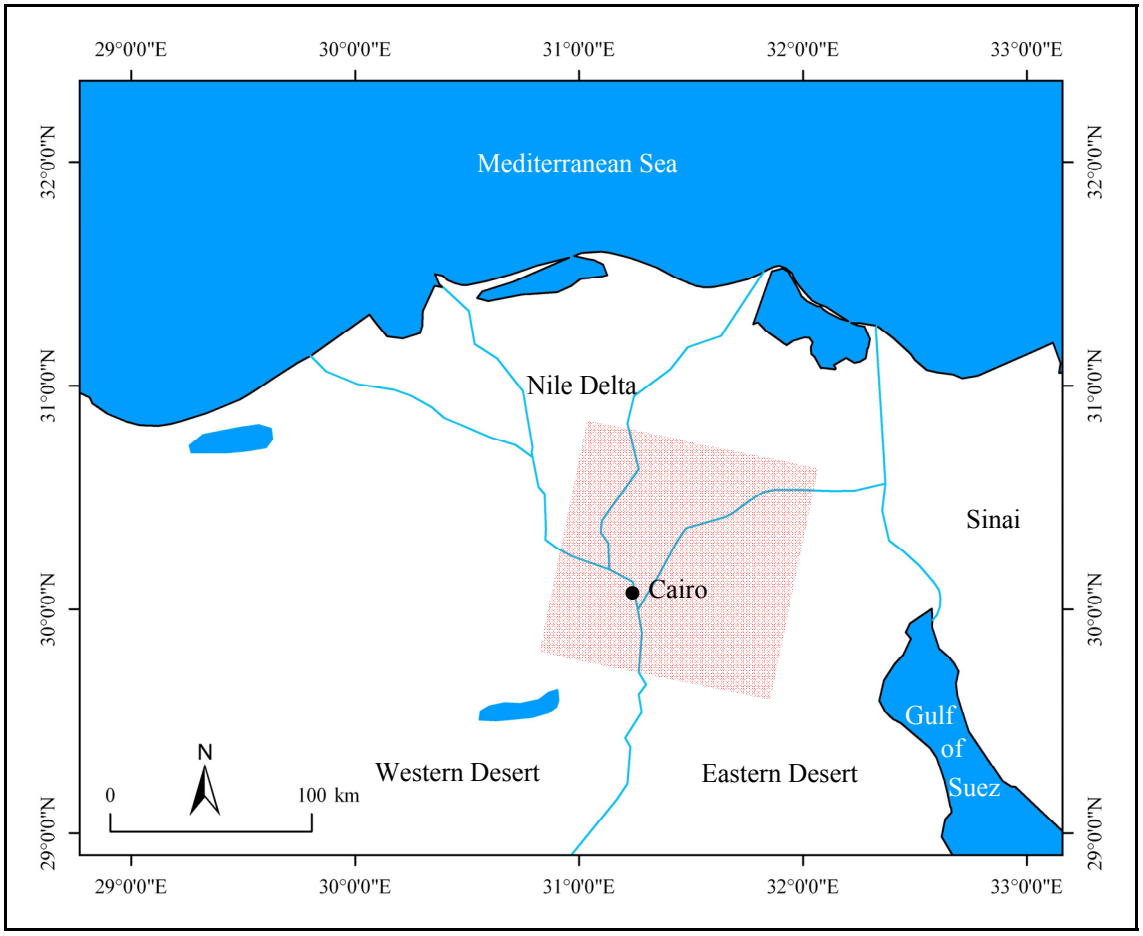

Figure 3.2. ERS coverage of greater Cairo (Track: 436, Frame: 2997) is highlighted in red

border are very dry. Because of these characteristics, greater Cairo is considered suitable for applying SAR interferometry and, therefore, has been selected for this study. The spatial density of the urban area is also sufficient to witness spatial variations in land subsidence. Figure 3.3 shows a coherence image for greater Cairo and its surroundings.

2. Data Acquisition

Thirty-four ERS-1/2 descending scenes (Track: 436, Frame: 2997) spanning eight years from 1993 to 2000 (Table 3.1) have been acquired taking into consideration the temporal and the spatial coverage of ERS archived data for the area of greater Cairo (Figure 3.2). Several ERS pairs of short perpendicular baseline, less than 200 m, were selected to limit the potential for geometric decorrelation in conventional InSAR processing, and several ERS tandem pairs were selected for tandem Digital Elevation Model (DEM) generation. Additionally, DEMs of 3-arc sec spatial resolution acquired by the Shuttle Radar Topography Mission (SRTM) have been collected and used as external DEMs for topographic corrections.

3. Permanent Scatterer Interferometry

Decorrelation of the interferometric phase in the densely vegetated Nile Delta occurs primarily because of seasonal cultivation, flood irrigation, and vegetation growth. The vegetation cover in the delta is seasonal crops and, thus, it is dynamically changing. Land use classes change approximately every four months. This situation hampers the application of SAR interferometry. But the Nile Delta also has urban areas that can preserve the phase coherence over relatively long time spans. However, construction

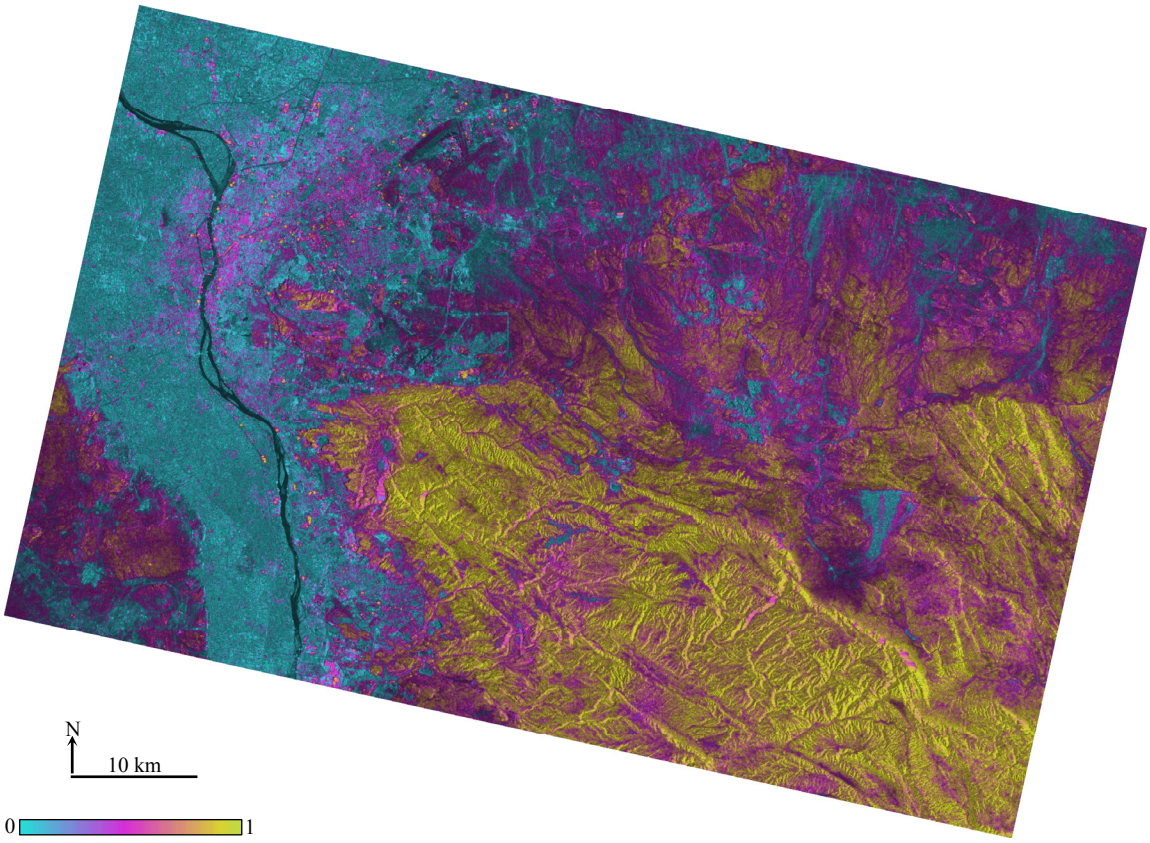

Figure 3.3. Coherence image created from InSAR scenes dated 01/20/2000, and 05/17/1993, superimposed on the amplitude image of 01/20/2000

Table 3.1. ERS dataset for greater Cairo

#	Date[a]	$B_{\perp}$ (m)[b]	B_T (day)[c]	ERS
1	19930412	617.0048	-1004	1
2	19930517	-77.6699	-969	1
3	19930726	249.5015	-899	1
4	19931004	-50.3564	-829	1
5	19950614	-87.0998	-211	1
6	19950823	-22.3913	-141	1
7	19950824	-122.5054	-140	2
8	19950927	150.3387	-106	1
9	19950928	567.0938	-105	2
10	19951206	169.0418	-36	1
11	19960110	125.4489	-1	1
12	19960111	0.0000	0	2
13	19960214	655.5337	34	1
14	19960215	663.9315	35	2
15	19960424	872.8420	104	1
16	19960529	-354.5767	139	1
17	19960530	-463.0765	140	2
18	19970515	35.2625	490	2
19	19980709	-438.0561	910	2
20	19980917	-770.1791	980	2
21	19981231	-783.9076	1085	2
22	19990311	-64.2046	1155	2
23	19990415	749.9412	1190	2
24	19990520	-187.5423	1225	2
25	19991007	-302.3993	1365	2
26	19991216	552.6185	1435	2
27	20000120	-126.4835	1470	2
28	20000223	-897.5716	1504	1
29	20000224	-728.0547	1505	2
30	20000330	-300.7856	1540	2
31	20000504	-224.0248	1575	2
32	20000608	-140.1180	1610	2
33	20001026	-310.1321	1750	2
34	20001130	-234.8034	1785	2

[a]Date is YYYYMMDD.
[b]$B_{\perp}$ is the Perpendicular baseline.
[c]B_T is the temporal baseline.

activities may cause a local loss of the phase coherence.

With an approximate 5 mm yr^{-1} subsidence in the delta, approximately 1.12 radians of slant range phase change per year are expected in the topographically corrected interferograms generated from ERS images. Considering the slow rate of land subsidence in the densely vegetated delta and phase ambiguity problems related to temporal and geometrical decorrelations, as well as tropospheric effects, obtaining reliable measurements of subsidence using conventional SAR interferometric approaches is difficult.

All possible combinations of collected ERS InSAR pairs with baselines of less than 200 m were processed and topographically corrected interferograms were produced using two-, three- and four-pass interferometric approaches. All interferograms created from summer and winter acquisitions were found dramatically affected by atmospheric artifacts. Additionally, complete phase decorrelation occurred over vegetated areas and most of the urban areas. Figure 3.4 shows a topographically corrected interferogram created for greater Cairo and its adjacent mountains using the two-pass interferometric approach. ERS InSAR pairs dated January 20, 2000, and May 17, 1993, were used to create the interferogram. Each color fringe represents 28 mm of surface deformation in the Line-Of-Sight direction. However, most of the color change close to the Nile River is basically related to the effect of atmospheric artifacts. The topographic phase was removed using an external SRTM DEM of 3-arc sec spatial resolution.

To overcome cycle ambiguity problems and detect the slow rate of deformation and its temporal and spatial patterns in greater Cairo, the Permanent Scatterer interferometric approach is applied in this study using thirty-four descending ERS scenes

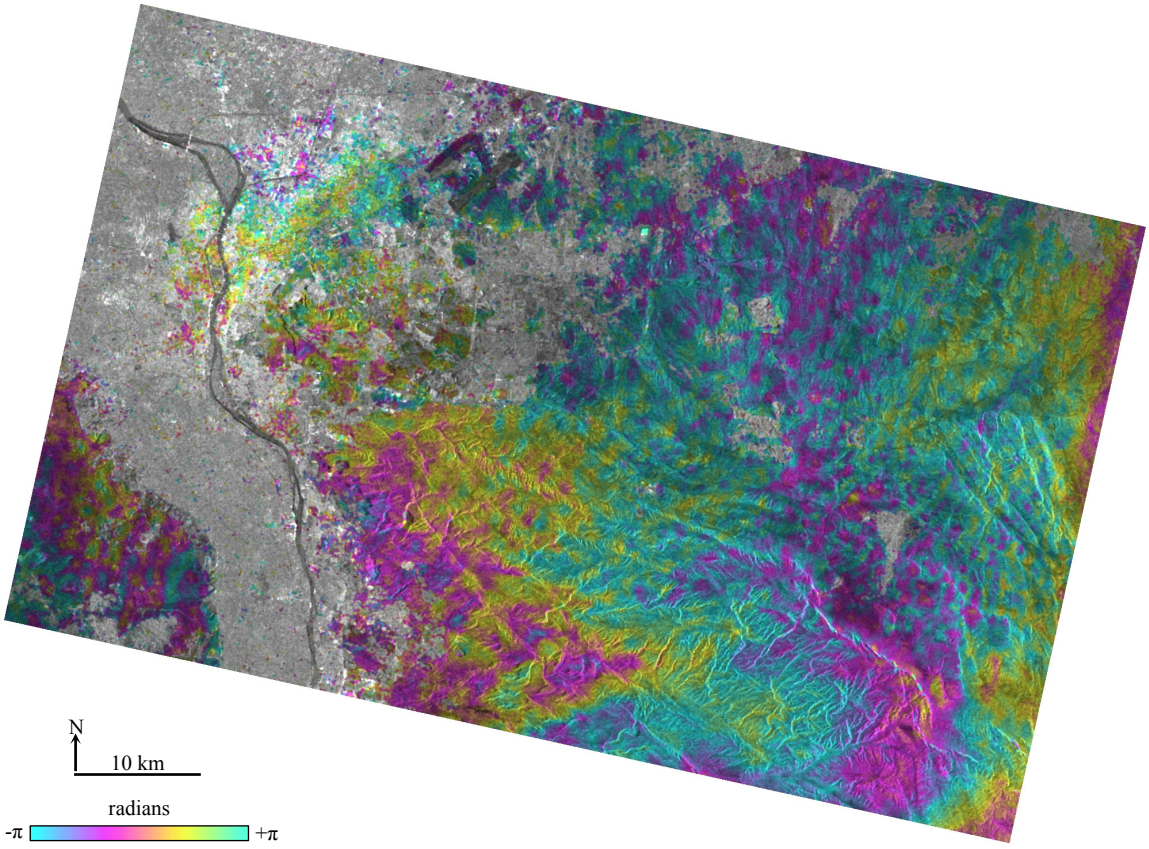

Figure 3.4. Topographically corrected interferogram created from InSAR scenes dated 01/20/2000, and 05/17/1993, superimposed on the amplitude image of 01/20/2000

spanning eight years from 1993 to 2000 (Table 3.1). Since it has been introduced by Ferretti et al. (2000), the Permanent Scatterer interferometric approach has been successfully applied in several crustal deformation studies such as estimation of the nonlinear subsidence rate (Ferretti et al., 2000), monitoring landslides and tectonic motions (Colesanti et al., 2003), and detection of mining related ground instabilities (Colesanti et al., 2005). Since then, several approaches with further improvements and some deviations in the processing procedure have also been developed; e.g., Dehls et al. (2002), Adam et al. (2003), Crosetto et al. (2003), and Hooper et al. (2004).

The Permanent Scatterer approach can be accomplished in various ways depending on the cultural characteristics and problems in each InSAR dataset. The major processing steps applied in this research included SLC image formation, coregistration of all selected SAR acquisitions to a unique reference image, Permanent Scatterers (PSs) selection, generation of the complex interferograms for the selected PSs, topographic phase removal, phase noise reduction, spatial and temporal phase unwrapping, estimation and removal of atmospheric artifacts, calculation of the LOS surface displacements, and geocoding.

3.1. Single look complex image formation and coregistration

The thirty-four selected ERS descending scenes (Table 3.1) were automatically checked and corrected for missing lines. Then, they were processed to a Doppler Centroid independent of range sample to generate Single Look Complex (SLC) images. A small subset of the ERS scenes covering greater Cairo has been used for applying the PS technique to avoid the densely vegetated areas of very low coherence. Figure 3.5

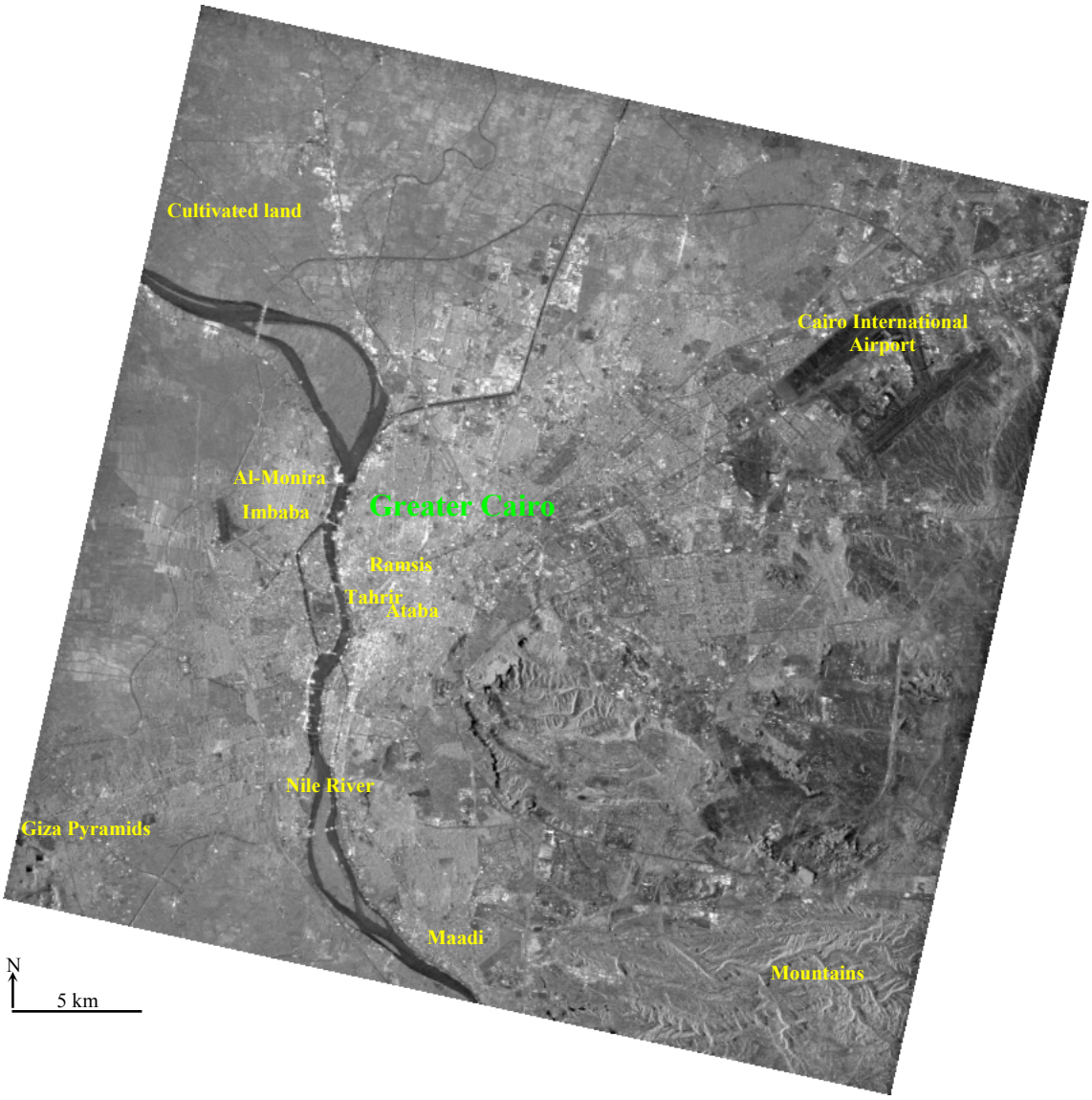

Figure 3.5. Average amplitude image for greater Cairo

shows the average amplitude image of the thirty-four ERS sub-scenes for the area of interest. The average amplitude image shows the mean intensities of the radar backscatters for the selected ERS images. It reveals features of the surface of Earth of the area of interest. Built up areas in greater Cairo have a bright radar response, whereas cultivated areas appear in a light grey color, and major roads as well as the Nile River appear in a dark grey color. Cairo International Airport appears also in a dark grey color in the northeastern part of greater Cairo.

As ERS SAR images are taken from slightly different angles at different times, offsets do occur among them. Consequently, all SLC images have to be resampled to a reference image. This is done by determining the offsets between corresponding pixels in the two SLCs (reference and resampled images) and by calculating a rotation and skew matrix that registers the resampled SLC image to the reference image.

To select a unique reference image, interferometric pairs with limited atmospheric artifacts have to be determined. The approach of pairwise comparison of interferograms developed by Massonnet and Feigl (1995) was applied for this purpose. The approach provides an assessment of initial interferograms without requiring statistical analysis of higher-level products and does not require ancillary data spatially and temporally coincident with the SAR acquisitions.

Interferograms with high correlation were generated using several ERS tandem pairs (Table 3.1). These tandem interferograms were compared using the pairwise comparison approach to assess the degree to which atmospheric variations are present in each selected ERS pair. The comparison revealed that interferograms generated from the summer acquisitions during August and September were affected highly by large

amplitude, high frequency atmospheric artifacts as a result of significant summer heating. Interferograms generated from the winter acquisitions were less affected by atmospheric artifacts.

Based on these comparisons, the ERS-2 scene acquired on January 11, 1996, has been selected as the reference, as it has low atmospheric distortions, and it minimizes both perpendicular and temporal baselines. It has also a Doppler Centroid near the average Doppler Centroid of other SAR acquisitions.

The coregistration accuracy assessment revealed that all ERS SLCs were precisely coregistered to the selected reference, as the standard deviations of the individual range and azimuth offset estimates from the regression fit were less than 0.15 pixel. The ERS scenes were oversampled by a factor of two to avoid aliasing in the coregistration process using amplitude values.

The initial spatial resolution of the ERS images is approximately 4x20 m in azimuth and range directions, respectively. They were multi-looked, ten looks in the azimuth direction and two looks in the range direction, to produce interferograms with 40 m resolution in both azimuth and range directions. The multi looking is an averaging process that reduces the phase noise.

3.2. Selection of permanent scatterers

The selection of Permanent Scatterers (PSs) is one of two major important processes in any Permanent Scatterer approach, as all the processing is conducted on the only selected PSs. The other critical process is to correctly unwrap the interferometric interferograms and correct them for potential errors. Ferretti et al. (2001) used the

amplitude dispersion index (D_A), which is the ratio of the standard deviation of the amplitude (σ_A) to its mean (μ_A), to identify PSs.

$$D_A = \frac{\sigma_A}{\mu_A} \tag{3.1}$$

According to Ferretti et al. (2001), all images in the dataset have to be radiometrically calibrated to make them comparable before conducting the statistical analysis on the amplitude values. They scaled the amplitude images using calibration factors provided by the European Space Agency (ESA). Then they averaged the amplitude images and calculated the mean of the stack and the standard deviation from the mean. Points of low amplitude dispersion, D_A<0.25, were selected as Permanent Scatterers. The amplitude dispersion index is used as a measure of phase stability and is practically proved to be powerful in detecting PSs over bare rocks and man-made structures such as buildings. The lower the amplitude dispersion index, the higher the phase stability.

The amplitude dispersion index is applied in this present study to identify Permanent Scatterers over greater Cairo; however, calculated calibration factors from the processed ERS dataset were used rather than using calibration factors from ESA. The average calibration factor for each image in the stack is calculated using the ratio of the amplitude of each image to the mean amplitude of the entire stack. An average density of 157 PS Km^{-2} has been identified, which is sufficient for aliasing any spatial variations of land subsidence in greater Cairo.

3.3. Generation of the complex interferograms

Single Look Complex (SLC) values were extracted for only selected PSs, and the interferometric complex interferograms were calculated from these values by multiplying the reference image with the complex conjugate of the resampled image according to equation (2.7), yielding the phase difference between the two SAR acquisitions for each selected PS. The complex interferometric phase (ϕ) at pixel (p) in interferogram (i) is nominally a summation of five phase components, which are:

$$\phi_{p,i} = \phi_{def,p,i} + \phi_{topo,p,i} + \phi_{orb,p,i} + \phi_{atm,p,i} + \phi_{noise,p,i} \qquad (3.2)$$

where ϕ_{def} is the deformation phase, ϕ_{topo} is the topographic phase, ϕ_{orb} is the orbital phase, ϕ_{atm} is the atmospheric phase, and ϕ_{noise} is the phase noise.

3.4. Topographic phase removal and phase unwrapping

The basic strategy in Permanent Scatterer processing is to separate these phase components from the phase resulting from the surface deformation for each selected PS. The topographic phases were removed using SRTM DEMs, and the produced interferograms were then filtered using the nonlinear adaptive filter developed by Goldstein and Werner (1998) to reduce the amount of phase noise, which is always present in SAR images. The DEOS precise ERS-1/2 state vectors (Scharroo and Visser, 1998) were used in this dissertation to compensate for orbital inaccuracies. For more information about DEOS orbital accuracies, the reader is directed to section (6.1) in

Chapter II.

The calculated interferograms are still wrapped at this level. Both spatial and temporal phase unwrapping were conducted on the topographically corrected interferograms for the selected PSs. The filtered interferograms were first spatially unwrapped with the minimum coast network flow (MCF) algorithm developed by Costantini (1998). The spatially unwrapped values of PSs were then integrated in time to produce the unwrapped phase time series for each selected PS.

Careful inspection of interferograms is a first-order approximation of phase errors. Temporal and spatial consistencies of features in the topographically corrected interferograms are good indicators for discriminating deformation features. Persistent phase signals are most likely related to real surface deformation as deformation patterns usually occur at the same location in several interferograms over considerable time spans. In contrast, atmospheric artifacts because of their dynamic nature are expected not to occur exactly at the same location in a time series of interferograms.

Taking into consideration the information mentioned above, all patterns that were observable in several interferograms at the same locations were considered true deformation, and sparse features lacking temporal and spatial consistency were assumed atmospheric artifacts rather than real surface deformation and, thus, filtered out. Furthermore, phase signals in the topographically corrected interferograms of very short time spans (e.g., 1, 34, 35, and 36 days in Table 3.1) were assumed topographic residuals and/or tropospheric effects and, thus, were eliminated, as no surface deformation is expected to occur in greater Cairo within these few days.

Topographic-induced artifacts and effects of soil moisture content may be misinterpreted in SAR interferometry. Phase signals may be affected by tropospheric variations as a function of altitude. Tropospheric variations may cause errors similar to topographic residuals (Delacourt et al., 1998). However, topographic-induced effects are not expected in greater Cairo because the area is relatively flat. Soil moisture content is a major concern in the densely vegetated, humid Nile Delta especially in the cultivated areas because of crop watering. But the Permanent Scatterer processing is conducted basically for the urbanized areas in greater Cairo; therefore, the effect of soil moisture content is not believed to be a considerable source of error.

Estimations of the phase components were undertaken iteratively to remove perfectly the residual topographic phase, the atmospheric phase, the phase noise, and the phase related to inaccuracies in calculations of the satellite orbits from the interferometric phase, leaving only the phase change related to the surface movements. Ultimately, the Line-Of-Sight (LOS) surface displacements were calculated from the corrected, unwrapped interferograms and the outputs were geocoded.

4. Results and Discussion

Surface movements in the Line-Of-Sight direction were calculated by converting the measured phase into displacement values. Thirty-four surface displacement maps referenced to the ERS acquisition dated January 11, 1996, were generated. In this research, all deformation associated with land subsidence is assumed to be vertical. Figure 3.6 shows the average surface displacement calculated from the 34 displacement maps over eight years (1993-2000) in the LOS direction. The mean displacement in LOS

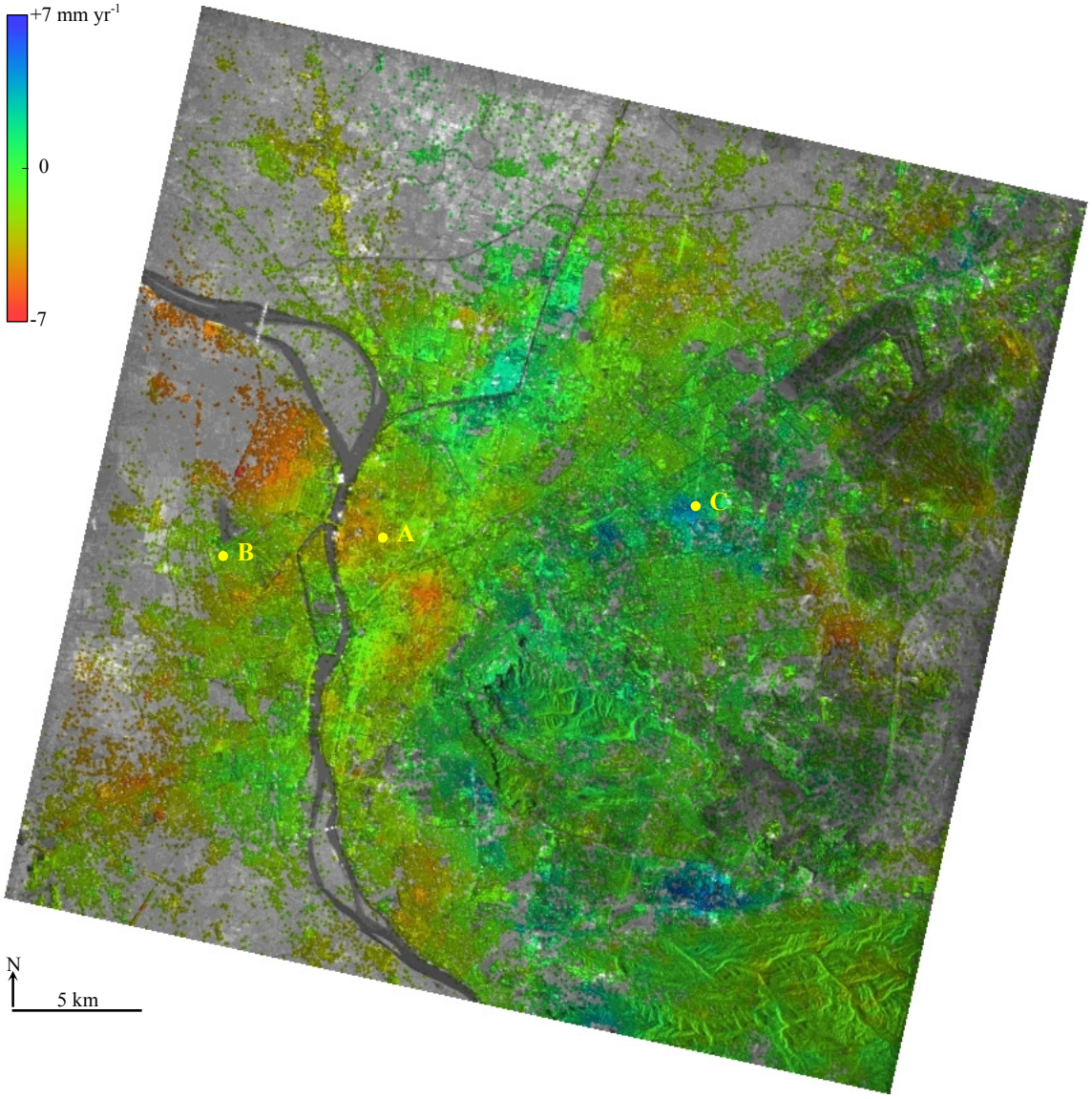

Figure 3.6. Mean LOS surface displacement in the 1993-2000 period, superimposed on the average amplitude image of greater Cairo

has a minimum negative (subsidence) value -7 mm yr^{-1}, and a maximum positive (uplift) value +7 mm yr^{-1}.

Deformation phase histories of three selected pints A, B and C are shown in Figures 3.7, 3.8 and 3.9, respectively to demonstrate the various behavior of PSs during the 1993-2000 period. Locations of the selected points are shown in Figure 3.6. The deformation phase history of point A (Figure 3.7) demonstrates about 37 mm of surface displacement in the Line-Of-Sight (LOS) between 1993 and 2000. All deformation occurred away from the satellite (subsidence) with an approximate constant rate over time. The deformation phase history of point B (Figure 3.8) shows the non-linear behavior of deformation during the 1993-2000 period. About 10 mm of surface displacement away from the satellite in LOS occurred; however, local displacement towards the satellite (uplift) occurred during 1995-1997 (Figure 3.8). The deformation phase history of point C demonstrates about 13 mm of non-linear surface displacement towards the sensor in LOS between 1993 and 2000. It is obvious that the deformation rate was not constant over time (Figure 3.9).

To demonstrate the progression of land subsidence in greater Cairo over time, a time series of LOS surface displacement maps interpolated spatially from the selected PSs and referenced temporally to the earliest ERS acquisition dated April 12, 1993, was created. Eight snapshots with approximately 1-year sampling time interval were then taken referenced temporally to July 1, 1993. No ERS SAR acquisitions are available for the area of interest during 1994. Therefore, no record is generated for that year.

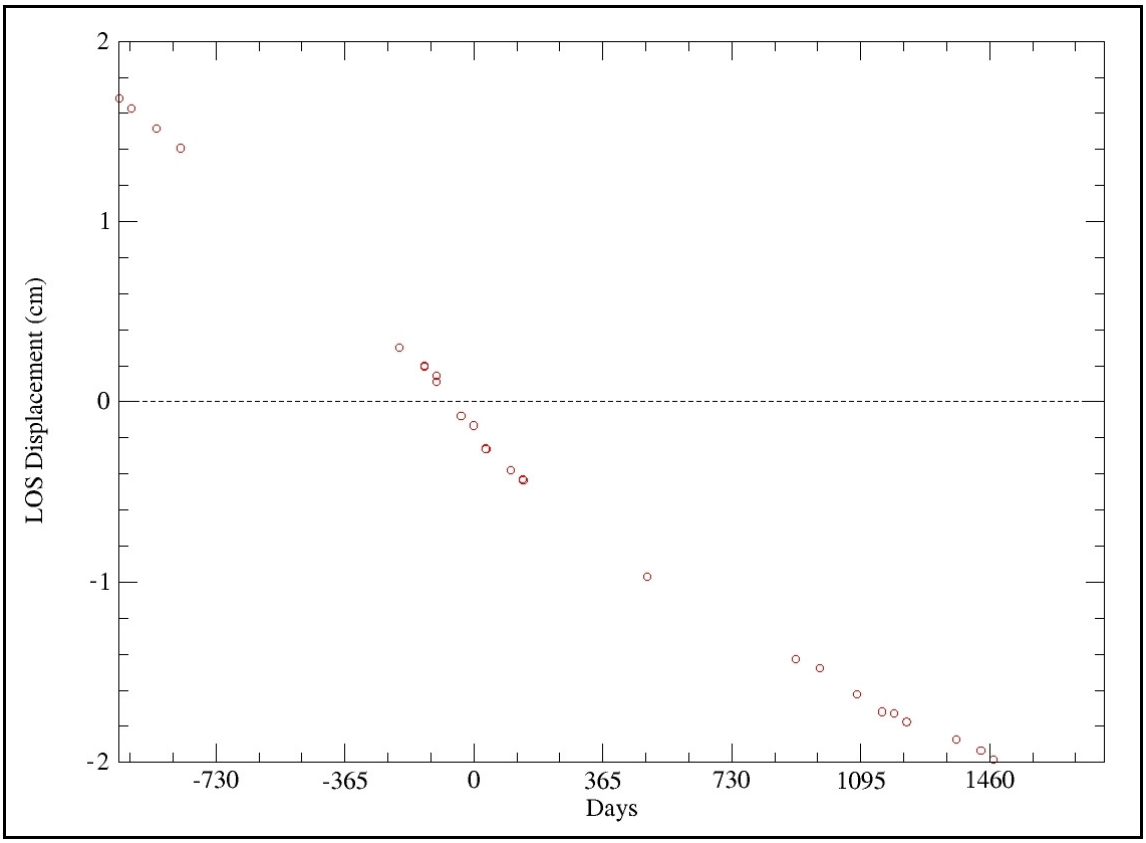

Figure 3.7. Deformation phase history of point A in greater Cairo during the 1993-2000 period

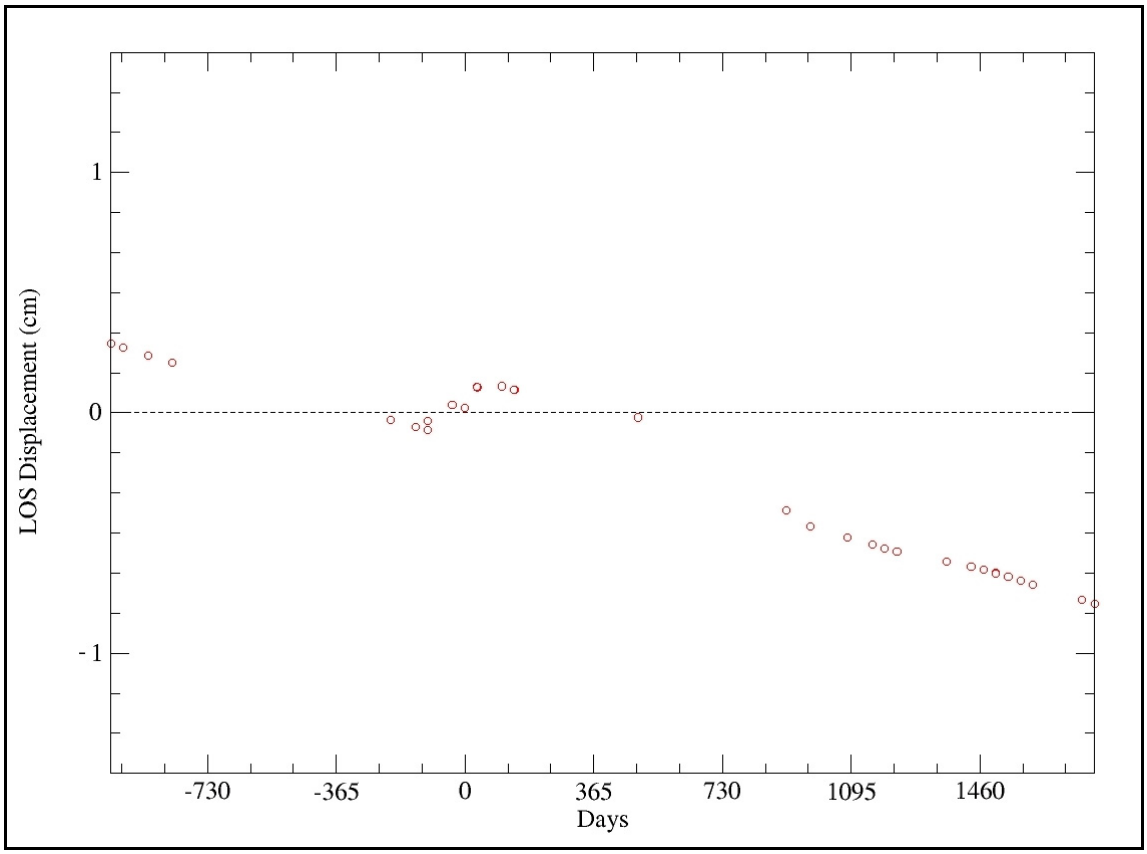

Figure 3.8. Deformation phase history of point B in greater Cairo during the 1993-2000 period

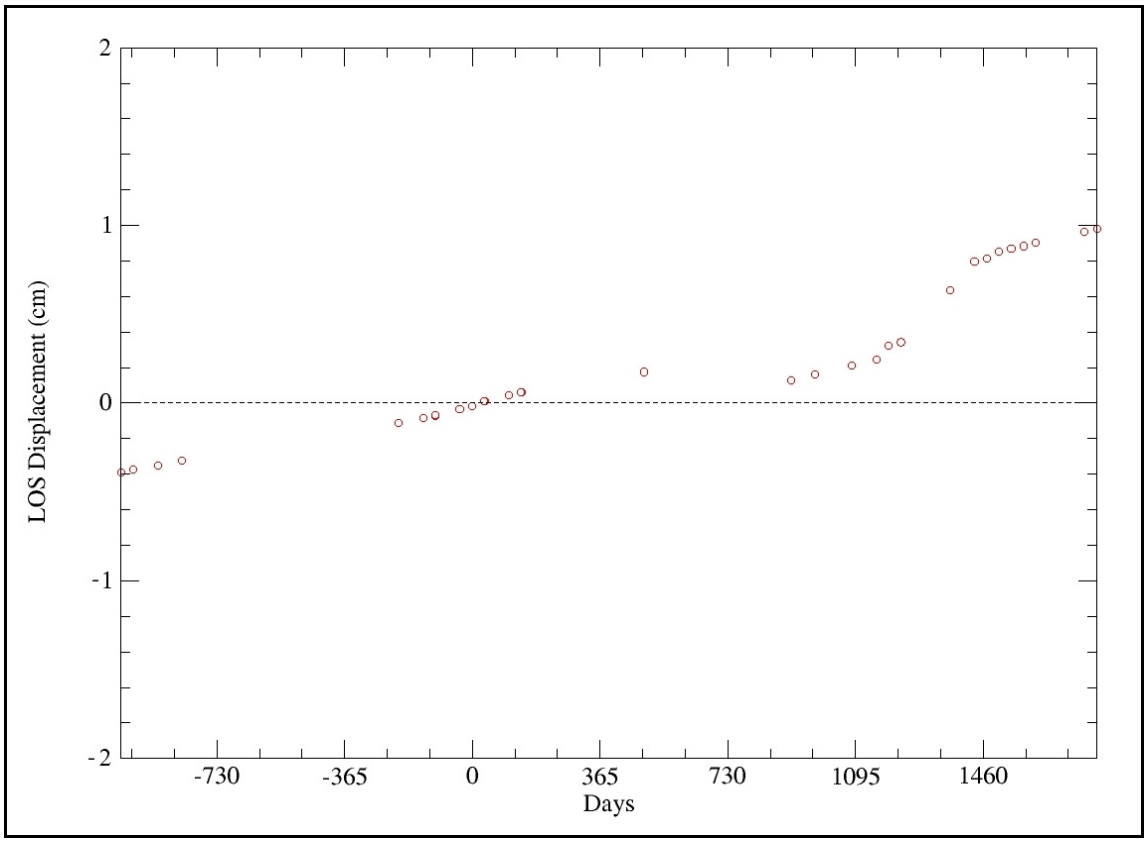

Figure 3.9. Deformation phase history of point C in greater Cairo during the 1993-2000 period

The signals of subsidence shown in Figures 3.10-3.16 coincide mainly with the highly urbanized areas. Despite the fact that historical records and locations of groundwater pumping are not available for this research, the coincidence of the signals with the highly populated districts implies that the detected signals are mainly of a pumping-induced subsidence. The highest subsidence rates are observable over the congested, highly populated districts in greater Cairo such as Imbaba, Al-Monira, Ramsis, Ataba, Tahrir, and Maadi (Figure 3.5). The slight positive values are of limited spatial extent and are most likely related to groundwater level recovery and local rebound of the aquifer system rather than gradual uplift that may be caused by a slow tectonic movement.

The pumping-induced subsidence rates may be recoverable or permanent based upon whether the effective stresses are less or greater than the pre-consolidation stresses (Sneed et al., 2001). From my past experience of living in this area, I can say there is no doubt that the rate of groundwater pumping in greater Cairo changes seasonally. For greater Cairo, pumping is higher in the summer time than other seasons in the year period. The non-linear deformation histories demonstrated in Figures 3.7, 3.8, and 3.9 imply that the pumping-induced subsidence in greater Cairo might be at least partially recoverable. But the petrophysical and hydrological characteristics of the aquifer system still have to be addressed. More research has to be undertaken to study the nature and magnitude of seasonal subsidence in greater Cairo, as this is not addressed in any previous work. This point is discussed in more depth in Chapter VI.

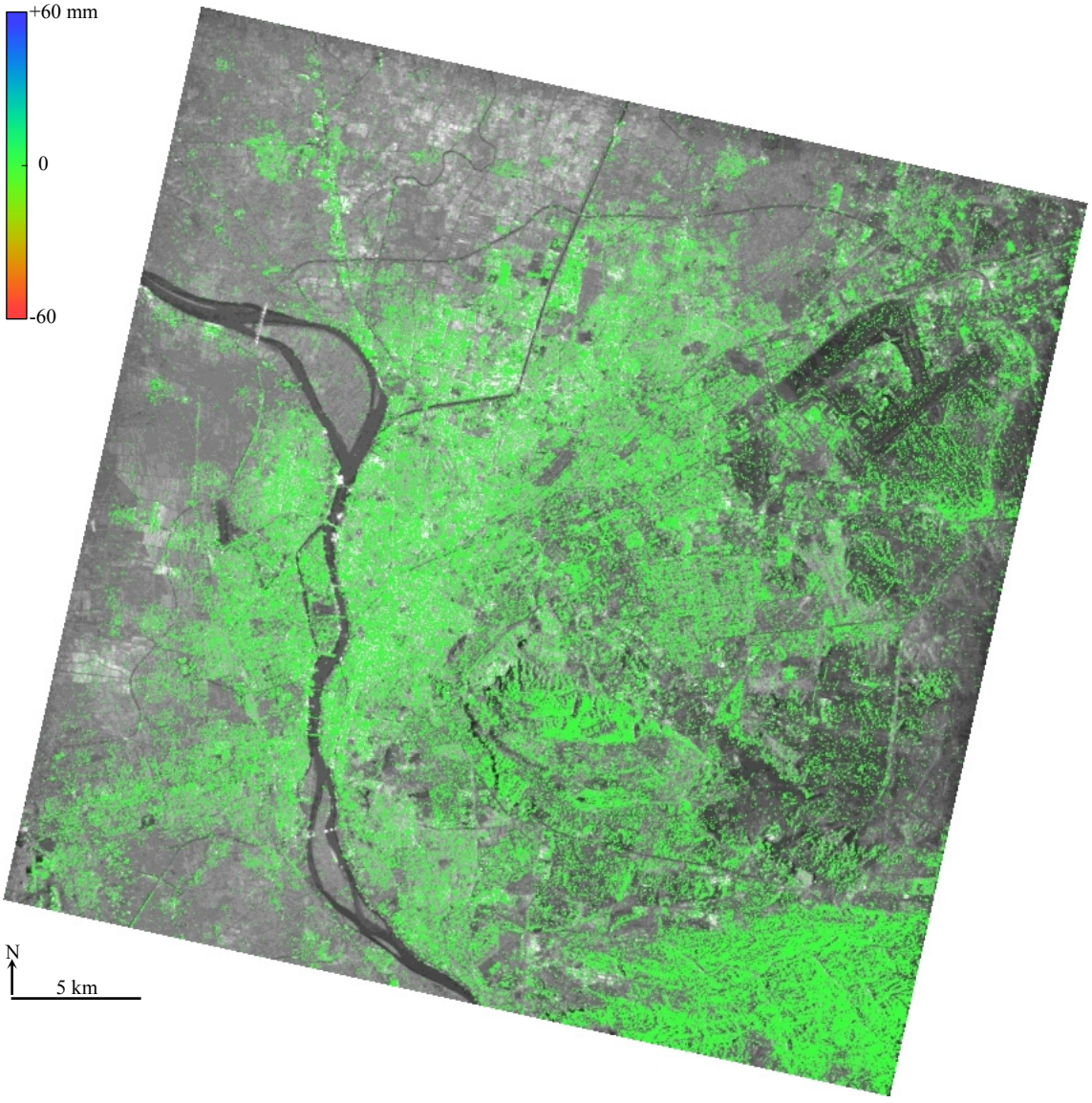

Figure 3.10. Estimated LOS surface displacement for July 1, 1993, superimposed on the average amplitude image of greater Cairo

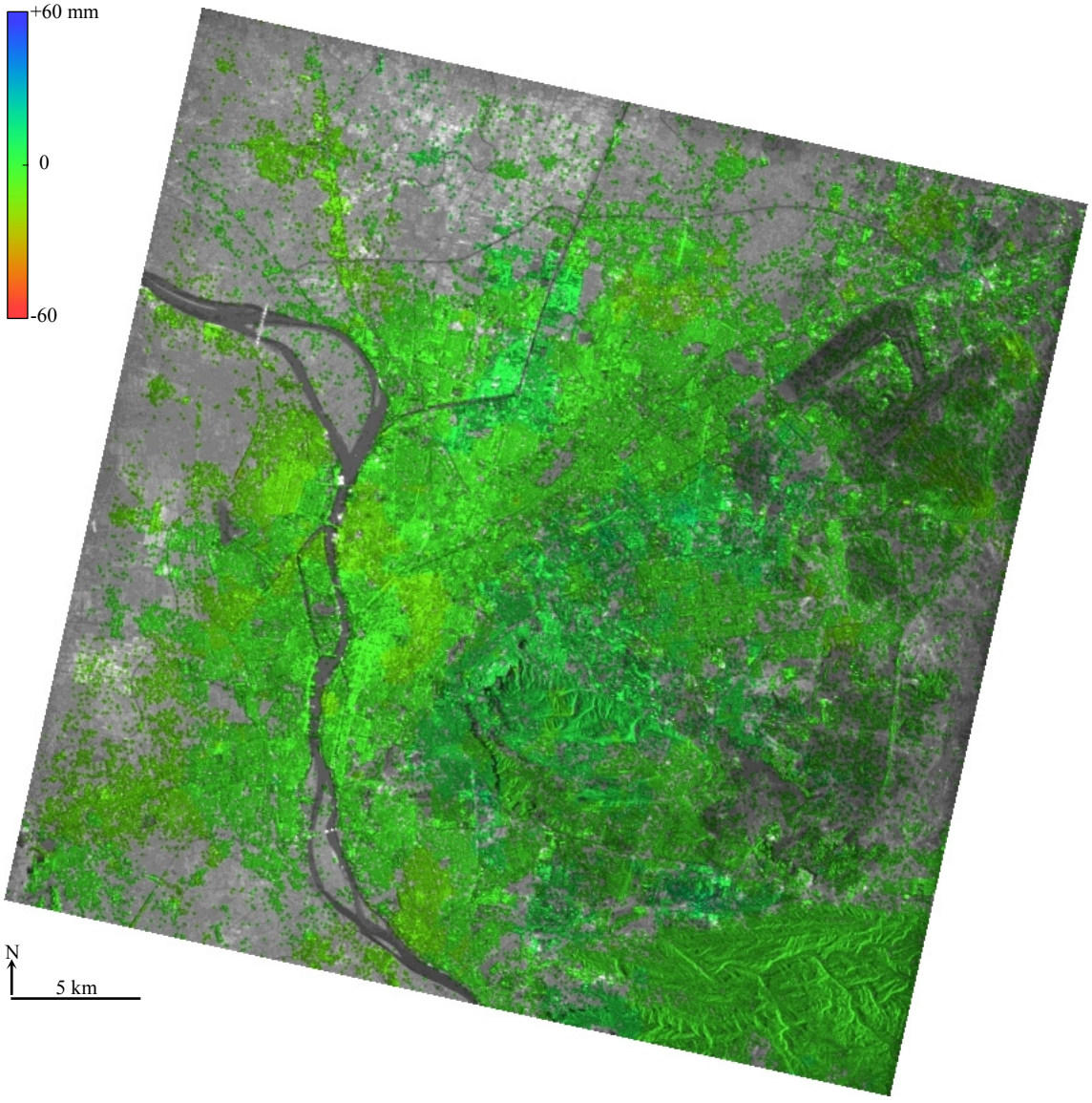

Figure 3.11. Estimated LOS surface displacement for July 1, 1995, superimposed on the average amplitude image of greater Cairo

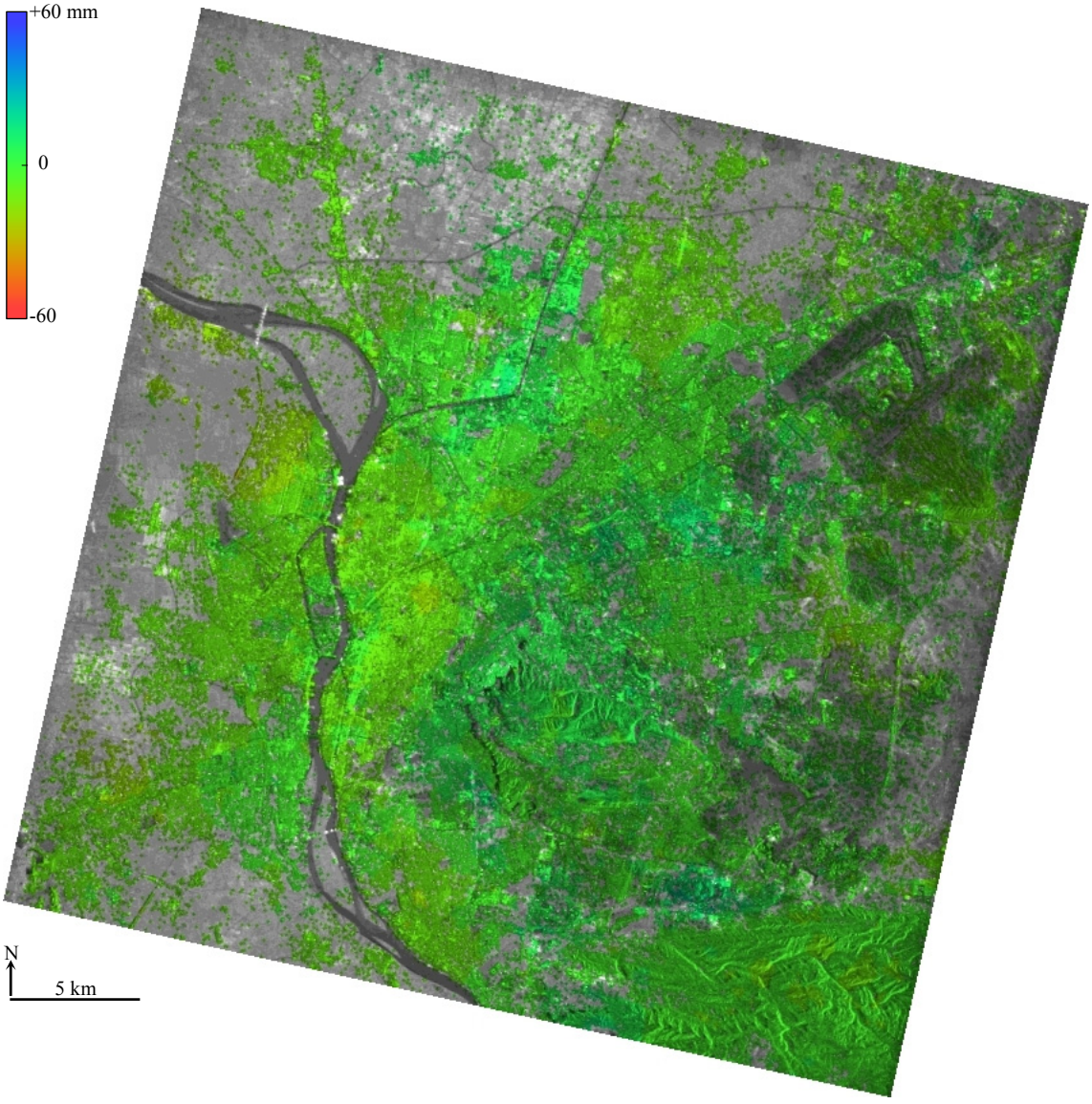

Figure 3.12. Estimated LOS surface displacement for July 1, 1996, superimposed on the average amplitude image of greater Cairo

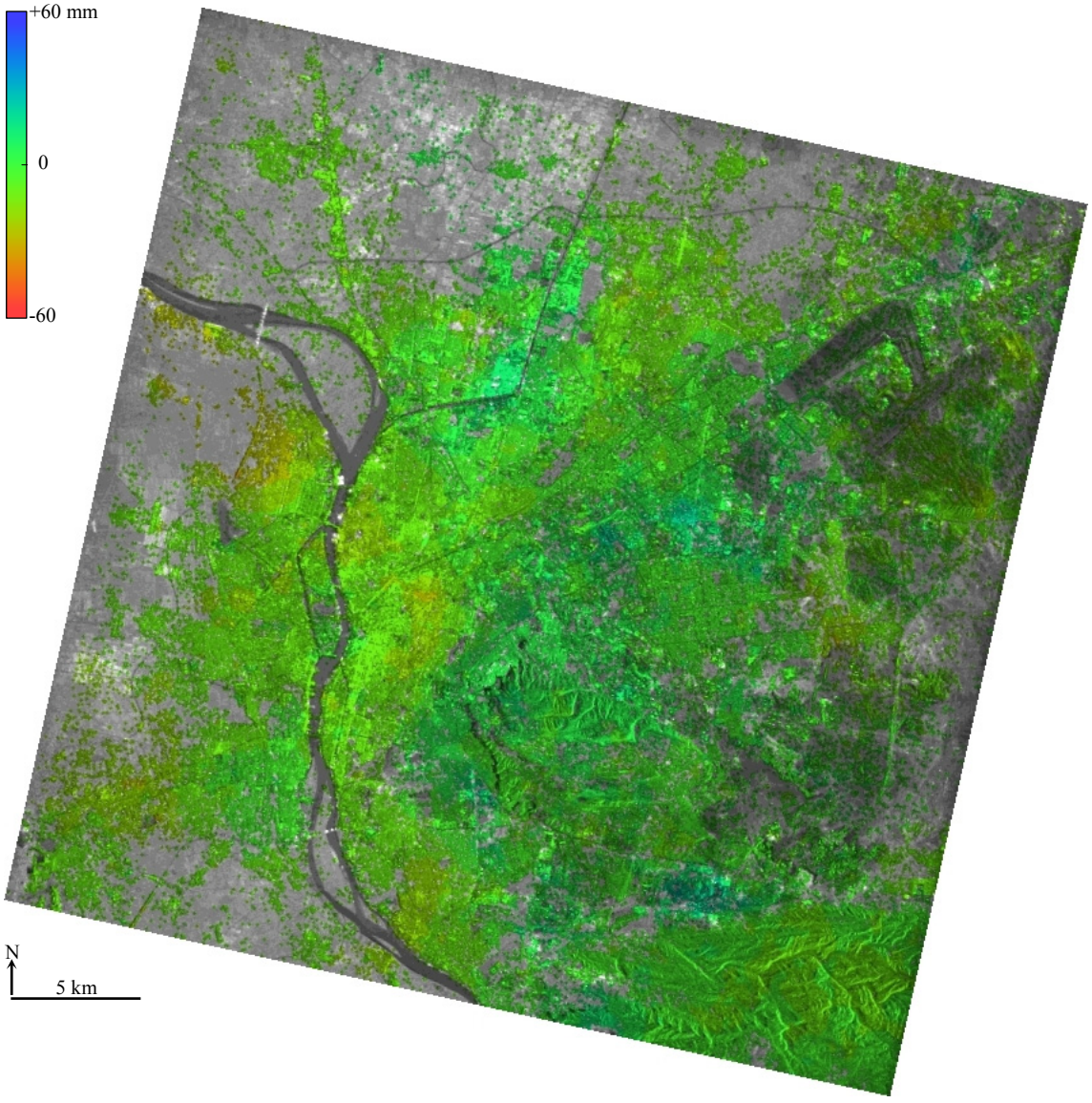

Figure 3.13. Estimated LOS surface displacement for July 1, 1997, superimposed on the average amplitude image of greater Cairo

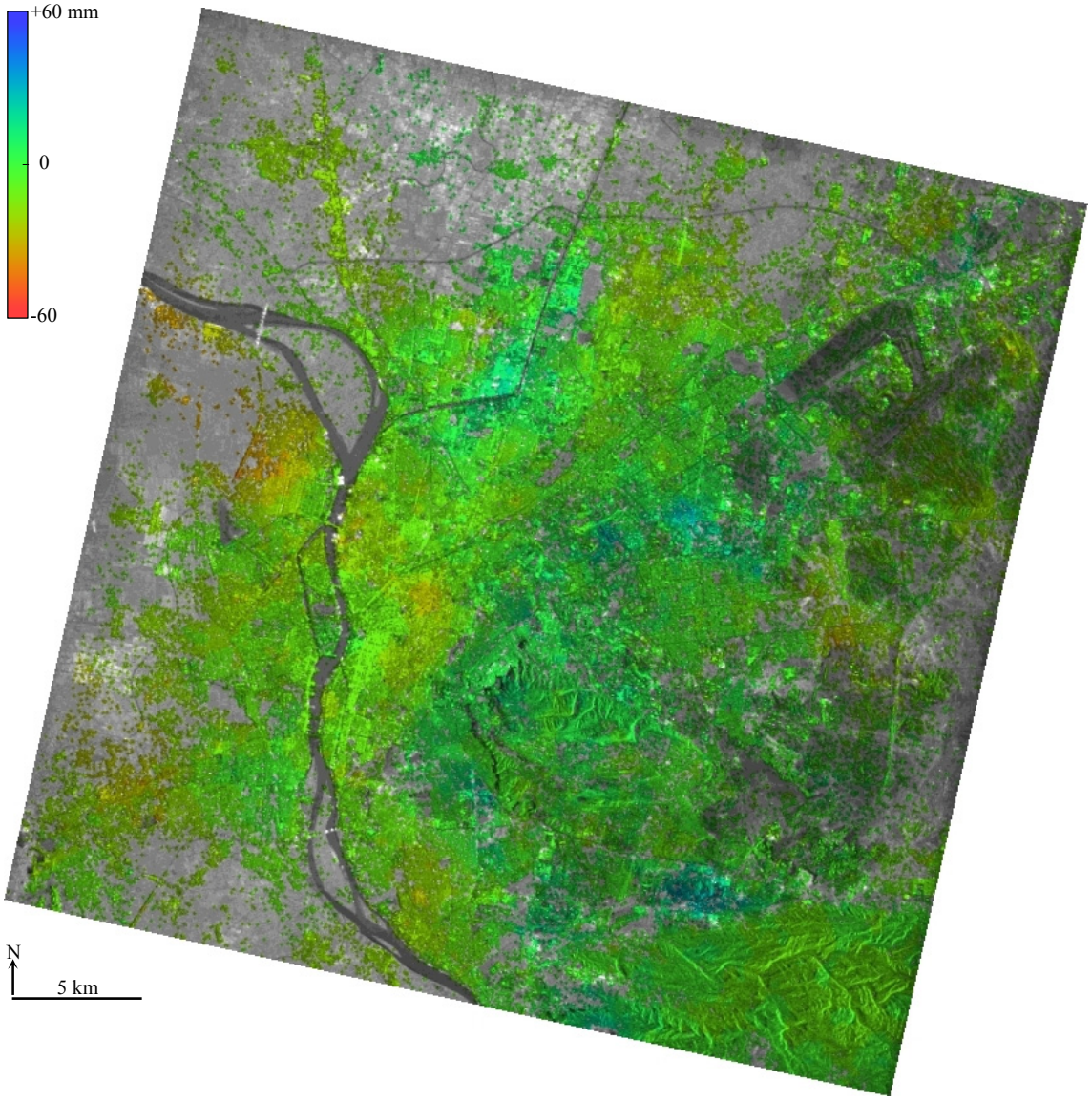

Figure 3.14. Estimated LOS surface displacement for July 1, 1998, superimposed on the average amplitude image of greater Cairo

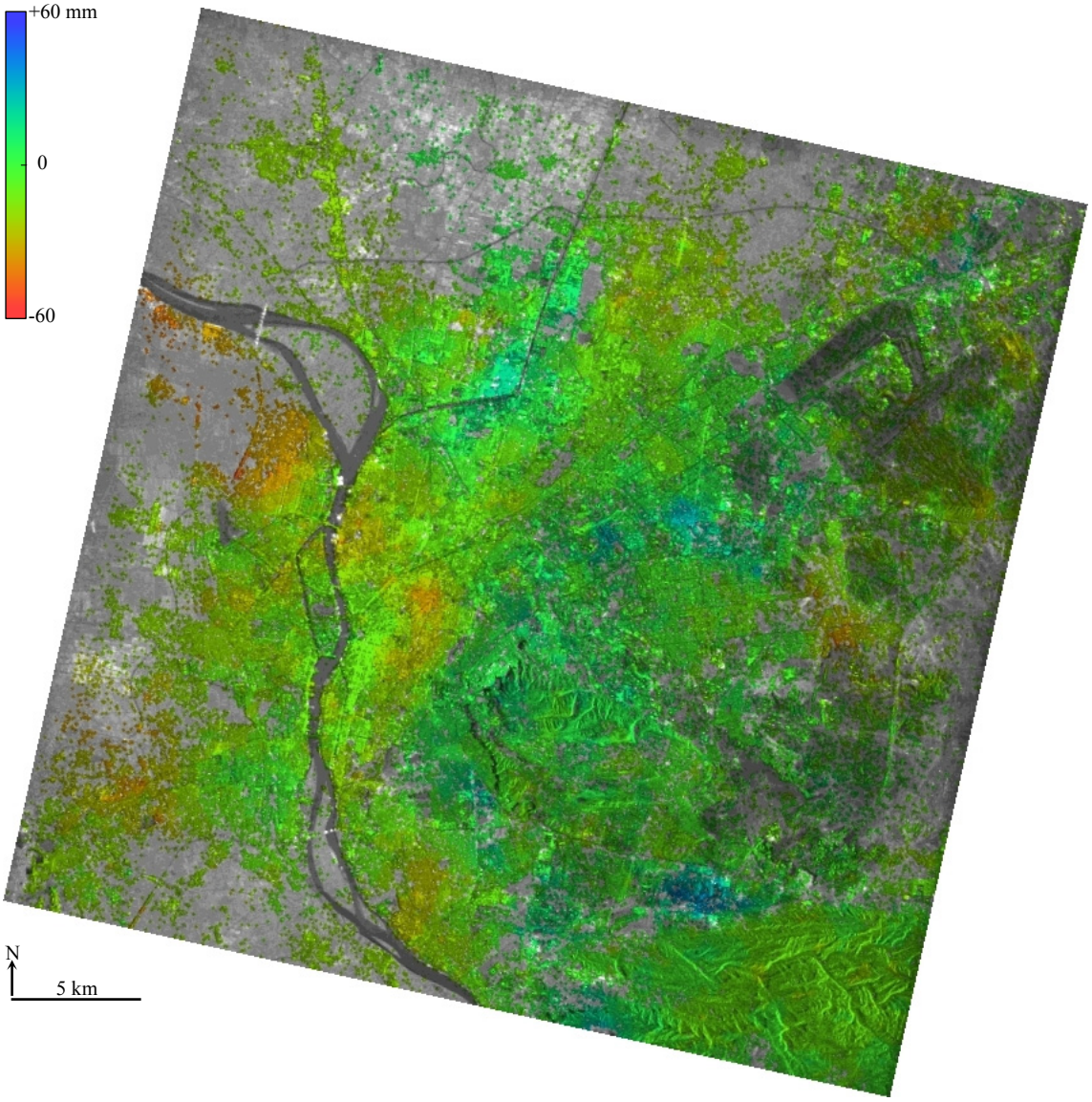

Figure 3.15. Estimated LOS surface displacement for July 1999, superimposed on the average amplitude image of greater Cairo

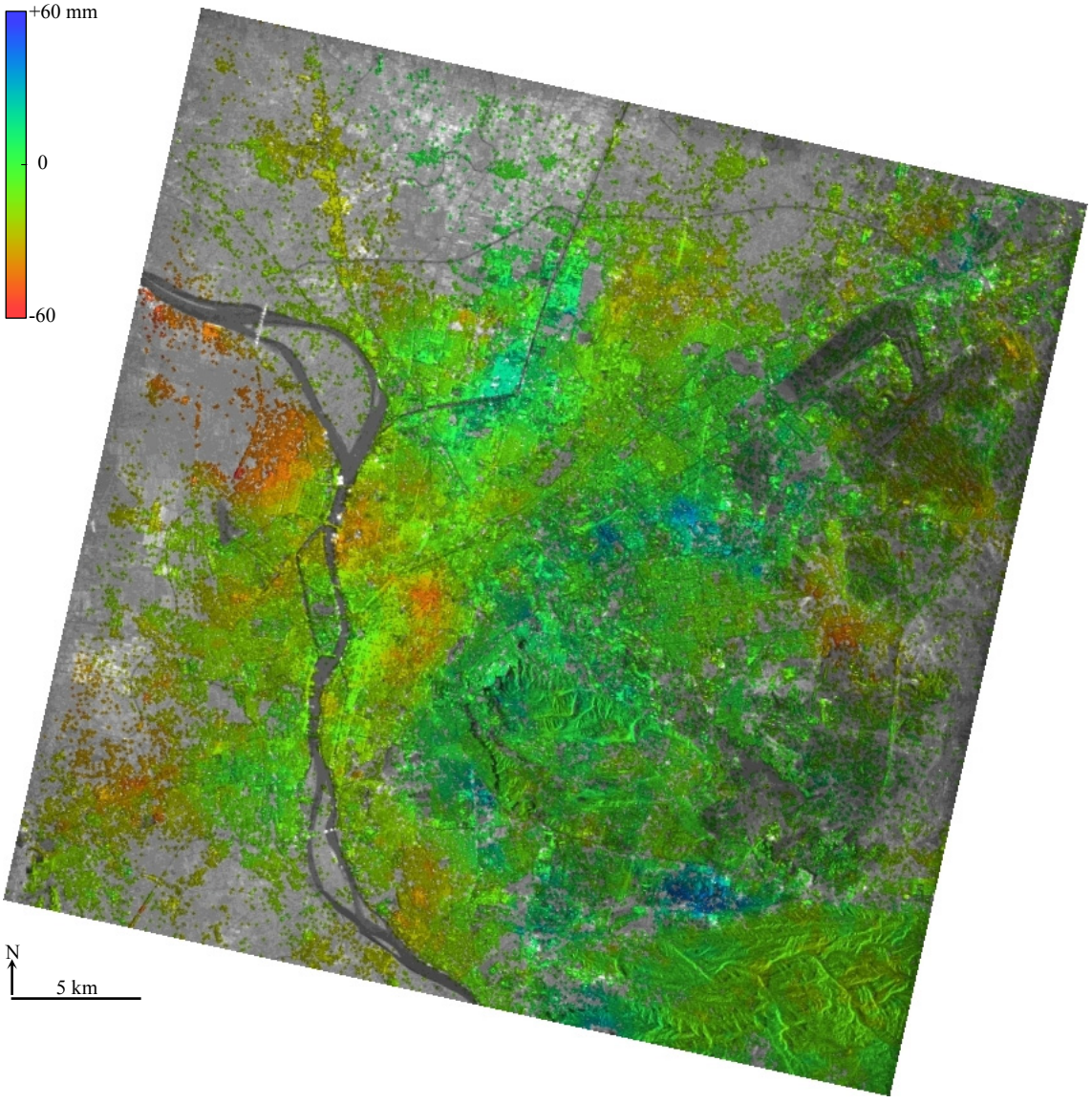

Figure 3.16. Estimated LOS surface displacement for July 1, 2000, superimposed on the average amplitude image of greater Cairo

The tectonic setting of greater Cairo is also believed to make a considerable contribution to the measured subsidence rate. Differential subsidence is observable along the major subsurface fault, no. 1, trending NE-SW (Figure 3.17). The average rate of differential subsidence along the fault is 4 mm yr^{-1}. Differential subsidence also occurred along several surface faults, including faults no. 2, 3, 4, 5, and 6, with average rates of 3, 4, 3, 3, and 5 mm yr^{-1}, respectively. Subsidence occurred on both sides of the historic surface faults no. 7 and 8, and the subsurface fault no 9.

Several studies, such as Badawy and Monus (1995), Badawy and Abdel-Fattah (2002), and Korrat et al. (2005), showed that north Egypt especially the area to the south of Cairo is tectonically active (Figure 3.18). During the last 15 years, several earthquakes have been recorded in northern Egypt, e.g., October 12, 1992; July 30, 1993; August 3, 1993; November 22, 1995; October 11, 1999; December 28, 1999; June 12, 2001 (Badawy and Abdel-Fattah 2001). Seismic activities in and around Cairo along with the ongoing land subsidence may cause a disaster in the future by activating inactive faults.

There is one more potential contributing factor to the rate of land subsidence in greater Cairo that has never been reported. This potential factor is the subway network that commenced in Cairo in 1982. The location, extent and magnitude of land subsidence in greater Cairo match very well with the subway lines and stations (Figure 3.19). The subway in greater Cairo consists of three major lines and approximately 86 stations. It passes through the most important residential and business districts in Cairo. Lines no. 1 and no. 2 have been used for several years, but line no. 3 is still under construction. About six million passengers per day are using the subway network (Egyptian Tunneling

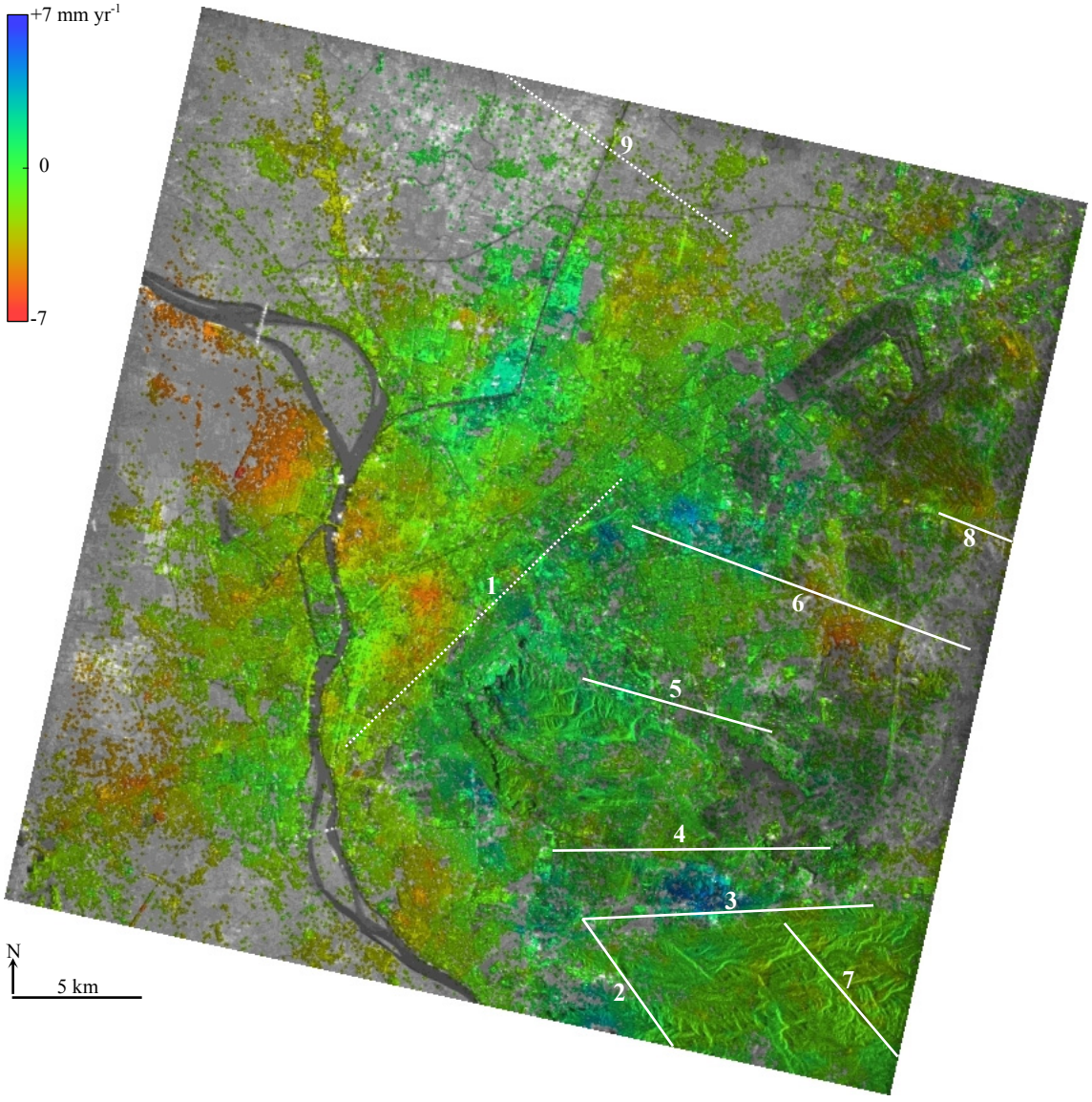

Figure 3.17. Mean velocity in LOS superimposed on the average amplitude image of greater Cairo with major faults. Dotted white lines are subsurface faults; solid white lines are surface faults from El Araby and Sultan (2000)

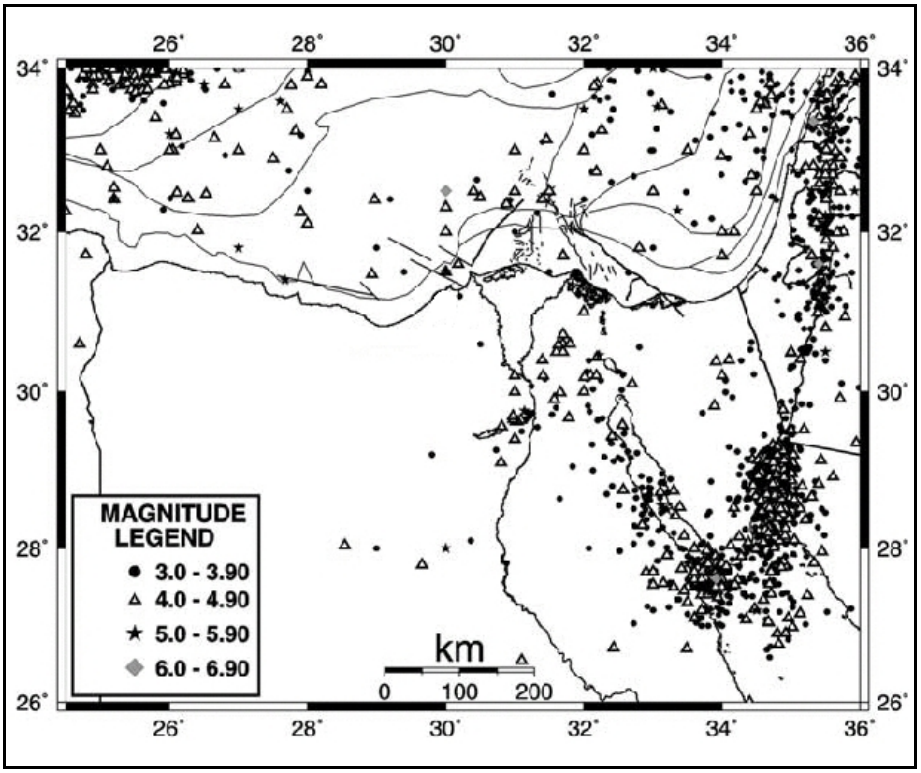

Figure 3.18. Seismicity of Egypt for the period 1900–2001 (Korrat et al., 2005)

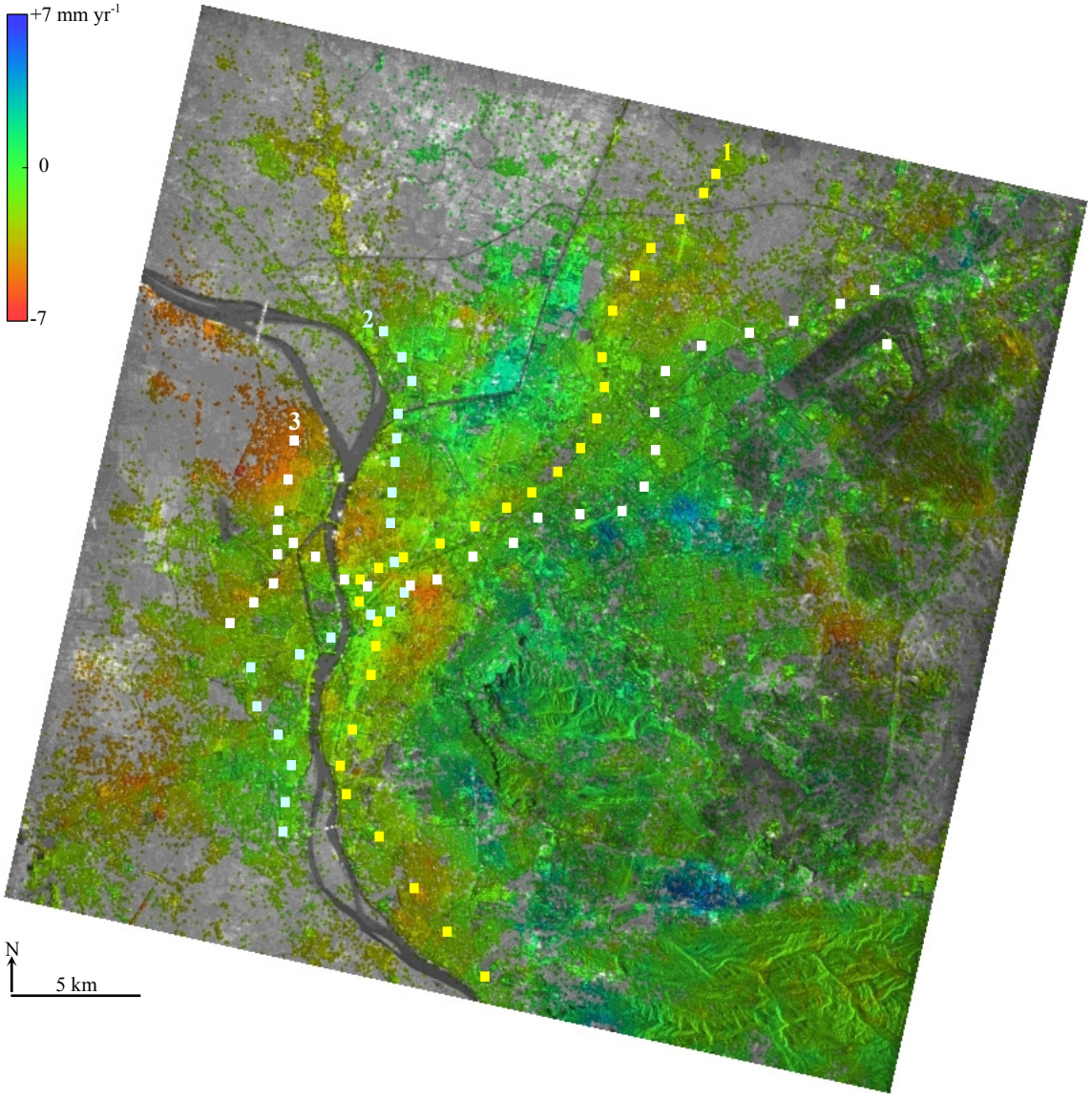

Figure 3.19. Mean velocity in LOS superimposed on the average amplitude image of greater Cairo with subway stations

Society, 2005).

Excavation and construction of tunnels, as well as the load of trains and millions of passengers every day might be potential causes of slight subsidence on the long run, particularly because the stratigraphic sequence in greater Cairo consists mainly of unconsolidated clays, silts and sands. It is remarkable that areas hosting extensive subway stations such as Ramsis, Ataba, and Tahrir are experiencing the highest rate of land subsidence. These areas also have the highest population densities in Cairo. It is also noticeable that a long section of the subway network line no. 1 passes in the subsiding side parallel to the major subsurface fault no. 1, trending NE-SW. The subway line no. 1 started in 1989 and since then it is always overloaded. This might be one of the potential causes of subsidence in this side.

It is not the objective of this research to find a remediation to the land subsidence problem in greater Cairo. However, it is recommended that the contribution of the anthropogenic factors, including the subway network and groundwater pumping be comprehensively re-assessed and differentiated from the contribution of the natural factors. In contrast with the natural factors, such as the tectonic setting and natural sediment compaction that are not controllable, anthropogenic factors can be stopped or at least mitigated. For example, subway stations in areas that experienced a high rate of land subsidence can be closed. The effect of groundwater pumping can also be mitigated by closing pumping stations in sensitive areas or it can be compensated by injecting water into the aquifer system. The city planers and decision makers may also consider moving ministries and public-related organizations out of Cairo, as it was proposed several years ago to relieve the pressure on the very congested ancient city.

CHAPTER IV

LAND SUBSIDENCE IN MANSURA AND MAHALA

1. Introduction

Urban subsidence can be expected in all cities in the Nile Delta because groundwater is main source of utility water and because the stratigraphic sequence is relatively the same in the entire delta, which consists basically of clays, silts and sands. Possible causes of land subsidence in Mansura and Mahala are believed to be limited to natural sediment compaction and groundwater pumping. The tectonic setting has no role to play, and there is no subway network in the two cities.

Studying land subsidence in the Nile Delta is very challenging because of the significant content of water vapor, soil moisture content, and dense vegetation cover. Even the urban areas in the Nile Delta are of limited spatial extent (Figure 1.1). Acting together the characteristics of the Nile Delta mentioned above with the very slow rate of surface deformation impede the application of conventional SAR interferometric approaches to obtain reliable subsidence measurements.

To overcome phase decorrelation problems with conventional SAR interferometry, the Permanent Sactterers interferometric approach is employed to detect subsidence patterns and measure its magnitude in the two largest cities in the central part of the Nile Delta; namely Mansura, which is home to approximately 450,000 people and Mahala, which is home to approximately 525,000 people. The two cities were selected away from the Mediterranean coast to reduce the amount of water vapor in the air and,

thus, minimize the atmospheric artifacts in SAR acquisitions. Land subsidence measurements in Mansura and Mahala, as well as in other cities in the delta can provide a broad understanding of the subsidence phenomenon and an estimation of the associated hazards with subsidence in the delta.

2. Data Acquisition

The short wavelength of the C-band (5.66 cm) and the temporal coverage of the ERS SAR interferometric data are well suited for studying the slow rate of surface deformation in the Nile Delta. Thirty-nine ERS descending scenes (Track: 436, Frame: 2979, Figure 4.1) were acquired over an eight year period from 1993 to 2000 (Table 4.1). Five ERS tandem pairs were collected for topographic and tropospheric estimations. SAR interferometric DEMs of 3-arc sec created from data acquired by the Shuttle Radar Topographic Mission (SRTM) were also obtained for topographic phase removal. Although SRTM DEMs are of coarse spatial resolution, this is not a real constraint as the study area has hyper flat terrain.

3. Permanent Scatterer Interferometry

Processing ERS InSAR data for Mansura and Mahala followed the same procedure applied in processing the ERS dataset for greater Cairo in Chapter III. Single Look Complex (SLC) images were generated and coregistered to the ERS-2 scene acquired on January 11, 1996.

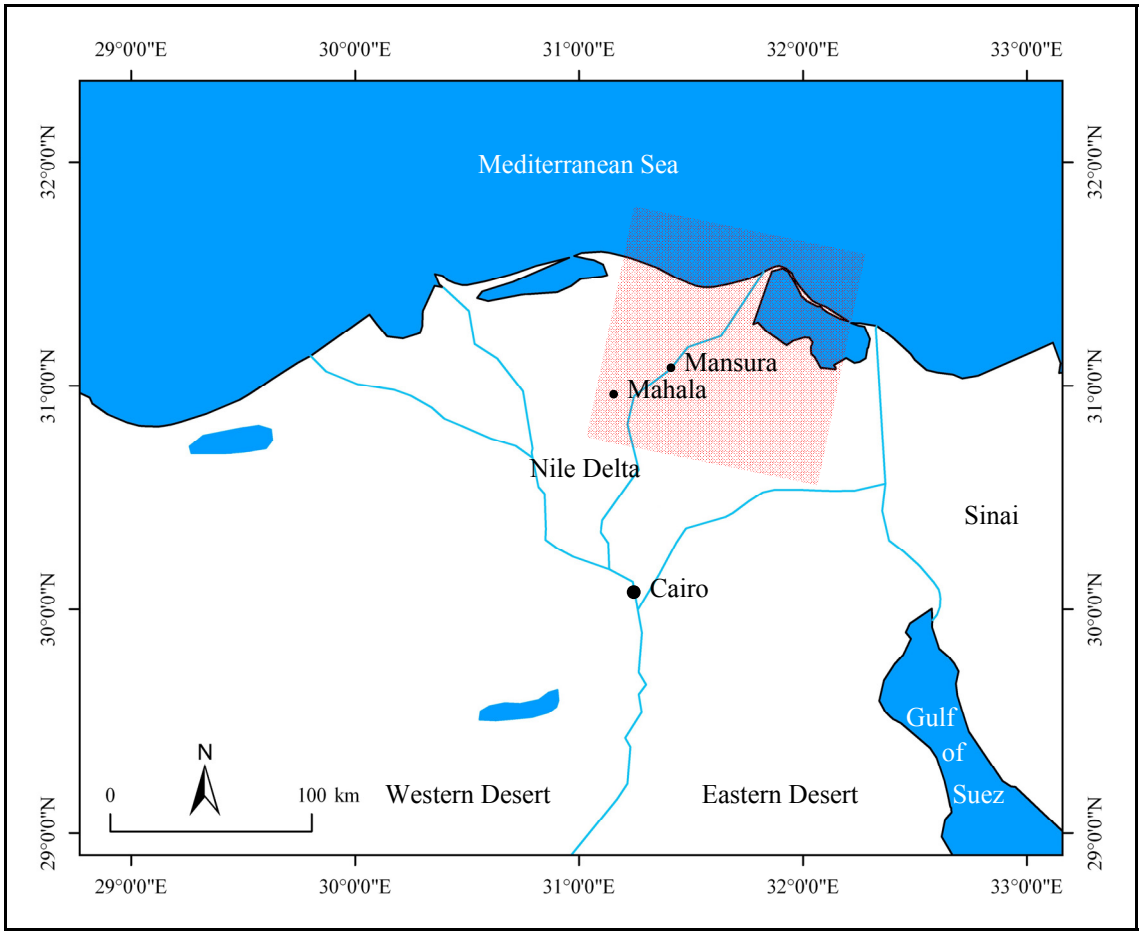

Figure 4.1. ERS coverage of Mansura and Mahala (Track: 436, Frame: 2979) is highlighted in red

Table 4.1. ERS dataset for Mansura and Mahala

#	Date[a]	$B_{\perp}$ (m)[b]	B_T (day)[c]	ERS
1	19930201	-698.4072	-1074	1
2	19930412	613.3302	-1004	1
3	19930517	-94.7692	-969	1
4	19930726	231.6942	-899	1
5	19930830	-400.5836	-864	1
6	19931004	-51.6256	-829	1
7	19931108	165.0499	-794	1
8	19950720	42.9351	-175	2
9	19950823	-27.9726	-141	1
10	19950824	-126.1882	-140	2
11	19950927	139.3528	-106	1
12	19950928	549.8912	-105	2
13	19960111	0.0000	0	2
14	19960214	638.1264	34	1
15	19960215	648.0047	35	2
16	19960529	-357.2229	139	1
17	19960530	-463.6777	140	2
18	19970515	24.4539	490	2
19	19980917	-764.5666	980	2
20	19981231	-782.0326	1085	2
21	19990311	-77.6046	1155	2
22	19990415	726.9202	1190	2
23	19990520	-188.5021	1225	2
24	19991007	-309.1264	1365	2
25	19991111	318.2996	1400	2
26	19991216	531.7678	1435	2
27	20000120	-131.4232	1470	2
28	20000223	-891.4721	1504	2
29	20000224	-725.9152	1505	2
30	20000330	-297.6116	1540	1
31	20000504	-217.8680	1575	2
32	20000608	-158.1932	1610	2
33	20000713	-985.9117	1645	2
34	20000817	-35.7963	1680	2
35	20000921	690.2563	1715	2
36	20001026	-305.6683	1750	2
37	20001130	-223.2472	1785	2

[a]Date is YYYYMMDD.
[b]$B_{\perp}$ is the Perpendicular baseline.
[c]B_T is the temporal baseline.

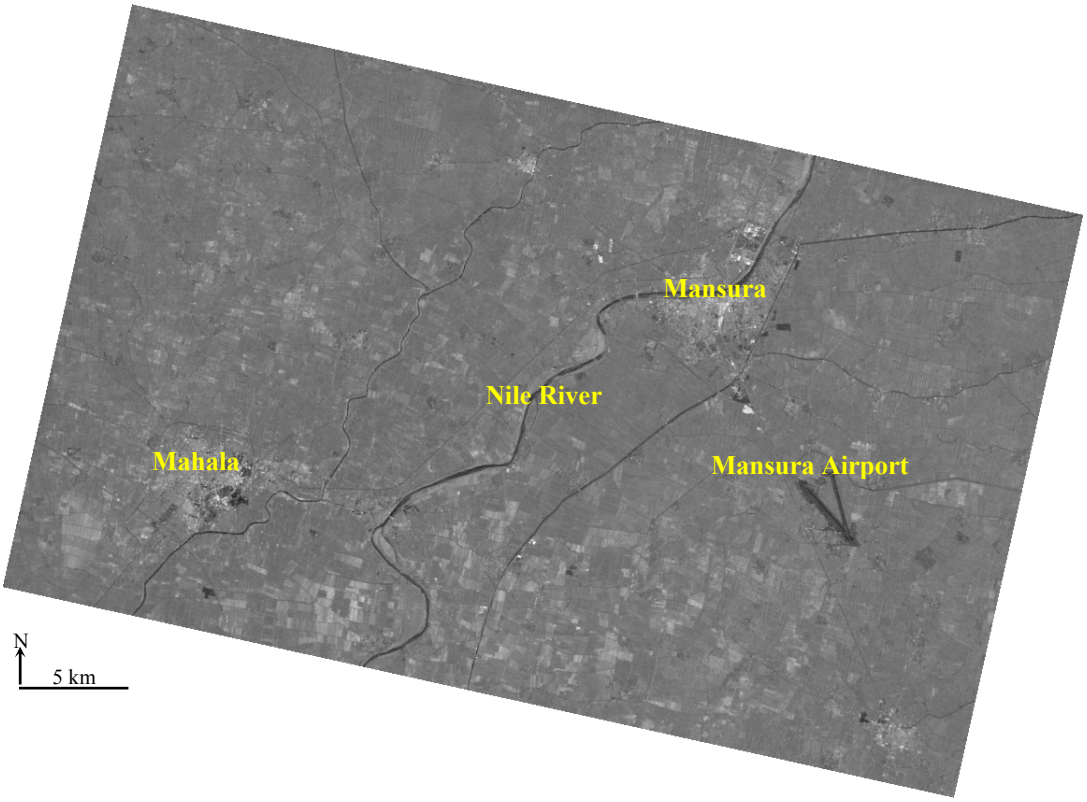

Figure 4.2. Average amplitude image of Mansura and Mahala

The average amplitude image of the processed 37 ERS subscenes for the two cities is shown in Figure 4.2. Mansura and Mahala metropolitan areas appear as bright radar responses in Figure 4.2. The Mansura Airport and the Nile River are also visible in the image. The fine dark lines correspond to irrigation channels and major roads. Some crop fields appear in light grey color. The general lack of contrast over much of the land area is related to various kinds of cultivated crops, which change seasonally.

Permanent Scatterers were selected and processed independently for each city. An average of 64 PS km^{-2} and 51 PS km^{-2} has been identified for Mansura and Mahala, respectively using the amplitude dispersion index, as explained in Chapter III. The preliminary inspection of interferograms revealed that winter acquisitions were generally less affected by atmospheric artifacts than summer acquisitions. The ERS acquisitions dated July 9, 1998, and August 13, 1998, were found plagued by atmospheric artifacts and, thus, were excluded from further processing.

The interferograms created for Mansura and Mahala were generally very noisy compared to those created for greater Cairo. The PS density in the two cities is less by a factor of three over greater Cairo as well. One explanation might be that Mansura and Mahala are surrounded by cultivated land from all directions and their spatial extents are significantly limited compared to Cairo. The location of Mansura and Mahala in the center of the densely vegetated delta, in addition to their limited spatial extents make the local troposphere over the two cities be significantly saturated by the water vapor.

Local interferometric decorrelations are also expected because of construction activities in Mansura and Mahala. The two cities are known of their fast rate of urban

sprawl during the last decade. The vertical extent of urban development is generally faster than the spatial extent because of the rigid constraints established by the Egyptian Government to preserve the fertilized cultivated land in the Nile Delta. Increasing the heights of buildings leads to local phase decorrelation.

The ERS interferograms created independently for the two cities were unwrapped and corrected as explained in Chapter III. Topographic phase residuals, atmospheric artifacts, and phase error caused by orbital inaccuracies, as well as phase noise were assessed and carefully removed. The iteration concept was applied to refine the estimated interferometric phase components. The Line-Of-Sight (LOS) surface displacement maps were created from the corrected interferograms and ultimately the final outputs were geocoded.

4. Results and Discussion

All deformation associated with land subsidence in Mansura and Mahala is assumed to be vertical. Thirty-seven LOS displacement maps were generated to demonstrate the deformation phase history for the two cities. The average measured velocity away from (subsidence) the satellite in LOS is -9 mm yr^{-1} in Mansura and -5 mm yr^{-1} in Mahala.

The calculated mean velocity in LOS superimposed on the average amplitude image of Mansura is shown in Figure 4.3. Three PSs were selected to demonstrate deformation behavior in sensitive areas in Mansura. Locations of the selected PSs are shown in Figure 4.3, and their deformation phase histories are shown in Figures 4.4-4.6.

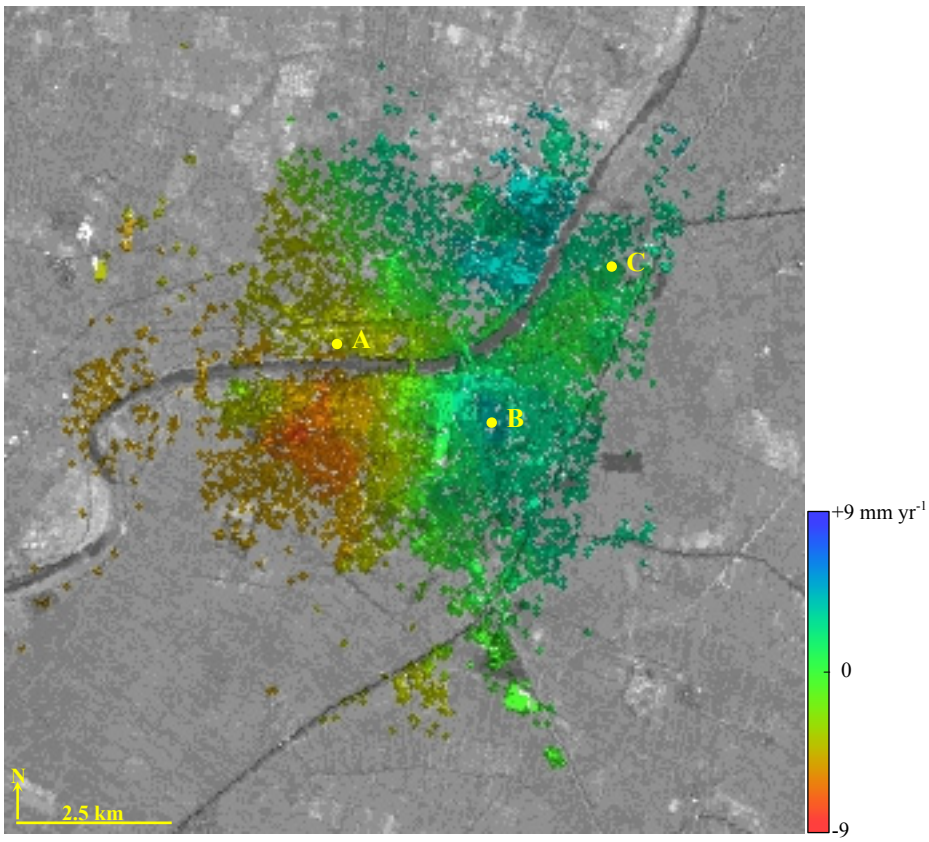

Figure 4.3. Mean LOS velocity in the 1993-2000 period, superimposed on the average amplitude image of Mansura

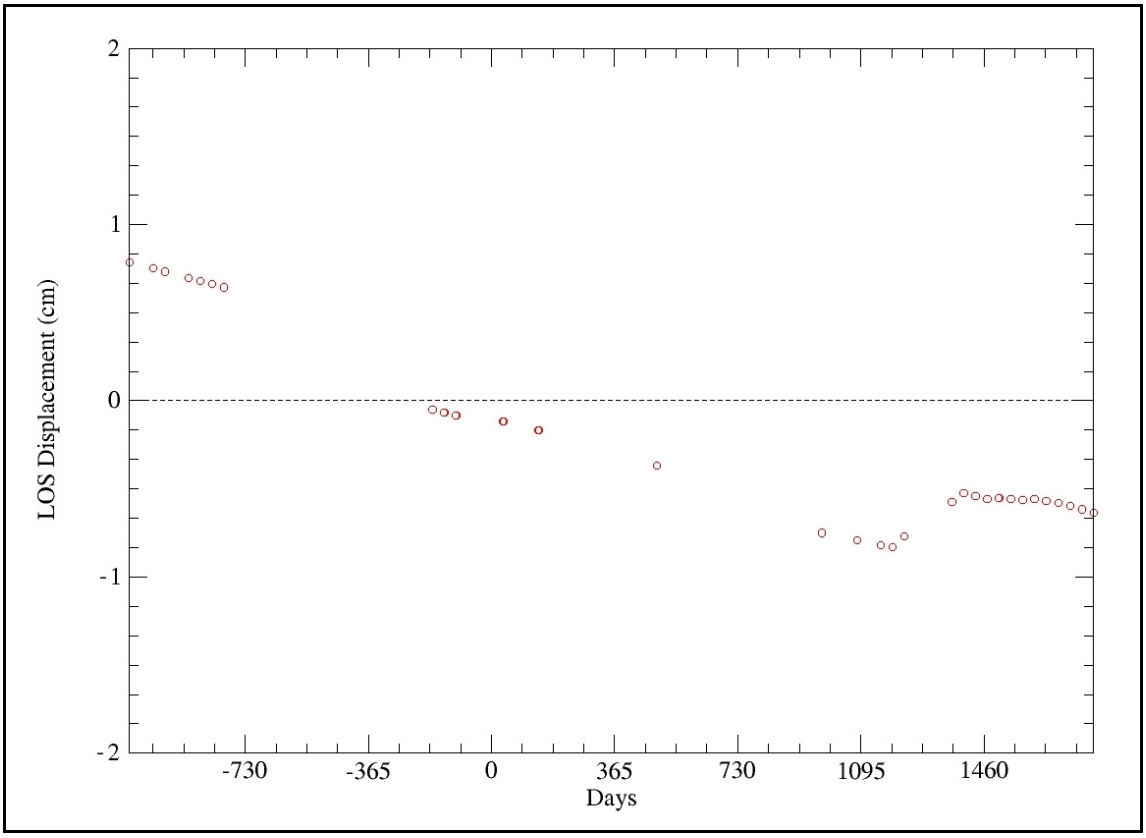

Figure 4.4. Deformation phase history of point A in Mansura during the 1993-2000 period

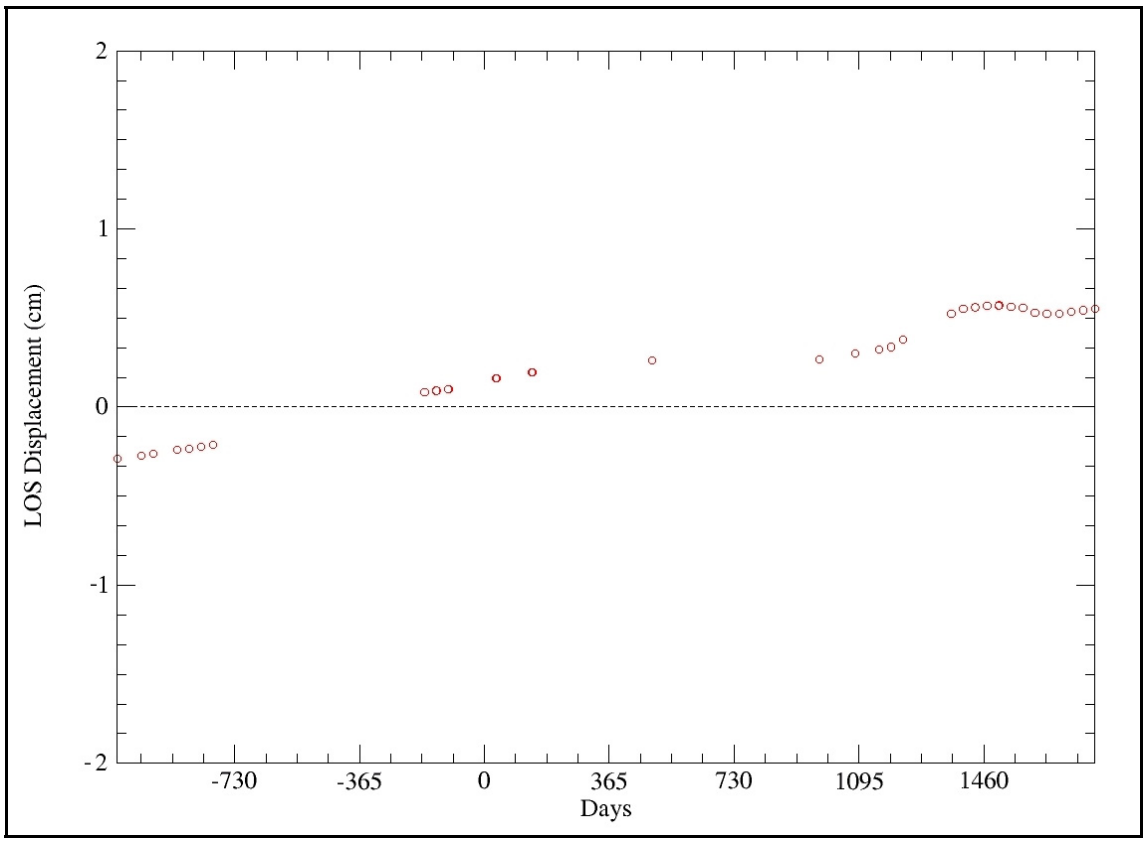

Figure 4.5. Deformation phase history of point B in Mansura during the 1993-2000 period

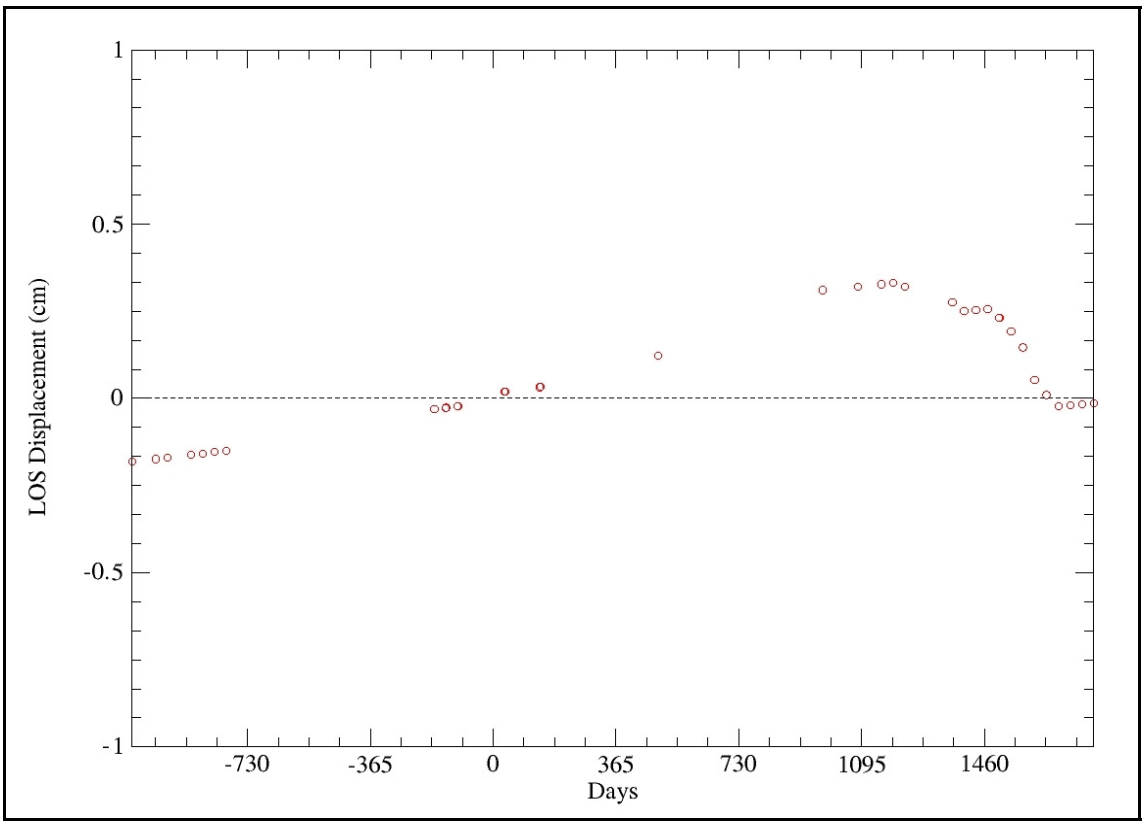

Figure 4.6. Deformation phase history of point C in Mansura during the 1993-2000 period

The deformation phase history of point A (Figure 4.4) demonstrates about 14 mm of non-linear surface displacement away from the satellite in the Line-Of-Sight (LOS) between 1993 and 2000. The rate of deformation during the 1998-2000 period was slower than the rate of deformation between 1993 and 1997. The deformation phase history of point B (Figure 4.5) shows the non-linear behavior of deformation during the 1993-2000 period. About 9 mm of surface displacement towards the satellite in LOS occurred. The deformation phase history of point C demonstrates about 5 mm of non-linear surface displacement towards the sensor in LOS between 1993 and 1999 and about 4 mm away from the satellite during 1999 and the first 6 months of 2000. During the last 6 months of 2000 the point was almost stable (Figure 4.6).

The calculated mean LOS velocity superimposed on the average amplitude image of Mahala is shown in Figure 4.7. Three points A, B and C were selected to demonstrate deformation behavior in sensitive areas in Mahala. Locations of the selected PSs are shown in Figure 4.7, and their deformation phase histories are shown in Figures 4.8-4.10.

The deformation phase history of point A (Figure 4.8) demonstrates about 23 mm of surface displacement in the Line-Of-Sight (LOS) between 1993 and 2000. Linear deformation occurred away from the satellite (subsidence) with an approximate constant rate over time from 1993 to 1999. Non-linear deformation was observable with a slower rate through 1999-2000. The deformation phase history of point B (Figure 4.9) shows the non-linear behavior of deformation during the 1993-2000 period. About 4 mm of

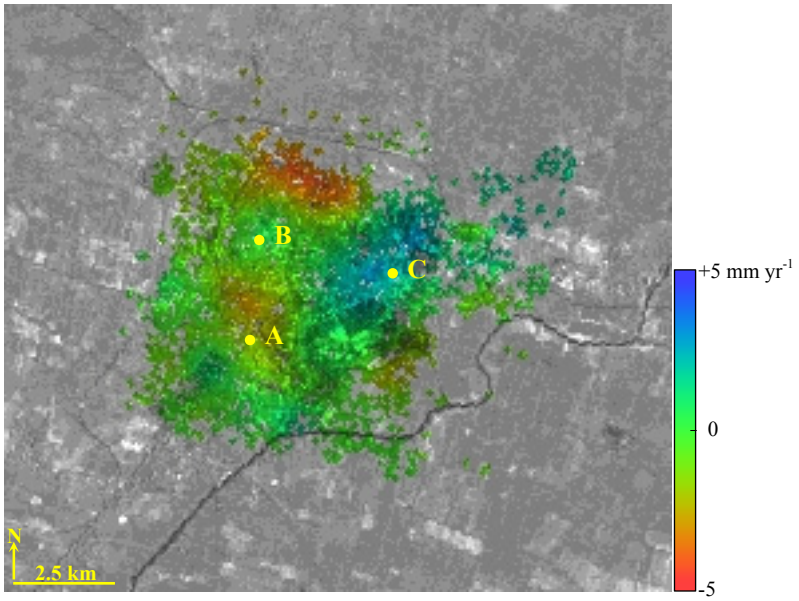

Figure 4.7. Mean LOS velocity in the 1993-2000 period, superimposed on the average amplitude image of Mahala

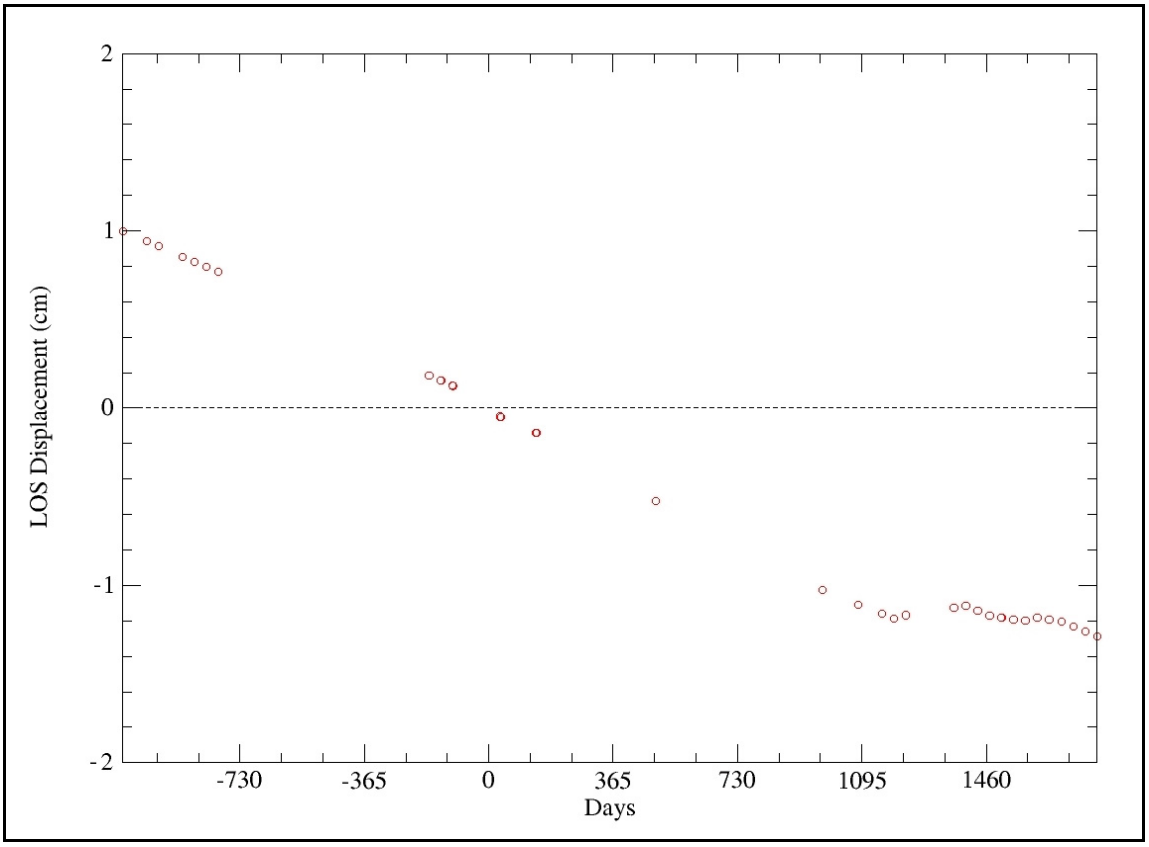

Figure 4.8. Deformation phase history of point A in Mahala during the 1993-2000 period

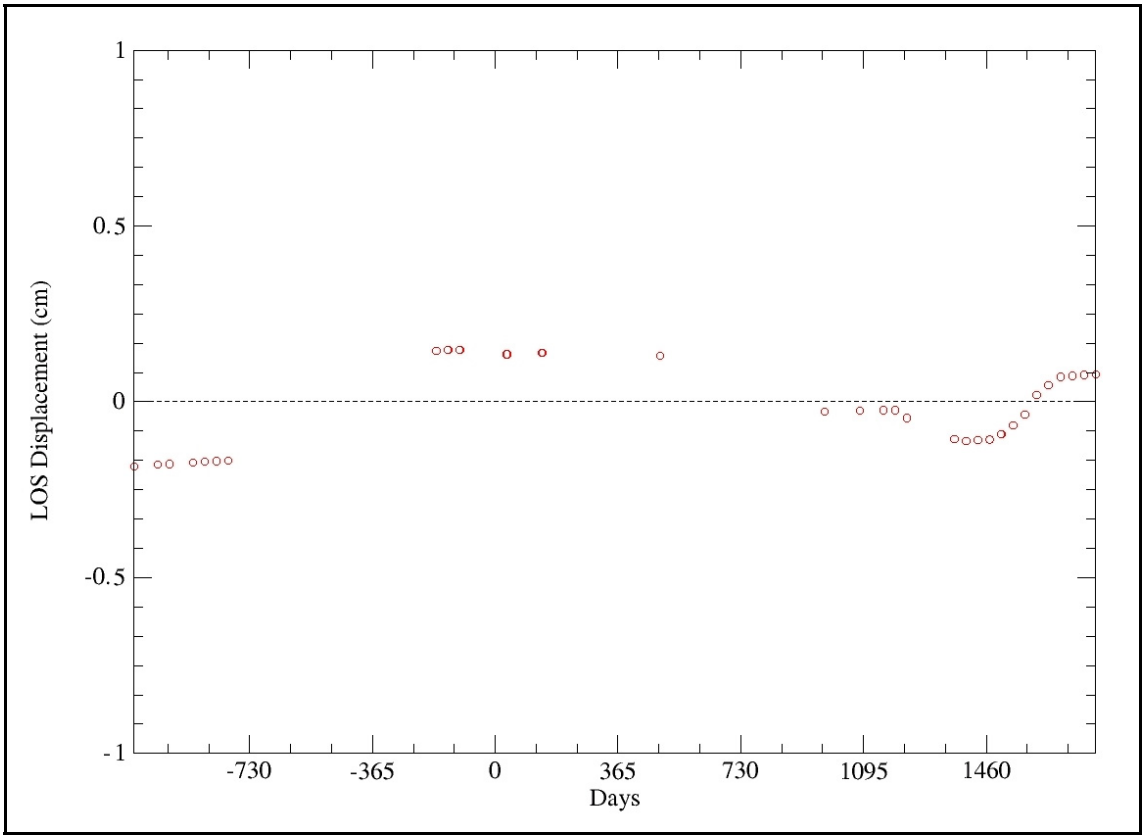

Figure 4.9. Deformation phase history of point B in Mahala during the 1993-2000 period

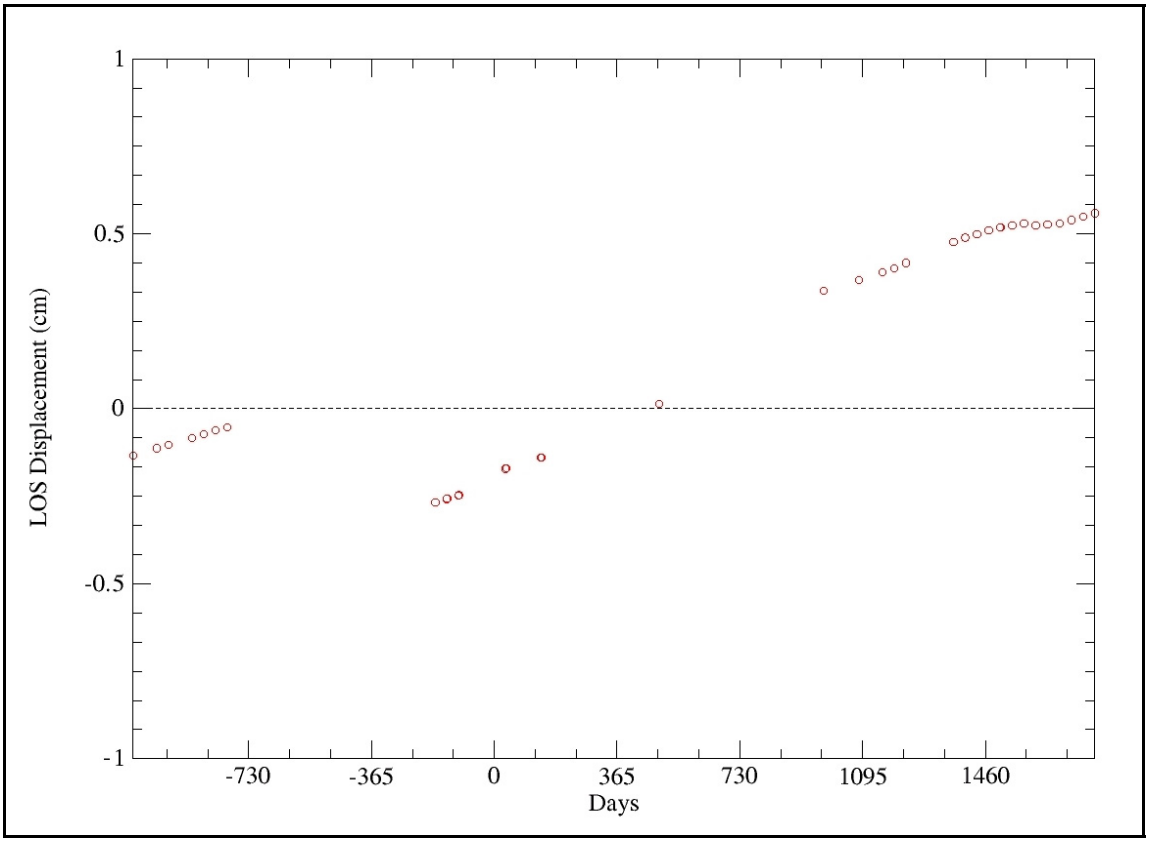

Figure 4.10. Deformation phase history of point C in Mahala during the 1993-2000 period

surface displacement towards and away from the satellite in LOS occurred. The deformation phase history of point C demonstrates about 9 mm of non-linear surface displacement towards the sensor in LOS between 1993 and 2000. It is obvious that the deformation rate in 2000 was slower than the deformation rate before 2000 (Figure 4.10).

A time series of 37 LOS displacement maps interpolated spatially from the selected PSs and referenced temporally to the earliest ERS acquisition on April 12, 1993, was created. Eight snapshots referenced to July 1, 1993, with approximately a 1-year sampling time interval were than taken to show progression of land subsidence in space and time for Mansura and Mahala (Figures 4.11 and 4.12, respectively). As no ERS acquisitions are available for 1994, no deformation record was created for that year.

The signal of land subsidence coincides with the highly populated districts in both Mansura and Mahala but with varying rates. The highest rate of land subsidence is observable in the southern part only of Mansura, whereas it is noticeable in the center and the northern part of Mahala. The time-series for Mahala shows that the subsidence bowl in the center of the city is decreasing over time. The positive values in the surface displacement maps created for the two cities suggest a local system rebound as a result of groundwater level recovery. Unfortunately, historical records of groundwater pumping and census data are not available for this research. Therefore, the suggestion can not be verified. Furthermore, no *in situ* measurement of land subsidence has been conducted in either Mansura or Mahala.

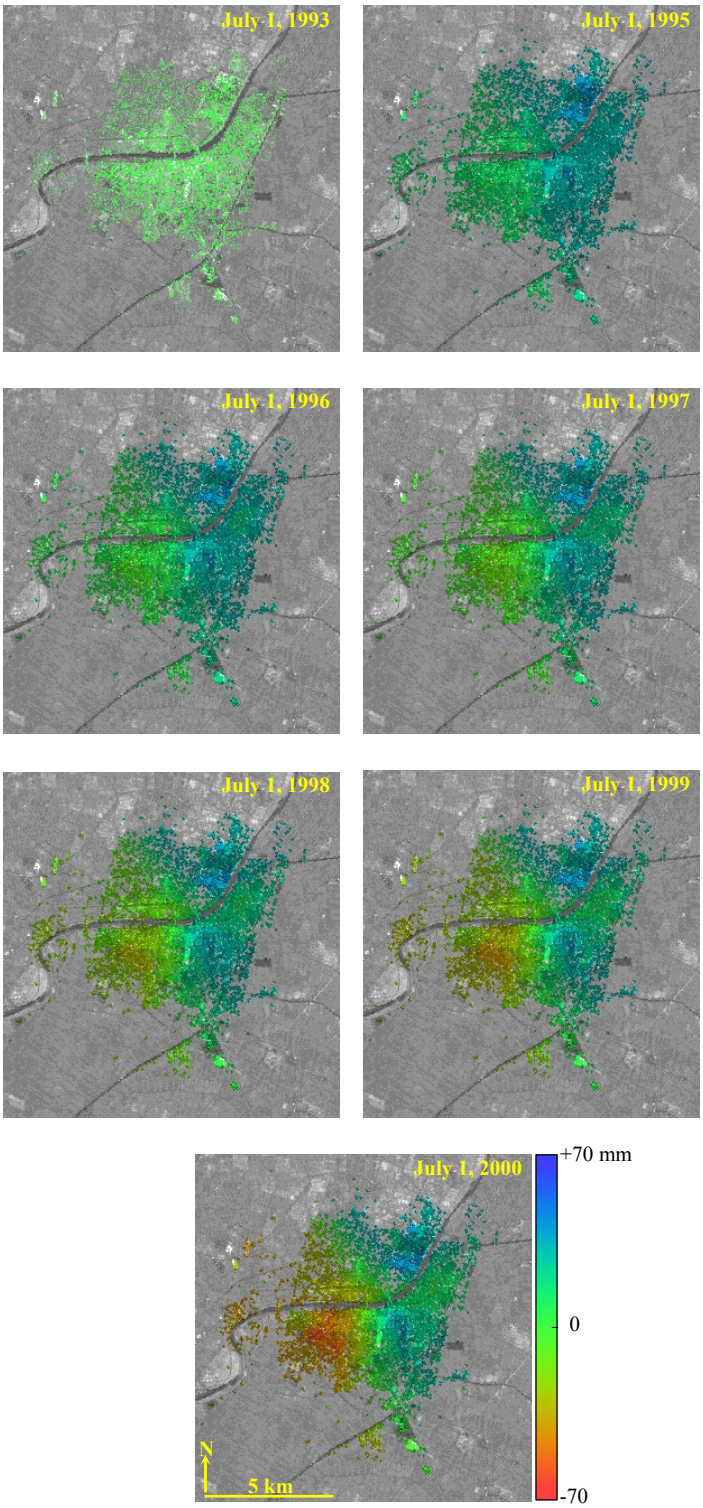

Figure 4.11. Estimated LOS surface displacement (1993-2000), superimposed on the average amplitude image of Mansura

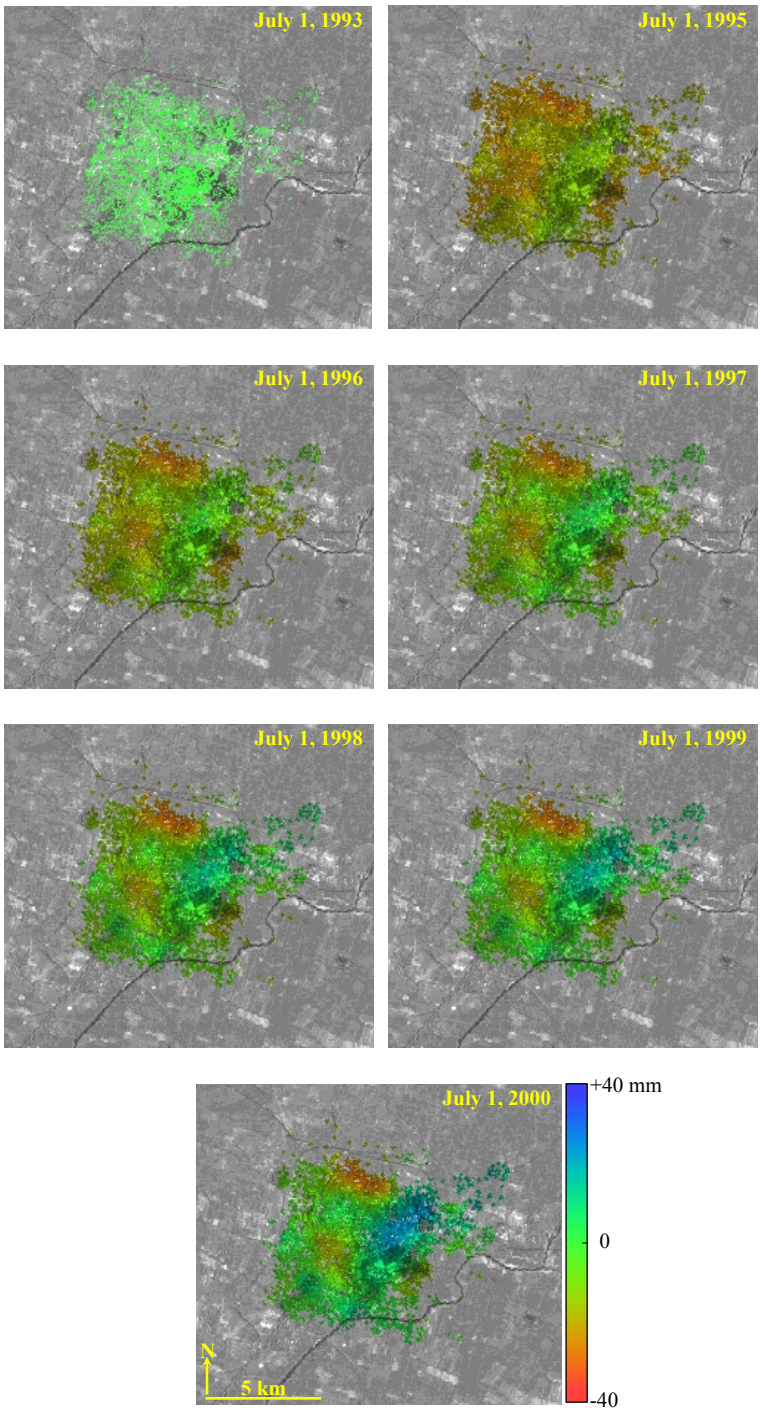

Figure 4.12. Estimated LOS surface displacement (1993-2000), superimposed on the average amplitude image of Mahala

As the spatial extents of both Mansura and Mahala are limited, the long-term subsidence resulting from natural sediment compaction can be assumed mainly affected by the seasonal variations in the rate of groundwater pumping in the two cities. Problems associated with pumping-induced subsidence can be handled by controlling the rate of groundwater pumping, by injecting water into the aquifer system, or even by eliminating pumping stations in the sensitive areas of high rates of land subsidence.

CHAPTER V

COASTAL CHANGE AT DAMIETTA PROMONTORY

1. Introduction

Coastal erosion is a major geomorphic problem along the coastal zone of the Nile Delta. Significant erosion has been observed along various segments of the coastline of the Nile Delta since the beginning of the 20th century. Promontories formed at the two Nile branch mouths (Figure. 5.1) have experienced the greatest amount of coastline retreat. Since the 1960s, shoreline retreat in some years has exceeded 100 m yr^{-1} at Rosetta Promontory and 50 m yr^{-1} at Damietta Promontory (Inman and Jenkins, 1980; Smith and Abdel-Kader, 1988; Frihy, 1992).

The accelerated erosion in the delta coast is attributed to the construction of two large dams at Aswan (the Low Dam in 1902 and the High Dam in 1964), and the subsequent entrapment of sediments in Lake Nasser behind the High Dam, as well as the effects of river control structures on the Nile River. Natural factors, including the delta subsidence, the sea level rise, and the pronounced coastal processes are also important contributors to the coastal retreat (UNDP/UNESCO, 1978; Sestini, 1992; Stanley, 1996).

Beaches are an important coastal environment along the Nile Delta, as most human settlements and economic activities are located on low-lying land directly behind beaches. Erosion can seriously damage and threaten communities, settlements, coastal roads, recreational resorts, valuable agricultural land, and development of the coast,

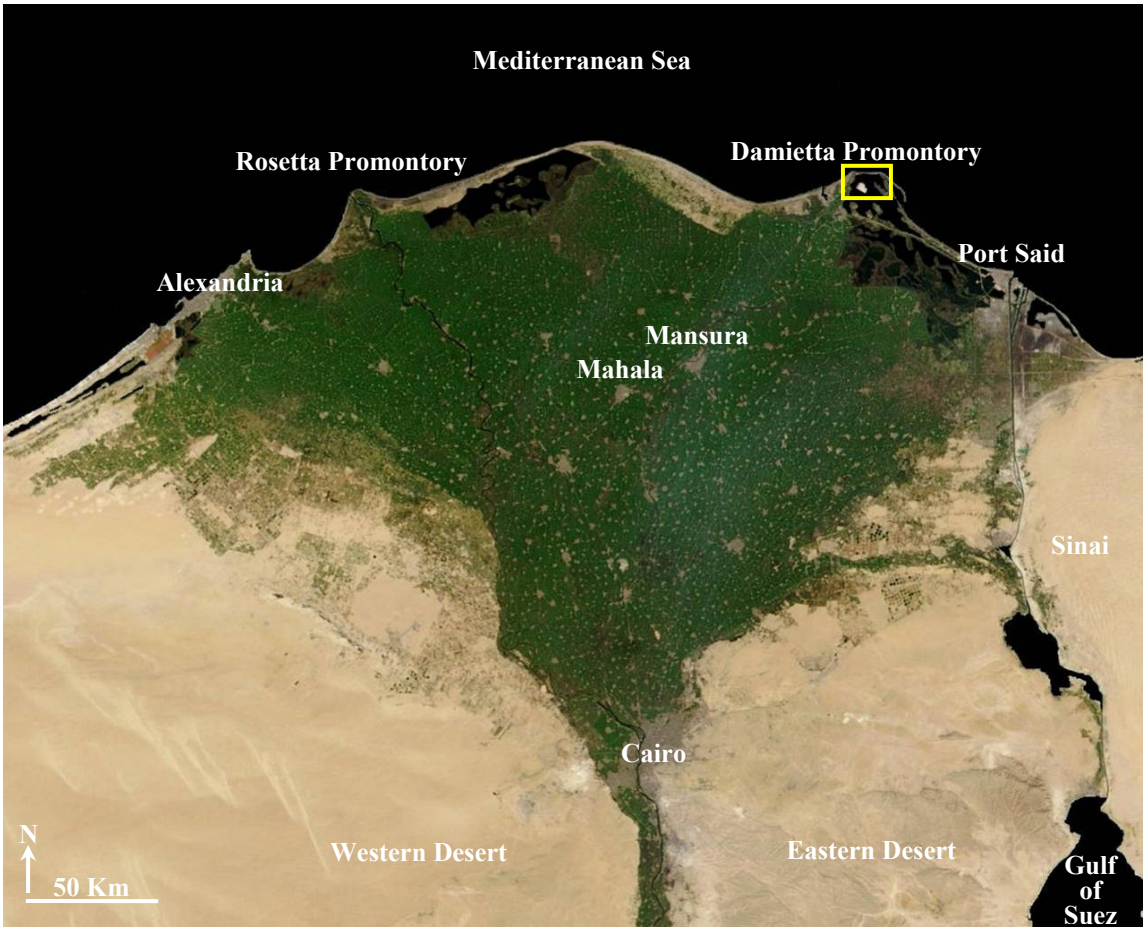

Figure 5.1. Damietta Promontory along the coast of the Nile Delta as seen by MODIS acquired on February 05, 2003

which poses a considerable hazard and an urgent management issue in the delta (Frihy, 1996; Stanley, 1996). Additionally, coastal erosion in the delta increases salination of groundwater and incursion of salt water (El kashef, 1983).

Coastal erosion is predicted to continue into the 21st century, with serious consequences for coastal developments (Stanley and Warne, 1993). Therefore, there is an increasing demand for regular monitoring, accurate measuring of coastal change for coastal zone management and integrated sustainable developmental of the Nile Delta.

Traditional survey tools and various remote sensing techniques have been widely used to monitor coastal changes. However, terrestrial survey tools are point measurements and, thus, provide a spatially limited view of the ongoing coastal changes. Remote sensing techniques provide more cost-effective and higher spatial coverage for coastal monitoring.

Numerous studies have been conducted to measure coastal change across the Nile Delta using optical remote sensing data; e.g., Klemas and Abdel-Kader (1982), Frihy et al. (1990), El Raey et al. (1995), and Ahmed et al. (2000a,b). Most of these studies have been accomplished using Landsat Thematic Mapper images. However, the low spatial resolution of the Landsat TM images (28.5 m) restricts their use in coastal erosion studies to situations where changes are greater than the pixel size. Using optical remote sensing data for coastal monitoring is also limited by the data availability and clear weather conditions.

Spatial and temporal resolutions should be carefully considered when exploiting remote sensing data for monitoring coastal change along the Nile Delta because of the

dynamic nature of its coastline. Radar interferometric data that can be acquired in all-weather conditions, both day and night, can provide subtle measurements of coastal change at a significantly improved spatial resolution and over large areas (100 km^2). In the study, ERS SAR interferometric data of approximately 20 m resolution are used to address coastal change at Damietta Promontory in the Eastern side of the Nile Delta (Figure 5.1). Using data collected by the ERS satellites, monitoring can be accomplished as frequently as every 35 days, the orbital period of the satellites.

2. Methodology

ERS SAR data acquired on February 1, 1993, May 29 and 30, 1996, and February 23 and 24, 2000, have been used in this study to identify coastline positions at Damietta Promontory during the 1993-2000 period. The selected ERS raw data (Track: 436, Frame: 2979, Figure 4.1) were checked and corrected for missing lines. They were then processed to a Doppler Centroid independent of range to generate Single Look Complex (SLC) images. The four ERS images acquired in 1996 and 2000 were precisely coregistered with a sub-pixel accuracy (~0.10 pixel) to produce two tandem coherence images (Figure 5.2). The produced images were multi looked to reduce speckle density. One look was taken in the range direction and five looks were taken in the azimuth direction to produce images of 20 m resolution in both directions. All products were then geocoded.

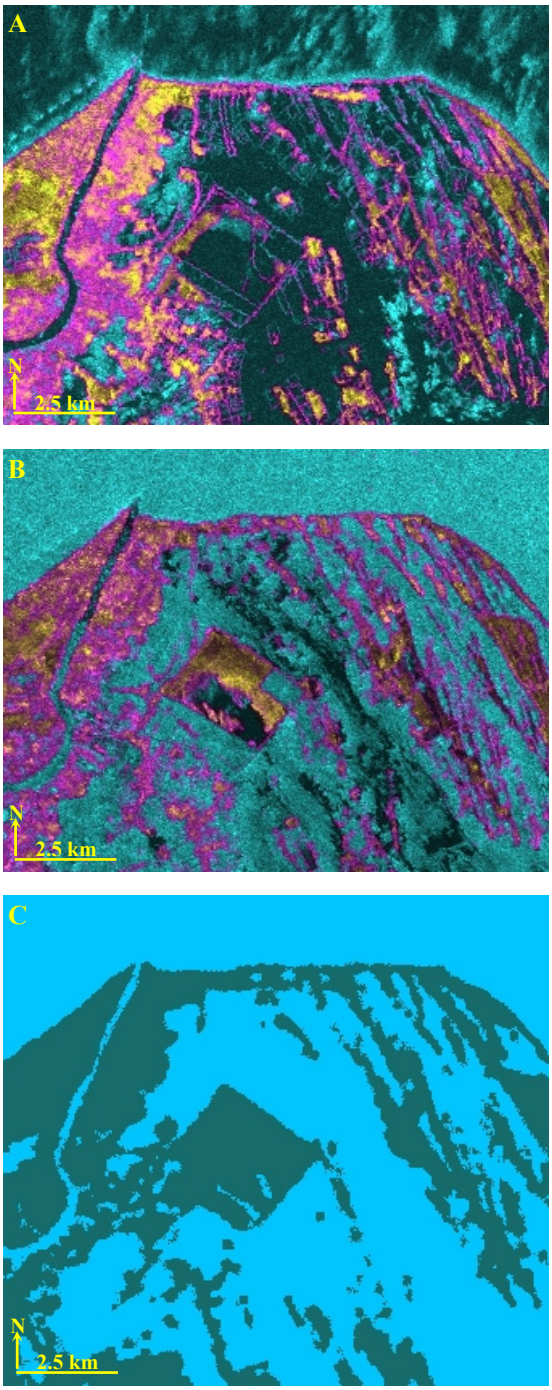

Figure 5.2. ERS tandem coherence and classified amplitude images, showing the water/land boundary at Damietta Promontory. (A) is the tandem coherence of February 23 and 24, 2000, (B) is the tandem coherence of May 29 and 30, 1996, and (C) is the classified amplitude image of February 1, 1993

The complex coherence is the degree of correlation between the two complex interferometric signals. Coherence values vary from zero to one as a quality measure of the stability of the scatterers between the two ERS SAR acquisitions. The complex coherence can be expressed as:

$$|\gamma| = \frac{\left|\sum_{i=1}^{N} C_1^{(i)} C_2^{*(i)}\right|}{\sqrt{\sum_{i=1}^{N}\left|C_1^{(i)}\right|^2 \sum_{i=1}^{N}\left|C_2^{(i)}\right|^2}} \qquad (5.1)$$

where $|\gamma|$ is the complex coherence, C_1 and C_2 are the phases of the two complex images, and $C_1 C_2^*$ is the complex interferogram.

Askne and Hagberg (1993) demonstrated the use of the InSAR phase coherence as both a classification tool and a change detection tool. Coherence magnitudes can be used to distinguish between land use/cover types. As the water surface is highly dynamic as opposed to the land surface, the coherence images (Figure 5.2) were used to accurately detect the water/land boundary at Damietta Promontory.

Several remote sensing techniques can be used to detect coastline positions, including digitization, supervised classification, and image segmentation (Wilson, 1997; White and El-Asmar, 1999). Two different approaches can be used for image segmentation: edge detection and growing homogenous regions. In edge detection, spatial convolution filters are passed over the image to find and link high frequency edges around regions. In the second approach, pixels are merged based on a specific

similarity criterion (Lemoigne and Tilton, 1995). In addition, wave spectra information can be used to model coastline changes by investigating the wave refraction patterns. TOPSAR wave spectra model was applied to detect coastline changes along the Terengganu coast, Malaysia (Marghany, 2001).

Supervised classification and edge detection techniques were applied in this research to detect coastline positions from the ERS interferometric data. Because of the lack of ERS tandem data before 1995, the amplitude image generated from the ERS scene acquired on February 1, 1993, was used to determine the coastline position in 1993. The amplitude image was filtered for speckle reduction and linearly stretched for visualization enhancement to overcome the poor contrast between water and land in SAR amplitude images. The filtering and linear stretching enhanced the contrast between water and land and, thus, enabled accurate detection of the coastline position by classifying the image into two major classes; water and land (Figure 5.2).

The edge detection technique has been accomplished by passing spatial convolution filters through the coherence images to accurately detect coastline positions in 1996 and 2000. The detected coastlines in 1993, 1996 and 2000 were then processed and analyzed via a Geographical Information System (GIS) to determine the pattern and magnitude of erosion and accretion at Damietta Promontory.

3. Results and Discussion

Areas of erosion and accretion were detected and identified at Damietta Promontory using ERS SAR interferometric data during the 1993-2000 period (Figures

5.3 and 5.4). Three locations (A, B and C) of erosion and accretion were identified and detected (Figures 5.3 and 5.4; Table 5.1). The average rate of measured erosion at location (A) is -5.98 m yr^{-1} and at location (B) is -13.17 m yr^{-1}. The average measured rate of accretion at location (C) is +5.44 m yr^{-1}. Based on results from this SAR interferometric study, the measured rate of erosion averaged for locations (A) and (B) together is -9.57 m yr^{-1}. The average is very close to the rate obtained from a field survey study by Frihy and Komar (1993), -10.40 m yr^{-1}, which adds confidence to the results.

Recognition of patterns and long-term trends of changes in the coastline along the Nile Delta is crucial for coastal zone management. Therefore, changes between different dates of acquisition were calculated separately (Table 5.1). This enabled the identification of areas of accelerating coastal change in the 1993-2000 period and, thus, the determination of which areas are likely to be most problematic in the future. Based on the average of measurements of coastal retreat at Damietta Promontory, location (B) (Figures 5.3 and 5.4) is experiencing an accelerating rate of erosion.

The Mediterranean Sea at the coast of the Nile Delta is almost microtidal (25-30 cm), and the coastline of the delta is affected mainly by waves and littoral currents. The prevailing wave and wind direction is southeast, which drives littoral currents to the east (UNDP/UNESCO, 1978; Manohar, 1981; Frihy, 1996). This clearly explains why areas of accretion are mostly located east of areas of erosion and points of sediment discharge (Smith and Abdel-Kader, 1988; Frihy and khafagy, 1991).

Table 5.1. Measured values of erosion and accretion

	Erosion (m)		Accretion (m)
	Location A	Location B	Location C
1993-1996	-21.56	-43.15	+20.91
1996-2000	-26.24	-62.17	+22.60
1993-2000	-47.80	-105.32	+43.51

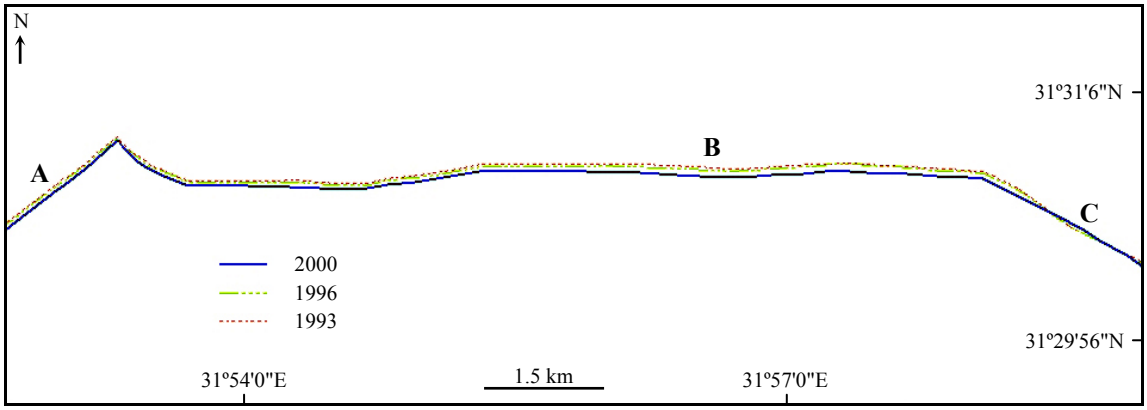

Figure 5.3. Coastline positions at Damietta Promontory detected by ERS SAR data acquired in the 1993-2000 period

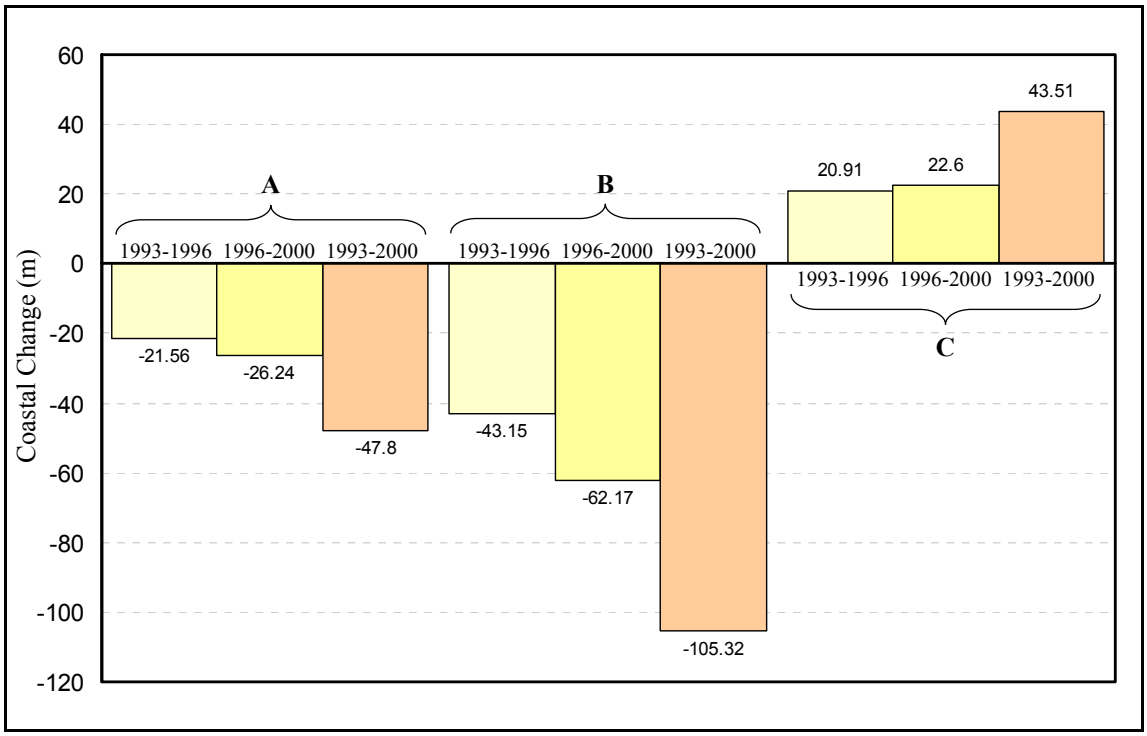

Figure 5.4. Measured erosion and accretion at locations A, B and C

In remote sensing studies for coastline detection, diurnal and long-term changes in sea level should be considered as a potential source of error, especially where the intertidal zone has a very shallow gradient (Mason et al., 1995). At the coast of the delta, effects of tides and changes in sea level are minimal. Therefore, they were not considered a significant source of error in locating the coastline at Damietta Promontory.

Potential sources of errors in coastline detection using remote sensing techniques include errors in the process of coregistration of the remotely sensed images, errors related to the applied technique for detecting coastline positions, and errors in measurements of the rate of coastal change, as well as errors related to effects of tides and changes in sea level. The spatial and temporal resolutions of the remotely sensed data should be appropriate to the measured rate of coastal change.

As most dramatic coastal changes occur in bad weather conditions, Synthetic Aperture Radar (SAR) data are very useful in coastal geomorphic studies because they can be acquired in all weather conditions. Furthermore, complex coherence images contain valuable information about the water/land boundary and thus, they can be used to accurately detect coastline positions. But only tandem coherence can be used, as no significant coastal change expected to occur within one day, the time period between the SAR acquisitions.

COnstellation of Small Satellites for Mediterranean basin Observation (COSMO-SkyMed) is one of the planned remote sensing missions in the near future. COSMO-SkyMed is an Earth observation program financed and managed by the Italian Space Agency (ASI). The system will be focused on the Mediterranean area, but it will be

capable of offering global services. The system will be equipped with four radar (X-band, metric resolution), hyperspectral, and optical satellites, providing images of high resolution with reduced revisit time over the observed sites (<8 hrs for Europe and 12 hrs for Equator). The first satellite will be launched in late 2006 and the constellation will be completed in 2007. COSMO-SkyMed data will enable comprehensive monitoring of coastlines in all weather conditions in the Mediterranean area. SAR, hyperspectral and optical data that will be provided by the COSMO-SkyMed satellite can be integrated for comprehensive monitoring and accurate measuring of the coastal change in the Nile Delta.

All coastal studies conducted on the Nile Delta revealed that the coastline of the delta is dynamic, particularly at Damietta Promontory, and requires regular monitoring. Coastal defense structures are needed to protect areas that are affected by significant coastal erosion. Results from this SAR interferometric study as well as results from previous coastal studies should be considered in the future for coastal zone management and sustainable development of the Nile Delta.

CHAPTER VI

CONCLUSIONS AND FUTURE DIRECTIONS

1. Conclusions

Land subsidence and coastal erosion are two interrelated long-term geomorphic problems in the Nile Delta. The rates of the ongoing land subsidence and coastline retreat require accurate measuring and regular monitoring. Current measures of land subsidence in the delta are rough estimates and assume uniformity over space and time. Current techniques used to measure coastal change in the Nile Delta are point measurements and, thus, provide a spatially limited view of the ongoing change. The overall objective of this interferometric study was to detect the spatial and temporal patterns, as well as the magnitudes of urban land subsidence and coastal change in the Nile Delta.

Synthetic Aperture Radar Interferometry (InSAR) has been successfully applied in this research to detect and measure land subsidence in greater Cairo, Mansura, and Mahala, as well as to detect and measure coastal change at Damietta Promontory in the eastern part of the Nile Delta in the 1993-2000 period. The average measured rates of land subsidence in greater Cairo, Mansura, and Mahala are 7, 9, and 5 mm yr^{-1}, respectively, and the average measured rates of erosion and accretion at Damietta Promontory are -9.57 and +5.44 m yr^{-1}, respectively. These measured rates indicate the pressing need for regular monitoring of land subsidence and coastline retreat in the Nile Delta.

The environment of the Nile Delta is not ideal for SAR interferometry because of the dense vegetation cover, high moisture content, and high humidity. The very slow rate of deformation in the delta is also a major constraint because it requires a long-time period to be measured. This, in turn, leads to interferometric phase decorrelation.

Phase decorrelation is a common interferometric problem in areas like the Nile Delta. Interferograms created for Cairo, Mansura, and Mahala were completely decorrelated over cultivated areas and even noisy over urban areas. Regardless of the very slow rate of deformation, the cultivation, flood irrigation, and crop growth make the application of SAR interferometry unfeasible over cultivated land. The vegetation cover in the delta is very dynamic. It is changing approximately every four months.

As expected, all interferograms created for any part of the delta have been affected by troposphere effects. However, interferograms created from winter acquisitions were found less affected by atmospheric artifacts than those created from summer acquisitions. Moreover, interferograms created for Mansura and Mahala were significantly impacted by troposphere effects compared to interferograms created for Cairo. Perhaps this occurred because of the limited spatial extent of urban areas in Mansura and Mahala and both of them are completely surrounded by cultivated land. Construction activities are also a potential source of local phase decorrelation over urban areas. This problem was noticeable in Mansura and Mahala more than Cairo because Mansura and Mahala have faster rate of construction activities.

To overcome phase decorrelation problems and detect the slow rate of land subsidence in the Nile Delta, the Permanent Scatterer approach has been applied to

measure urban land subsidence as the interferometric phase remains well correlated in urban areas over long time periods. SAR interferometric data acquired by the European Radar Satellites (ERS-1 and ERS-2) were used in this study because of their spatial and temporal coverage and, more importantly, because of their short wavelength, 5.66 cm, that can detect slight changes in the surface of Earth.

The amplitude dispersion index has been used to identify Permanent Scatterers (PSs) in greater Cairo, Mansura, and Mahala over the 1993-2000 period. The identified PSs for each city have been found of sufficient density to conduct the interferometric analysis and to produce reliable results. The Permanent Scatterer technique has been applied independently for each city on the selected PSs.

The Permanent Scatterer interferometric approach was capable of detecting the non-linear behavior of land subsidence in the selected sites. Additionally, the created surface displacement maps for greater Cairo, Mansura, and Mahala show the pattern and magnitude of land subsidence in each city. The main contributors to the rate of subsidence in greater Cairo are the natural sediment compaction, tectonic setting, and groundwater pumping. The deformation maps created for Cairo imply that the subway network in Cairo is a potential contributor to the rate of recent subsidence as well. In Mansura and Mahala, the major causes of land subsidence are limited to the natural sediment compaction and groundwater pumping. The bowl shape that appears in the deformation maps is common where pumping-induced subsidence exists.

Subsidence measurements in greater Cairo, Mansura and Mahala are still relative at this level and need to be validated against *in situ* measurements. However, the

accuracy of the Permanent Scatterer techniques has been tested previously in numerous studies. On average, it is approximately ±2 mm; whereas the approximate accuracy of conventional InSAR techniques is ±5 mm. Unfortunately, There are no GPS measurements or any other *in situ* measurements available to validate the findings from this interferometric study. The measured subsidence rates are comparable with the subsidence rates reported in previous works based on sedimentlogical studies and thickness correlations of stratigraphic units in the delta. However, the InSAR measurements are believed to be highly impacted by several anthropogenic factors.

Despite phase decorrelation problems over the cultivated land in the Nile Delta, this study highlighted the feasibility of applying Permanent Scatterer interferometry to detect urban subsidence in the densely vegetated delta. The need of continued InSAR monitoring is evident from the localized urban subsidence in each of the three study sites. The slow rate of deformation can be accurately detected by exploiting long-time period of InSAR data of short wavelength. Therefore, it is recommended that regular SAR acquisitions by ERS-2 and ENVISAT, as well as by other C-band platforms be continued over the Nile Delta.

The synoptic view of remote sensing in coastal studies is unsurpassed. However, the application of optical remote sensing data in such studies is limited by the resolution cell, data availability, and clear weather. In contrast, SAR interferometric data can be acquired in all weather conditions, day and night. Furthermore, the unprecedented interferometric coherence is a powerful tool for detecting land/water boundaries.

ERS InSAR data have been also employed in this study to detect the patterns and magnitude of coastal change at Damietta Promontory. Areas of erosions and accretion have been accurately identified using the ERS complex coherence and amplitude images. The tandem mode of the ERS satellites is appropriate for this purpose, as no significant coastal change is expected to occur within 24 hours. The measured rate of coastal erosion at Damietta Promontory using ERS InSAR data is very close the measured rate of erosion using terrestrial survey reported in previous work, which adds confidence to the obtained results.

2. Future Directions

Urban subsidence is expected in all cities in the Nile Delta. Further interferometric studies for urban subsidence in other major cities in the delta such as Alexandria in the west and Port Said in the east will give a broad understanding of the ongoing deformation in the delta. However, the measured localized urban subsidence can not be interpolated to witness the regional land subsidence in the entire delta. The wide separation between urban areas can introduce intolerable uncertainty to the interpolation process.

To observe regional subsidence across the entire delta, subsidence over the cultivated land has to be measured. Of course, this can be accomplished locally using traditional terrestrial survey tools. However, to detect the very slow rate of subsidence in the delta using InSAR, monitoring has to be continued for many years. This is unfeasible over cultivated land for the reasons explained before. Natural reflectors will decorrelate

with time and, thus, they are not appropriate for InSAR measurements. The alternative is to conduct the interferometric measurements using artificial stable reflectors.

Based on feasibility and limitations addressed in this chapter for InSAR use over the Nile Delta, artificial scatterers have to be used across wide areas in the delta over a long time period to measure regional subsidence. The artificial reflectors must be fixed at well known elevation points on the bedrock after removing the soil layer to avoid potential errors that may arise from soil swelling and/or contraction.

All SAR data used in this study are ERS descending; i.e., acquired during the day light. It is expected that ERS ascending data acquired at night will be less affected by atmospheric artifacts, which may permit better results from conventional SAR interferometry over large cities in the Delta such as greater Cairo. As ERS SAR and ENVISAT ASAR data are acquired by similar sensors, they can be integrated to enable long-term subsidence monitoring in the Nile Delta over approximately 15 years.

Seasonal InSAR data are needed to address the impact of pumping-induced subsidence on the long-term subsidence and to determine whether the pumping-induced subsidence is permanent or recoverable. Seasonal data at least for the winter and summer seasons need to be exploited over approximately 10 years to detect the slight seasonal subsidence in major cities.

REFERENCES

Abdel-Aal, M., J. Price, D. Vaitl, and A. Shrallow, Tectonic evolution of the Nile Delta, its impacts on sedimentation and hydrocarbon, in: *Twelfth Petroleum Exploration and Production Conference,* November 3-5, 19-34, 1994.

Adam, N., B. Kampes, M. Eineder, J. Worawattanamateekul, and M. Kircher, The development of a scientific Permanent Scatterer system, *High Resolution Mapping from Space, ISPRS/EARSeL Workshop Proceedings,* Hanover, Germany, October 6-8, http://www.ipi.uni-hannover.de/html/publikationen/2003/workshop/adam.pdf, 2003.

Ahmed, M., A. Hassan, and O. Frihy, Absence of environmental impact assessment legislations for project decommissioning phase: environmental consequences, *Proceedings of the 10th International Conference "Environmental Protection Is a Must",* Alexandria, Egypt, May 9-11, 7-19, 2000a.

Ahmed, M., J. Robert, and M. Yehia, Monitoring the Nile Delta: a key step in adaptation to long-term coastal change, *Proceedings of the 2nd International Conference, on Earth Observations and Environmental Information (EOEI),* Cairo, Egypt, November 11-14, 3-17, 2000b.

Allen, C., Interferometric synthetic aperture radar, *IEEE Geoscience and Remote Sensing Society Newsletter,* September, *96*, 6-13, 1995.

Amelung, F., D. Galloway, J. Bell, H. Zebker, and R. Laczniak, Sensing the ups and downs of Las Vegas: InSAR reveals structural control of land subsidence and aquifer system deformation, *Geology, 27*(6), 483-486, 1999.

Askne, J., and J. Hagberg, Potential of interferometric SAR for classification of land surfaces, *Proceedings of the Int. Geosci. and Remote Sensing Symposium,* Tokyo, Japan, August 18-21, 985-987, 1993.

Badawy, A., and A. Abdel-Fattah, Source parameters and fault plane determinations of the 28 December 1999 northeastern Cairo earthquakes, *Tectonophysics, 343*(1-2), 63-77, 2001.

Badawy, A., and A. Abdel-Fattah, Analysis of the southeast Beni-Suef, northern Egypt earthquake sequence, *J. of Geodyn., 33,* 219-234, 2002.

Badawy, A., E. Issawy, G. Hassan, and A. Tealeb, Kinematics engine of the ongoing deformation field around Cairo, Egypt, *ACTA Geophysica Polonica, 51*(4), 447-458, 2003.

Badawy, A., and P. Monus, Dynamic source parameters of the 12th October 1992 Earthquake, Cairo, Egypt, *J. Geodyn., 20,* 99-109, 1995.

Bawden, G., W. Thatcher, R. Stein, K. Hudnut, and G. Peltzer, Tectonic contraction across Los Angeles after removal of groundwater pumping effects, *Nature, 412,* 812-815, 2001.

Beaumont, P., G. Blake, and J. Wagstaff, *The Middle East: a geographical study*, London, Wiley, 572 p., 1976.

Bloom, A., *Geomorphology: a systematic analysis of late Cenozoic landforms*, Upper Saddle River, N.J., Prentice Hall, 482 p., 1998.

Buckley, S., P. Rosen, S. Hensley, and B. Tapley, Land subsidence in Houston, Texas measured by radar interferometry and constrained by extensometers, *J. Geophys. Res., 108*(B11), 2542, 2003.

Bürgmann, R., P. Rosen, and E. Fielding, Synthetic aperture radar interferometry to measure Earth's surface topography and its deformation, *Annu. Rev. Earth Plannet. Sci., 28,* 169-209, 2000.

Carnec, C., D. Massonnet, and C. King, Two examples of the application of SAR interferometry to sites of small extent, *Geophys. Res. Lett., 23,* 3579-3582, 1996.

Chen, C., *Statistical-cost network-flow approaches to two dimensional phase unwrapping for radar interferometry,* PhD thesis, Stanford University, Stanford, California, June, 2001.

Colesanti, C., A. Ferretti, C. Prati, and F. Rocca, Monitoring landslides and tectonic motions with the Permanent Scatterers technique, *Engineering Geology, 68*, 3-14, 2003.

Colesanti, C., S. Le Mouelic, M. Bennani, D. Raucoules, C. Carnec, and A. Ferretti, Detection of mining related ground instabilities using the Permanent Scatterers technique - a case study in the east of France, *International J. of Remote Sensing, 26*(1), 201-207, 2005.

Costantini, M., A novel phase unwrapping method based on network programming, *IEEE Transactions on Geoscience and Remote Sensing, 36*(3), 813-821, 1998.

Crosetto, M., A. Arnaud, J. Duro, E. Biescas, and M. Agudo, Deformation monitoring using remotely sensed radar interferometric data, *Proceedings of the 11th FIG Symposium on Deformation Measurements,* Santorini, Greece, 2003.

Curlander, J., and R. McDonough, *Synthetic aperture radar: systems and signal processing,* New York, Wiley-Intersci., 647 p., 1991.

Dehls, J., M. Basilio, and C. Colesanti, Ground deformation monitoring in the Ranafjord area of Norway by means of the permanent scatterer technique, *IEEE Int., Geosci. and Remote Sensing Symposium, IGARSS,* 203-207, 2002.

Delacourt, C., P. Briole, and J. Achache, Tropospheric corrections of SAR interferograms with strong topography, Application to Etna, *Geophys. Res. Lett., 25*, 2849-52, 1998.

Dixon, T., F. Amelung, A. Ferretti, F. Novali, F. Rocca, R. Dokka, G. Sella, S. Kim, S. Wdowinski, and D. Whitman, New Orleans subsidence: space geodesy and Hurricane Katrina Flooding, *Nature, 441,* 587-588, 2006.

Egyptian Tunneling Society (ETS), Greater Cairo metro network: http://www.egypts.com/index.htm, 2005.

Elachi, C., *Spaceborne radar remote sensing: applications and techniques*, New York, IEEE, 255 p., 1988.

El Araby, H., and M. Sultan, Integrated seismic risk map of Egypt, *Seismological Research Letters, 71,* 52-65, 2000.

El-Fiky, G., C. Reddy, and A. Tealeb, GPS derived velocity and crustal strain field in the vicinity of Cairo city, Egypt, *J. Soc. India, 63,* 449-452, 2004.

El Kashef, A., Salt water intrusion in the Nile delta, *Ground Water*, *21*, 160-167, 1983.

El Raey, M., Vulnerability assessment of the coastal zone of the Nile Delta of Egypt, to the impacts of sea level rise, *Ocean & Coastal Management, 37*(1), 22-40, 1997.

El Raey, M., S. Nasr, O. Frihy, and M. El Hattab, Change detection of Rosetta promontory over the last forty years, *International J. of Remote Sensing, 16,* 825-834, 1995.

Evans, D., T. Farr, H. Zebker, and P. Mouginis-Mark, Radar interferometry studies of the Earth's topography, *EOS, Trans. American Geophysical Union, 73*(553), 557-558, 1992.

Ferretti, A., A. Monti-Guarnieri, C. Prati, and F. Rocca, Multi-baseline interferometric techniques and applications, in: *Proceedings of FRINGE '96 Workshop,* Zurich, Switzerland, September 30 - October 2, 243-253, 1996.

Ferretti, A., C. Prati, and F. Rocca, Nonlinear subsidence rate estimation using Permanent Scatterers in differential SAR interferometry, *IEEE Trans. Geosci. Remote Sensing, 38*(5), 2202-2212, 2000.

Ferretti, A., C. Prati, and F. Rocca, Permanent Scatterers in SAR interferometry, *IEEE Trans. Geosci. Remote Sensing*, *39*(1), 8-20, 2001.

Fielding, E., R. Bloom, and R. Goldstein, Rapid subsidence over oil fields measured by SAR interferometry, *Geophys. Res. Lett., 27*, 3215-3218, 1998.

Frihy, O., Sea-level rise and shoreline retreat of the Nile Delta promontories, Egypt, *Natural Hazards, 5,* 65-81, 1992.

Frihy, O., Some proposals for coastal management of the Nile Delta coast, *Ocean and Coastal Management, 30*, 43-59, 1996.

Frihy, O., and A. Khafagy, Climate and human induced changes in relation to shoreline migration trends at the Nile Delta promontories, Egypt, *Catena, 18*, 197-211, 1991.

Frihy, O. and P. Komar, Long-term shoreline changes and the concentration of heavy minerals in beach sands of the Nile Delta, Egypt, *Marine Geology, 115*, 253-261, 1983.

Frihy, O., S. Nasr, M. Ahmed, and M. El Raey, Temporal shoreline and bottom changes of the inner continental shelf of the Nile Delta, Egypt, Egypt, *J. Coastal Research, 7*(2), 465-476, 1990.

Fruneau, B., J. Rudent, D. Obert, and D. Raymond, Small displacements detected by SAR interferometry on the City of Paris (France), *Proceedings of IGARSS '99*, Hamburg, Germany, June 28 - July 2, (CD ROM), 1999.

Fujiwara, S., P. Rosen, M. Tobita, and M. Murakami, Crustal deformation measurements using repeat-pass JERS-1 synthetic aperture radar interferometry near the Izu Peninsula, Japan, *J. Geophys. Res., 103*, 2411-26, 1998a.

Gabriel, A., and R. Goldstein, Crossed orbit interferometry: Theory and experimental results from SIR-B, *International J. of Remote Sensing, 9,* 857-872, 1988.

Gabriel, A., R. Goldstein, and H. Zebker, Mapping small elevation changes over large areas-differential radar interferometry, *J. Geophys. Res., 94*, 9183-9191, 1989.

Galloway, D., K. Hudnut, S. Ingebritsen, S. Phillips, G. Peltzer, F. Rogez, and P. Rosen, Detection of aquifer system compaction and land subsidence using interferometric synthetic aperture radar, Antelope Valley, Mojave Desert, California, *Water Resour. Res., 34,* 2573-2585, 1998.

Goldstein, R., Atmospheric limitations to repeat-pass radar interferometry, *Geophys. Res. Lett., 22,* 2517-2520, 1995.

Goldstein, R., T. Barnett, and H. Zebker, Remote sensing of ocean currents, *Science, 246,* 1282-1285, 1989.

Goldstein, R., and C. Werner, Radar interferogram filtering for geophysical applications, *Geophys. Res. Lett., 25*(21), 4035-4038, 1998.

Goldstein, R., and H. Zebker, Interferometric radar measurement of ocean surface currents, *Nature, 328,* 707-709, 1987.

Graham, L., Synthetic interferometric radar for topographic mapping, *Proceedings of the IEEE 62*(2), 763-768, 1974.

Gray, A., and P. Farris-Manning, Repeat-pass interferometry with airborne synthetic aperture radar, *IEEE Trans. on Geosci. and Remote Sensing, 31*(1), 180-191, 1993.

Hanssen, R., *Radar interferometry: data interpretation and error analysis,* Kluwer Academic Publishers, Boston, 308 p., 2001.

Hernandez, B., F. Cotton, M. Campillo, and D. Massonnet, A comparison between short term (co-seismic) and long term (one year) slip for the Landers earthquake:

measurements from strong motion and SAR interferometry, *Geophys. Res. Lett., 24,* 1579-82, 1997.

Hilley, G., R. Bürgmann, A. Ferretti, F. Novali, and F. Rocca, Dynamics of slow-moving landslides from Permanent Scatterer Analysis, *Science, 304,* 1952-1955, 2004.

Hoffmann, J., H. Zebker, D. Galloway, and F. Amelung, Seasonal subsidence and rebound in Las Vegas Valley, Nevada, observed by synthetic aperture radar interferometry, *Water Resour. Res., 37(6),* 1551-1566, 2001.

Hooper, A., H. Zebker, P. Segall, and B. Kampes, A new method for measuring deformation on Volcanoes and other natural terrains using InSAR Persistent Scatterers, *Geophys. Res. Lett., 31,* L23611, doi:10.1029/2004GL021737, 2004.

Idris, H., and S. Nour, Present groundwater status in Egypt and the environmental impacts, *Environmental Geology and Water Sciences, 16(3),* 171-177, 1990.

Inman, D., and S. Jenkins, The Nile littoral cell and man's impact on the coastal littoral zone in SE Mediterranean, in: *Proceedings of the 17th International Coastal Engineering Conference,* ASCE, Sydney, Australia, March 23-28, 1600-1617, 1980.

Klemas, V., and A. Abdel-Kader, Remote sensing of coastal processes with emphasis on the Nile Delta, in: *International Symposium on Remote Sensing of Environments,* Cairo, 27 p., 1982.

Korrat, I., N. El Agami, H. Hussein, and M. El-Gabry, Seismotectonics of the passive continental margin of Egypt, *J. of African Earth Sciences, 41*(1-2), 145-150, 2005.

Lemoigne, J., and J. Tilton, Refining image segmentation by integration of edge and region data, *IEEE Trans. on Geosci. and Remote Sensing, 33*(3), 605-615, 1995.

Li, F., and R. Goldstein, Studies of multi-baseline spaceborne interferometric synthetic aperture radars, *IEEE Trans. Geosci. Remote Sensing, 28*(1), 88-96, 1990.

Lu, Z., R. Fatland, M. Wyss, S. Li, and J. Eichelberer, Deformation of New Trident volcano measured by ERS-1 SAR interferometry, Kalmia National Park, Alaska, *Geophys. Res. Lett., 24,* 695-98, 1997.

Manohar, M., Coastal processes at the Nile Delta coast, *Shore and Beach, 49*, 8-15, 1981.

Marghany, M., TOPSAR wave spectra model and coastal erosion detection, *International J. of Applied Earth Observation and Geoinformation, 3*(4), 357-385, 2001.

Marom, M., L. Shemer, and E. Thornton, Energy density directional spectra of a nearshore wave field measured by interferometric synthetic aperture radar, *J. Geophys. Res., 96,* 22125-22134, 1991.

Mason, D., I. Davenport, R. Flather, B. McCartney, and G. Robinson, Construction of an inter-tidal digital elevation model by the water-line method, *Geophys. Res. Lett., 22,* 3187-3190, 1995.

Massonnet, D., P. Briole, and A. Arnaud, Deflation of Mount Etna monitored by spaceborne radar interferometry, *Nature, 375,* 567-570, 1995.

Massonnet, D., and K. Feigl, Discrimination of geophysical phenomena in satellite radar interferograms, *Geophys. Res. Lett., 22*(12), 1537-1540, 1995a.

Massonnet, D., and K. Feigl, Satellite radar interferometric map of the coseismic deformation field of the M = 6.1 Eureka Valley, California, earthquake of May 17, 1993, *Geophys. Res. Lett., 22*(12), 1541-1544, 1995b.

Massonnet, D., and K. Feigl, Radar interferometry and its application to changes in the Earth's surface, *Reviews of Geophysics, 36,* 441-500, 1998.

Massonnet, D., K. Feigle, M. Rossi, and F. Adragna, Radar interferometric mapping of deformation in the year after the Landers earthquake, *Nature, 369,* 227-230, 1994.

Massonnet, D., T. Holzer, and H. Vadon, Land subsidence caused by the East Mesa geothermal field, California, observed using SAR interferometry, *Geophys. Res. Lett., 24,* 901-904, 1997.

Massonnet, D., M. Rossi, C. Carmona, F. Adragna, G. Pletzer, K. Feigle, and T. Rabaute, The displacement field of the Landers earthquake mapped by radar interferometry, *Nature, 364,* 138-142, 1993.

Meshref, W., *Tectonic framework of Egypt,* in: R. Said (ed.), Geology of Egypt, A.A. Balkema Publisher, Rotterdam, Netherlands, 113-153, 1990.

Mosconi, A., A. Rebora, G. Venturino, P. Bocc, and M. Khalil, Egypt-Nile Delta and North Sinai Cenozoic tectonic evolutionary model: a proposal, *Proceedings of*

the 13th Egypt Gen. Petrol. Corp. Explor. and Prod. Conference, Cairo, Egypt, February 21-25, *1,* 203-223, 1996.

Orwig, E., Tectonic framework of northern Egypt and the eastern Mediterranean, *EGPC, 5th Exploration Seminar,* Cairo, Egypt, March 16-20, 20 p., 1982.

Orwig, L., and D. Held, Interferometric ocean surface mapping and moving object relocation with a Norden Systems Ku-band SAR, *Proc. of the International Geoscience and Remote Sensing Symposium (IGARSS '92),* Houston, Texas, May 26-29, (Piscataway, N.J., IEEE) 1598-1600, 1990.

Pletzer, G., K. Hudnut, and K. Feigl, Analysis of coseismic surface displacement gradients using radar interferometry: new insights into the Landers earthquake, *J. Geophys. Res., 99*(B11), 21971-21981, 1994.

Prati, C., and F. Rocca, Limits to the resolution of elevation maps from stereo SAR images, *International J. of Remote Sensing, 11*(12), 2215-2235, 1990.

Prati, C., and F. Rocca, Focusing SAR data with time varying Doppler cenroid, *IEEE Trans. on Geoscience and Remote Sensing, 30*(3), 550-559, 1992.

Price, E., and D. Sandwell, Small-scale deformations associated with the 1992 Landers, California, earthquake mapped by synthetic aperture radar interferometry phase gradients, *J. Geophys. Res., 103,* 27001-27016, 1998.

Rabus, B., M. Eineder, A. Roth, and R. Bamler, The shuttle radar topography mission - a new class of digital elevation models acquired by spaceborne radar, *Photogrammetry & Remote Sensing, 57,* 241-262, 2003.

Rizzini, A., F. Wezzani, V. Cococcetta, and G. Milad, Stratigraphy and sedimentation of the Neogene Quaternary section in the Nile Delta area, *Marine Geology, 27,* 327-348, 1978.

Rodriguez, E., and J. Martin, Theory and design of interferometric synthetic-aperture radars, *Proc. of the IEEE, 139*(2), 147-59, 1992.

Rogers, A., and R. Ingalls, Venus: mapping the surface reflectivity by radar interferometry, *Science, 165,* 797-799, 1969.

Rosen, P., S. Hensley, H. Zebker, F. Webb, and E. Fielding, Surface deformation and coherence measurements of Kilauea Volcano, Hawaii, from SIR-C radar interferometry, *J. Geophys. Res., 101,* 23109-23125, 1996.

Rott, H., T. Nagler, and F. Rocca, InSAR techniques and applications for monitoring landslides and subsidence, in: T. Benes (ed.), *Proceedings of EARSeL Assembly Geoinformation for European-wide Integration,* Prague, June 2002, Millpress, Rotterdam 25-31, 2003.

Rumsey, H., G. Morris, R. Green, and R. Goldstein, A radar brightness and altitude image of a portion of Venus, *Icarus, 23,* 1-7, 1974.

Said, R., *The River Nile,* Berlin: Springer-Verlag, 151 p., 1981.

Scharroo, R., and P. Visser, Precise orbit determination and gravity field improvement for the ERS satellites, *J. Geophys. Res., 103*(C4), 8113-8127, 1998.

Schlumberger, *Well Evaluation Conference Egypt*, Paris: Schlumberger Middle East, Editions Galilee, 248 p., 1984.

Sestini, G., Nile Delta: a review of depositional environments and geological history, in: Whateley, M., and K. Pickerring, (eds.), *Deltas sites and traps for fossil fuels,* London, Geological Society Spatial Publication, *41,* 99-127, 1989.

Sestini, G., Implications of climatic changes for the Nile Delta, in: Jeftic, L., J. Milliman, and G. Sestini, (eds.), *Climatic change and the Mediterranean,* Edward Arnold, New York, 535-601, 1992.

Shawky Abdine, A., Egypt's petroleum geology: good grounds for optimisim, *World Oil,* December, 99-112, 1981.

Singhroy, V., K. Mattar, and L. Gray, Landslide characterization in Canada using interferometric SAR and combined SAR and TM images, *Advances in Space Research, 2*(3), 465-476, 1998.

Smith, E., and A. Abdel-Kader, Coastal erosion along the Egyptian Delta, *J. of Coastal Res., 4,* 245-255, 1988.

Sneed, M., M. Ikehara, D. Galloway, and F. Amelung, Detection and measuring of land subsidence using Global Positioning System and interferometric synthetic aperture radar, Coachella Valley, California, 1996-1998, U.S. Geological Survey, *Water-Resources Investigations Report, 01-4193,* 2001.

Stabel, E., and P. Fischer, Satellite radar interferometry products for the urban application domain, *Advances in Environmental Research, 5,* 425-433, 2001.

Stanley, D., Subsidence in the northeastern Nile Delta: rapid rates, possible causes, and consequences, *Science, 240,* 497-500, 1988.

Stanley, D., Recent subsidence and northeast tilting of the Nile delta, Egypt, *Marine Geology, 94,* 147-154, 1990.

Stanley, D., Nile Delta: extreme case of sediment entrapment on a delta plain and consequent coastal land loss, *Marine Geology, 129,* 189-195, 1996.

Stanley, D., and A. Warne, Nile Delta, recent geological evolution and human impact, *Science, 260,* 628-634, 1993.

Stanley, D., and A. Warne, Nile Delta in its destruction phase, the world deltas conference; a tribute to James Plummer Morgan (1919-1995), *J. of Coastal Research, 14*(3), 794-825, 1998.

Strozzi, T., L. Tosi, L. Carbognin, U. Wegmüler, and A. Galgaro, Monitoring land subsidence in the Euganean Geothermal Basin with differential SAR interferometry, *Proceedings of FRINGE '99,* Liège, Belgium, 10-12 November, http://earth.esa.int/services/esa_doc/doc_int.html, 1999a.

Strozzi, T., U. Wegmüler, and A. Luckman, and H. Balzter, Mapping deformation in Amazon with ERS SAR interferometry, *Proceedings of FRINGE '99,* Liège, Belgium, 10-12 November, http://earth.esa.int/services/esa_doc/doc_int.html, 1999b.

Strozzi, T., U. Wegmüler, Land subsidence in Mexico City mapped by ERS differential SAR interferometry, *Proceedings of IGARSS '99,* Hamburg, Germany, June 28 - July 2, 1940-1942, 1999.

Tarchi, D., N. Casagli, R. Fanti, D. Leva, G. Luzi, and A. Pasuto, Landslide monitoring by using ground-based SAR interferometry: an example of application to the Tessina landslide in Italy, *Engineering Geology, 68,* 15-30, 2003.

Thatcher, W., and D. Massonnet, Crustal deformation at Long Valley Caldera, eastern California, 1992-1996 inferred from satellite radar interferometry, *Geophys. Res. Lett., 24,* 2519-22, 1997.

UNDP/UNESCO, Arab Republic of Egypt: coastal protection studies, project findings and recommendations, *UNDP/EGY/73/063,* Final Report, FNR/SC/OSP/78/230, Paris, UNDP/UNESCO, 483 p., 1978.

Warne, A., and D. Stanley, Late quaternary evolution of the Northwest Nile Delta and adjacent coast in the Alexandria region, Egypt, *J. of Coastal Research, 9*(1), 26-64, 1993.

White, K., and H. El-Asmar, Monitoring changing position of the coastline using Thematic Mapper imagery, an example from the Nile Delta, *Geomorphology, 29,* 93-105, 1999.

Wicks, C., W. Thatcher, and D. Dzurisin, Migration of fluids beneath Yellowstone caldera inferred from satellite radar interferometry, *Science, 282*(5388), 458-462, 1998.

Wilson, P., Rule-based classification of water in Landsat MSS images using the variance filter, *Photogrammetric Engineering and Remote Sensing, 63,* 485-491, 1997.

World Bank, Arab Republic of Egypt: country economic memorandum, economic readjustment with growth, in: *World Bank Report no. 7447-EGT, 2,* 72 p., Washington, DC, 1990.

Zaghloul, Z., A. Abdel-Daiem, and A. Taha, Geomorphology, geologic evolution and subsidence of the Nile Delta during the Quaternary, *Bulletin of the Faculty of Science,* Mansura, Egypt, *17*(1), 471-495, 1990.

Zaghloul, Z., S. Andrawis, and S. Ayad, New contribution to the stratigraphy of Tertiary sediments of Kafr El Dawar well no. 1, NW Nile Delta, Egypt, *Annals of the Geological Survey of Egypt, 9,* 292-307, 1979.

Zaghloul, Z., A. Taha, O. Hegab, and F. El-Fawal, The Neogene Quaternery sedimentary basins of the Nile Delta, *Egyptian J. of Geology, 21,* 143-161, 1977a.

Zaghloul, Z., A. Taha, O. Hegab, and F. El-Fawal, The Plio-Pleistocene Nile Delta: sub-environments, stratigraphic section and genetic classification, *Annals of the Geological Survey of Egypt, 9,* 283-291, 1977b.

Zebker, H., F. Amelung, and S. Jonsson, Remote sensing of volcano surface and internal processes using radar interferometry, *AGU Geophysical Monograph, 116,* 179-205, 2000.

Zebker, H., and R. Goldstein, Topographic mapping from interferometric SAR observations, *J. Geophys. Res., 91,* 4993-4999, 1986.

Zebker, H., S. Madsen, J. Martin, K. Wheeler, and T. Miller, The TOPSAR interferometric radar topographic mapping instrument, *IEEE Trans. Geosci. Remote Sensing, 30,* 933-40, 1992.

Zebker, H., P. Rosen, R. Goldstein, A. Gabriel, and C. Werner, On the derivation of coseismic displacement fields using differential interferometery: the Landers earthquake, *J. Geophys. Res., 99,* 19617-19634, 1994a.

Zebker, H., P. Rosen, and S. Hensley, Atmospheric effects in interferometric synthetic aperture radar surface deformation and topographic maps, *J. Geophys. Res., 102*(B4), 7547-7563, 1997.

Zebker, H., and J. Villasenor, Decorrelation in interferometric radar echoes, *IEEE Trans. Geosci. Remote Sensing, 30,* 950-959, 1992.

Zebker, H., C. Werner, P. Rosen, and S. Hensley, Accuracy of topographic maps derived from ERS-1 interferomteric radar, *IEEE Trans. Geosci. Remote Sensing, 32,* 823-836, 1994b.

Zisk, S., Lunar topography: first radar-interferometer measurements of the Alphonsus-Ptolemaeus-Arzachel region, *Science, 178,* 977-980, 1972a.

Zisk, S., A new Earth-based radar technique for the measurement of lunar topography, *Moon, 4,* 296-306, 1972b.

VITA

Name:	Mohamed Hassan Aly
Address:	Texas A&M University Department of Geology & Geophysics College Station, Texas 77843-3115
Email:	aly@tamu.edu

Education: B.S., 1992, Geology, Zagazig University, Egypt

M.S., 1997, Geology, Zagazig University, Egypt

Research Interests: Integrating SAR Interferometry (InSAR) and Global Positioning System (GPS), as well as Geographic Information System (GIS) to study crustal deformation and geomorphic hazards.